Pattern Formation in Ultrafast Dynamics of Charge-density-wave States

Lingyu Yang
Chaozhou, Guangdong, China
M.S. Theoretical Physics, Sun Yat-sen University

A Dissertation presented to the Graduate Faculty
of the University of Virginia in Candidacy for the degree of
Doctor of Philosophy

Department of Physics
University of Virginia
June 2024

Professor Gia-Wei Chern
Research Advisor

Professor Jeffrey Teo

Professor Bellave Shivaram

Professor Prasanna Balachandran
GSAS Representative

Abstract

We investigate the post-quench dynamics of charge-density-wave (CDW) order in the square-lattice t-V model and Holstein model. Both systems exhibit a ground state characterized by a checkerboard modulation of electron density at half-filling. In the t-V model, we employ a generalized self-consistent mean-field method, based on the time-dependent variational principle, to describe the dynamical evolution of CDW states. By assuming a homogeneous CDW order throughout the quench process, this approach reduces to the Anderson pseudospin method. Quench simulations using the Bloch equation for pseudospins reveal three canonical behaviors of order-parameter dynamics: phase-locked persistent oscillation, Landau-damped oscillation, and dynamical vanishing of the CDW order.

To incorporate dynamical inhomogeneity into quench simulations, we develop an efficient real-space von Neumann equation method. Large-scale simulations uncover complex pattern formations in post-quench CDW states, particularly in the strong quench regime. These emergent spatial textures are characterized by super density modulations atop the short-period checkerboard CDW order, highlighting the significance of dynamical inhomogeneity in quantum quenches of many-body systems with broken Z_2 symmetry.

In addition, we address artifacts in time evolution introduced by the time-dependent mean-field theory by studying the non-adiabatic post-quench dynamics of CDW states in the Holstein model, which is numerically exact when lattice degrees of freedom are treated classically. We derive the Anderson pseudospin formulation and Newtonian

equations of motion for the electronic and lattice degrees of freedom, respectively, to describe the dynamical evolution of CDW states and lattice distortions. Quench simulations reveal three canonical behaviors of order-parameter and lattice dynamics, consistent with those observed in the t-V model.

Real-space simulations in the Holstein model explore two post-quench scenarios. In the first, the initial state is prepared with vanishing electron-lattice coupling, and quenching the coupling constant induces the formation of CDW domains, resulting in either anomalous coarsening or spontaneous glassy states depending on the final coupling constant. In the second scenario, starting from a checkerboard modulation of charge density, quenching to a different finite coupling constant results in spatial inhomogeneity that satisfies parametric instability. The rich physics observed in the post-quench dynamics of CDW states in the Holstein model arises from the interplay between electronic and lattice degrees of freedom.

Finally, we investigate the out-of-equilibrium dynamics of a photo-excited CDW state in the square-lattice Holstein model, similar to the setup in a pump-probe experiment. Our extensive simulations show that the energy injected by a short pump pulse results in the reduction of the CDW order and the generation of coherent phonons. For a pump pulse with a large fluence or a center frequency greater than the CDW bandgap, the photoexcitation leads to a complete melting of the CDW order. Furthermore, our simulations reveal a dynamical regime at intermediate fluence where the pump pulse induces complex pattern formation. These emergent spatial textures are characterized by super density modulations on top of the short-range checkerboard CDW order. Our findings highlight the significance of dynamical inhomogeneity in quantum many-body systems subjected to pump-probe experiments.

Acknowledgments

First and foremost, I want to express my deepest gratitude to my research advisor at UVA, Professor Gia-Wei Chern, for his guidance, insights, and continuous support, without which I could not have completed this thesis. He patiently taught me how to learn and explain physics intuitively, work on problems with the big picture in mind, and be a good scientist in general.

I am deeply grateful to Professor Jeffrey Teo for his many discussions and encouragement during the early stages of my graduate studies, as well as his generous support during the most challenging times of my PhD journey. I learned a lot from him through his classes and various conversations.

I would also like to thank the members of my defense committee, Prof. Bellave Shivaram and Prof. Prasanna Balachandran, for their suggestions on how to improve my thesis. I extend my gratitude to the physics department staff, especially Peter Cline, for his generous support for graduate students.

I am grateful to Dr. Shizeng Lin and Dr. Chunli Huang for their support during my time in Los Alamos. The many discussions with them have greatly shaped my perspective on physics. I also wish to thank Dr. Ryan Badman and Dr. Andrei Galiautdinov; without their help, I would not have been able to come to Charlottesville. I appreciate the company and support of my friends and fellow graduate students in Charlottesville, both academically and personally.

Lastly, I would like to thank my parents for their understanding of my pursuit of a PhD in physics. I also acknowledge the unwavering support of my wife, Peiling Wu, who has helped take care of our household and our daughter. I could not have finished my thesis without her support over the past few years.

Table of Contents

List of Figures

Chapter 1

Introduction

1.1 Background

Quantum quench is a theoretical protocol used to study the non-equilibrium time evolution of a physical observable in an isolated system. This is realized by preparing an initial state, such as the ground state of a system Hamiltonian, and then allowing it to evolve under a different Hamiltonian, achieved by abruptly changing a parameter of the original Hamiltonian, in a time scale much smaller than the inverse of the mass gap [2, 3]. The initial state is generally not an eigenstate of the new Hamiltonian. Consequently, the physical observable, such as the expectation value of local operators, becomes time-dependent, and its time evolution is referred to as post-quench dynamics.

The post-quench dynamics of quantum systems has attracted enormous attention in recent years [3–6]. The interest is partly spurred by tremendous experimental advances both in cold atom systems [7, 8] and in ultrafast techniques such as pump-

probe spectroscopy [9–14]. In particular, for cold-atomic gases trapped in an optical lattice, the parameters of the Hamiltonian, such as interaction strength between particles and lattice parameters can be tuned rapidly in time, thus providing a near-ideal platform for studying quench-induced nonequilibrium quantum behaviors. Moreover, as cold-atom systems can be well isolated from the environment, their post-quench dynamics is well approximated by a unitary evolution. In pump-probe spectroscopy, by exciting a sample with a short laser pulse (pump pulse), this technique allows one to study the ultrafast relaxation dynamics of quasiparticles [15, 16]. Recently, pump-probe techniques have also been utilized to investigate photo-induced ultrafast collective behaviors [17–23], for example, by measuring the time-resolved dynamics of order-parameter fields. Moreover, photo-induced phase transition [24, 25] with an intensive pump pulse offers an avenue to detect long-lasting meta-stable states or even the so-called hidden states which are nonequilibrium many-body states without equilibrium counterpart [26–36].

A central question is whether thermalization can be reached in such closed-system quantum evolution and, if yes, what are the mechanisms and time-scales [37–49]. Moreover, several nonequilibrium phases and dynamical phase transitions, some of which have no counterpart in equilibrium systems, have been demonstrated in the long-lasting prethermal states after a quantum quench [50–60]. Understanding the nature of such prethermal states is an ongoing active research.

1.2 Post-quench dynamics in symmetry breaking phases

For post-quench dynamics with spontaneous symmetry breaking phases, the interplay between the collective modes, as represented by order-parameter fields, and quasiparticle degrees of freedom dominates the nonequilibrium behaviors of the prethermal states [61, 62]. Extensive theoretical studies, including several pioneering works on the interaction quench of superconductor pairing field, have revealed three dynamical phases of the time-dependent order parameter in the collisionless limit [1, 63–66]. In the phase-locked regime, the dynamics of the collective modes locks with that of the quasiparticles, giving rise to a persistent oscillation of the order parameter. For intermediate quench amplitudes, the perturbed system relaxes to a state with a reduced order parameter through the Landau-damping mechanism. The energy transfer from the collective modes to quasipartiles in this regime leads to a damped oscillation of the order parameter. Finally, in the third strongly-damped regime, corresponding to a quench toward reduced interactions, the relaxation of the system is characterized by dynamically vanishing order parameters. While more complex dynamical behaviors have also been discussed, most symmetry-breaking phases, including the well-studied BCS superconductivity (SC) and spin density waves (SDW) as well as more complex order parameters, exhibit the above three major dynamical regimes [67–80].

It is worth noting that in most previous works the prethermal states induced by interaction quenches are assumed to be spatially homogeneous, including the three main dynamical phases discussed above. For example, the Anderson pseudospin ap-

proach [81], which is widely used in the study of quench dynamics of BCS superconductors, precludes the possibility of spatial fluctuation or inhomogeneity. On the other hand, since thermalization mechanisms are generally local, it is likely that the post-quench states would develop spatial inhomogeneity through a process similar to the Kibble-Zurek mechanism [82, 83]. The Kibble-Zurek mechanism, which was developed to understand the formation of topological defects in early universe, has been applied to study the post-quench dynamics in the symmetry-breaking phases [84]. For the case of interaction quench, significant amount of energy is uniformly injected into a system. The relaxation of local regions that are separated from each other by a distance greater than the coherent length would proceed independently. Such incoherent local relaxations lead to the generation of topological defects of the order parameter, giving rise to a heterogeneous post-quench state [84–89].

Even in the collisionless coherent regime, the highly nonlinear post-quench evolution renders the system susceptible to instabilities that could lead to inhomogeneous states. For example, it is shown that quench-induced large-amplitude coherent oscillations of the SC order parameter are unstable against parametric instability and the emergence of Cooper-pair turbulence [90]. Spontaneous formation of inhomogeneous superconducting states following an interaction quench has indeed been demonstrated in real-space dynamical simulations based on time-dependent Hartree-Fock-Bogoliubov theory [91, 92]. Similar scenario has also been observed in the context of Mott transitions in Hubbard models. Although the Mott metal-insulator transition

is not characterized by the broken-symmetry scenario, the on-site double occupation probability serves as an effective order parameter of a Mott transition. Interestingly, the double-occupancy of a quenched Hubbard model exhibits a coherent oscillation similar to that of conventional order parameters [93,94]. Real-space dynamical simulations of Mott phases in the coherent collisionless limit also found post-quench states with a highly inhomogeneous distribution of the double occupancy [95].

While dynamical inhomogeneity in quantum quenches of many-body systems remains to be systematically investigated, pattern formation phenomena are ubiquitous in nonequilibrium systems with highly nonlinear dynamics. In particular, the mechanisms and characterizations of pattern formation in classical physics, soft-matter, and biological systems have been intensively studied for decades [96–100]. Several unifying descriptions of pattern forming systems, such as the Swift-Hohenberg equation, as well as classifications of universal behaviors have also been developed. It remains to be seen whether some of the general mathematical frameworks can be applied to pattern formation induced by quantum quenches. However, the physical mechanisms of pattern-forming instabilities in quantum quenches are intrinsically different. For most classical examples, the formation of complex patterns often is driven by energy injection and the subsequent local dissipation in an open system. On the other hand, the complex textures of order-parameter field in post-quench states result from the unitary evolution of a closed quantum system.

Based upon the analysis above, it is important to systematically study the post-

quench dynamics in the symmetry-breaking phases and investigate the mechanism of pattern formation and emergence of spatial inhomogeneity.

1.3 Post-quench dynamics of charge-density-wave states

Charge density wave (CDW) states are one of the prominent platforms for exploring ultrafast phenomena associated with a symmetry breaking phase. This is partly due to the ubiquity of CDW states which have been observed in a wide class of materials, including metals, semiconductors, and Mott insulators [101–112]. Since many CDW states are stabilized by electron-phonon coupling, CDW order is often found to compete or coexist with a proximate superconducting state. Moreover, as the charge degrees of freedom directly couples to external electric field, CDW materials are idea candidates for manipulating and tracing photo-excited phase transitions. For example, photo-induced insulator-to-metal transitions through the melting of CDW order have been observed in many materials [113–130].

To study the post-quench dynamics of the CDW states, we consider the quantum quench dynamics of the spinless fermionic t-V model on a square lattice. This model, which can be viewed as a simplified version of the Hubbard model, describes the competition between delocalization of fermions on a lattice and the nearest-neighbor density-density repulsion. For a half-filled t-V model defined on a bipartite lattice, the ground state in the strong coupling limit $V \to \infty$ is obtained when one sublattice is fully occupied, while the other sublattice is empty. This staggered arrangement

of fermions breaks the Z_2 sublattice symmetry and can be described by an Ising order parameter. For the case that the fermionic particles are electrons, the resultant density modulation corresponds to a CDW order. Although the t-V model is also often used to describe charge-neutral fermionic cold atoms, we shall refer to a periodic particle-density modulation as a CDW for convenience. In the case of a square-lattice, a divergent Lindhard susceptibility due to a perfect Fermi surface nesting at half-filling indicates that the system is unstable against the formation of a checkerboard CDW order even in the small V limit. Therefore, t-V model provides an ideal platform for studying the time evolution of CDW states upon interaction quench.

While a CDW order can be induced through a purely electronic mechanism, as we will discuss in t-V model, the majority of CDW states are accompanied by a concomitant structural distortion. This points to an important role of electron-phonon coupling in both the static and dynamical behaviors of CDW states. In particular, the dynamics of CDW order is also intimately related to that of lattice degrees of freedom. The interplay between the photo-excited electron-hole pairs and the combined CDW and lattice dynamics could lead to rich dynamical phenomena. For example, it has been shown that the melting of a CDW is often accompanied by the generation of coherent phonons [128–132]. The Holstein model serves as a valuable platform for investigating the dynamic interplay between electrons and lattice vibrations, encapsulated by a localized electron-lattice coupling term. This model facilitates the exploration of interesting phenomena like CDW states, characterized by periodic al-

terations in electron density within the material. In the context of the hall-filled Holstein model on a square lattice, the system manifests as a band insulator, with the Brillouin zone folded owing to lattice symmetry, thereby confining the system to a restricted Brillouin zone in reciprocal space. Furthermore, Fermi surface nesting dictates that wave vectors differing by $\mathbf{K} = (\pi, \pi)$ are interconnected, consequently instigating CDW collective excitations. The electron-lattice coupling prompts lattice distortions, culminating in a gap formation at the nesting vector. This gap plays a crucial role in stabilizing the CDW phase by diminishing the kinetic energy of the system, and facilitating electron localization.

1.4 Organization and conventions

Here I make a brief outline of this thesis. In Chapter 2, we discuss the time-dependent mean-field methods for t-V model and show that it can be reduced to the Anderson pseudospin formalism. In Chapter 3, we formulate the real space von Neumann equation and perform a systematic investigations on the emergence of spatial inhomogeneity and pattern formation. After concluding the post-quench dynamics of CDW states in pure electronic system, we formulate the pseudospin formalism for Holstein model, and show that the CDW dynamics is described by the Bloch equation of pseudospin and Newtonian equations for lattice degrees of freedom in Chapter 4, upon the assumption that CDW states are spatially homogeneous. The real space dynamics is studied in Chapter 5, where anomalous coarsening is observed in inter-

action quench from a Fermi liquid state, and parametric instability of CDW order emerges in quench from an initial with finite electron-lattice coupling. Finally, we discuss the CDW melting, pattern formation, and generation of coherent phonons in photo-excitation of Holstein model in Chapter 6.

Chapter 2

Mean-field methods for t-V model

2.1 Introduction

We consider the quantum quench dynamics of the spinless fermionic t-V model on a square lattice. This model, which can be viewed as a simplified version of the Hubbard model, describes the competition between delocalization of fermions on a lattice and the nearest-neighbor density-density repulsion. Its Hamiltonian reads

$$\hat{\mathcal{H}} = -t_{\mathrm{nn}} \sum_{\langle ij \rangle} \hat{c}_i^\dagger \hat{c}_j + V \sum_{\langle ij \rangle} \hat{n}_i \hat{n}_j, \tag{2.1}$$

where $\hat{c}_i^\dagger$ ($\hat{c}_i$) denotes the creation (annihilation) operator of a spinless fermion at site-i, $\hat{n}_i = \hat{c}_i^\dagger \hat{c}_i$ is the fermion number operator. The first term above describes particle hopping between neighboring sites $\langle ij \rangle$ on a square lattice, with t_{nn} being the transfer coefficient. The second term with $V > 0$ represents a nearest-neighbor density-density repulsive interaction.

For a half-filled t-V model defined on a bipartite lattice, the ground state in the strong coupling limit $V \to \infty$ is obtained when one sublattice is fully occupied,

while the other sublattice is empty. This staggered arrangement of fermions breaks the Z_2 sublattice symmetry and can be described by an Ising order parameter. For the case that the fermionic particles are electrons, the resultant density modulation corresponds to a charge density wave (CDW) order. Although the t-V model is also often used to describe charge-neutral fermionic cold atoms, we shall refer to a periodic particle-density modulation as a CDW for convenience. In the case of a square-lattice, a divergent Lindhard susceptibility due to a perfect Fermi surface nesting at half-filling indicates that the system is unstable against the formation of a checkerboard CDW order even in the small V limit.

For a finite repulsive interaction, the t-V model cannot be exactly solved either for equilibrium states or dynamical evolution. The 1D version of this model can be efficiently solved with high accuracy using the density matrix renormalization group (DMRG) [133,134] and its time-dependent generalizations such as time-evolving block decimation (TEBD) algorithm [135, 136]. Although DMRG or tensor-network variational wave functions can also be applied to quasi-2D systems, e.g. with a cylinder geometry, such approaches are computationally more intensive with less well-controlled accuracy. Large-scale dynamical simulations of higher-dimensional systems are thus not feasible using such DMRG-based methods.

The rest of this chapter is organized Simulation results based on pseudospin methods show that the post-quench CDW order exhibits the three canonical dynamical phases: (I) phase-locked persistent oscillation, (II) Landau-damped oscillation with a

finite asymptotic value, and (III) dynamical vanishing of the CDW order parameter. Further characterizations of these dynamical phases will be discussed in the following sections.

2.2 Time-dependent Hartree-Fock Method for t-V model

The Hartree-Fock (HF) mean-field method proves an efficient approximation to the modeling of the emergent CDW states. The central idea of HF approximation, as in most mean-field type methods, is to reduce a many-body problem into an effective single-particle problem self-consistently. While such self-consistency can be achieved via the usual mean-field decoupling of the interaction terms, HF approximation is best understood as a variational method in which the trial many-fermion wave function has the form of a Slater determinant. The HF or its extension for superconducting pairing have also been generalized to include time dependence. Indeed, the time-dependent HF (TDHF) is widely used to describe dynamics of many-body systems in nuclear physics and quantum chemistry [137–139]. It is worth noting that the Anderson pseudospin approaches [1, 63–66] to quantum quenches of SC or SDW orders are also based on TDHF.

Generalization of the mean-field methods to dynamical evolution of interacting systems can be achieved via the Dirac-Frenkel time-dependent variational principle (TDVP) [140, 141]. By constraining a quantum state to a specific manifold of the Hilbert space through a variational wave function, the minimum action equation gives

an effective dynamical description for the variational parameters. For example, applying TDVP to variational matrix product states (MPS) offers an alternative approach to introduce time evolution in DRMG-based methods [142, 143]. The TDHF methods, or more generally the time-dependent self-consistent field methods for fermions, can similarly be derived by constraining the many-body wave function to the form of Slater determinant in the TDVP formalism. Here we outline the approach for a generalized t-V model with both particle hopping t_{ij} and density-density interaction V_{ij} extended to further neighbor pairs (ij). The derivation can be straightforwardly generalized to other lattice models.

We start with the Dirac-Frenkel action for a general quantum state $|\Psi(t)\rangle$ whose dynamics is governed by a Hamiltonian $\hat{\mathcal{H}}$.

$$S[\Psi] = \int dt \, \langle \Psi(t)| \left(i\hbar \frac{d}{dt} - \hat{\mathcal{H}} \right) |\Psi(t)\rangle \tag{2.2}$$

The equation of motion for the quantum state is given by the least action principle: $\partial S / \partial \langle \Psi| = 0$. Indeed, the minimum action equation simply reproduces the Schrödinger equation for an unconstrained wave function. Next we assume that the many-fermion quantum state is a Slater determinant, which can be expressed as a filled Fermi sea of self-consistently determined quasiparticles:

$$|\Psi(t)\rangle = \prod_{\mu} \hat{\gamma}_{\mu}^{\dagger}(t)|0\rangle, \tag{2.3}$$

where $\hat{\gamma}_{\mu}^{\dagger}(t)$ is the time-dependent creation operator of a quasiparticle with quantum number μ and $|0\rangle$ is the vacuum of the fermions. The quasiparticle operators are

related to the fermion operators $\hat{c}_i^\dagger$ through a time-dependent unitary transformation:

$$\hat{\gamma}_\mu^\dagger(t) = \sum_i \phi_i^\mu(t)\, \hat{c}_i^\dagger. \tag{2.4}$$

As will be shown below, the transformation coefficients ϕ_i^μ play the role of effective single-particle wave functions. The independence of the quasiparticles further imposes the orthogonality conditions for the wave functions $\sum_i \phi_i^{\mu *}(t)\phi_i^\nu(t) = \delta_{\mu\nu}$, which have to be satisfied at all times. Substituting the Slater determinant wave function into the Dirac-Frenkel action and using the Wick's theorem to compute the expectation values, we obtain

$$\begin{aligned} S[\{\phi\}] = \int dt \sum_\mu \sum_{ij} \left[\phi_i^{\mu *} \left(i\hbar\delta_{ij} \frac{d}{dt} + t_{ij} \right) \phi_j^\mu \right] \\ - \int dt \sum_{\mu,\nu} \sum_{ij} V_{ij} \left(|\phi_i^\mu|^2 |\phi_j^\nu|^2 - \phi_i^{\mu *} \phi_j^{\nu *} \phi_j^\mu \phi_i^\nu \right) \end{aligned} \tag{2.5}$$

The two terms in the second line above correspond to the familiar Hartree and Fock decoupling, respectively. The least action condition $\partial S/\partial \phi^{\mu *} = 0$ gives the following nonlinear single-particle Schrödinger equations

$$\begin{aligned} i\hbar \frac{d\phi_i^\mu}{dt} = &- \sum_j t_{ij} \phi_j^\mu + \sum_j \sum_\nu V_{ij} |\phi_j^\nu|^2 \phi_i^\mu \\ &- \sum_j \sum_\nu V_{ij} \phi_j^{\nu *} \phi_i^\nu \phi_j^\mu. \end{aligned} \tag{2.6}$$

The coupled differential equations of these single-particle wave functions give a complete dynamical description of the many-fermion systems. Importantly, for a given set of initial wave functions $\phi_i^\mu(t = 0)$ that are normalized and orthogonal to each

other, it can be shown that the orthogonality conditions are maintained by the above dynamical equations. Therefore, it needs to be awared that the evolution of the system is always described by a single Slater determinant, and effectively produces the behaviors of the system in the collisonless limit, which may not give us the asymptotic behavior of the true quantum system.

2.3 Anderson pseudospin formulation

In this section, we derive an effective spin formulation for the coherent dynamics of CDW from the general TDHF equations. For a bipartite lattice, the nearest-neighbor repulsive density-density interaction naturally leads to a disparity of particles on the two sublattices. The resultant long-range order corresponds to a commensurate CDW state with an ultra-short modulation period. In the case of square lattice, this CDW order is characterized by a checkerboard pattern associated with the wave vector $\mathbf{Q} = (\pi, \pi)$. For a time-dependent CDW state, an effective order parameter for the charge modulation is

$$\Delta(t) = \frac{1}{N} \sum_i \langle \Psi(t) | \hat{n}_i | \Psi(t) \rangle e^{i\mathbf{Q}\cdot\mathbf{r}_i}, \tag{2.7}$$

where $\hat{n}_i = \hat{c}_i^\dagger \hat{c}_i$ is the number operator of fermions at site-i, and the phase factor $\exp(\mathbf{Q} \cdot \mathbf{r}_i) = \pm 1$ for the two sublattices. Within the TDHF framework, the time-dependent many-fermion state $|\Psi(t)\rangle$ is to be approximated by the Slater determinant state in Eq. (2.3). Assuming that the post-quench system remains in a homogeneous CDW state, which means the $\mathbf{Q} = (\pi, \pi)$ checkerboard pattern is the only Fourier

mode of the particle fluctuations, there are only two different values of the on-site particle number depending on the sublattices:

$$n_{A/B}(t) = \overline{n} \pm \Delta(t). \tag{2.8}$$

Here $\overline{n} = 1/2$ is the average number of particles per site. Importantly, the assumption that the time-evolving post-quench system preserves a homogeneous CDW order indicates an emergent translation symmetry associated with the checkerboard pattern, which is a 45°-rotated square lattice with a doubled unit cell. This in turn implies that wave vectors $\mathbf{k}$, restricted to the reduced Brillouin zone, are good quantum numbers of the time-dependent CDW states. We thus introduce the following ansatz for the wave functions of quasiparticles

$$\phi_i^{\mathbf{k}}(t) = \frac{e^{i\mathbf{k}\cdot\mathbf{r}_i}}{\sqrt{N}} \eta_{\mathbf{k}}^{s_i}(t), \tag{2.9}$$

where $s_i = A, B$ denotes the sublattice of site-i. The time evolution of $\eta_{\mathbf{k}}^{s}(t)$ is governed by the Fourier transform of the time-dependent Schrödinger equation (2.6):

$$i\hbar \frac{d}{dt} \begin{pmatrix} \eta_{\mathbf{k}}^{A} \\ \\ \eta_{\mathbf{k}}^{B} \end{pmatrix} = \begin{pmatrix} -V\Delta(t) & \epsilon_{\mathbf{k}} \\ \\ \epsilon_{\mathbf{k}} & +V\Delta(t) \end{pmatrix} \begin{pmatrix} \eta_{\mathbf{k}}^{A} \\ \\ \eta_{\mathbf{k}}^{B} \end{pmatrix}, \tag{2.10}$$

where $\epsilon_{\mathbf{k}} = -2t_{\mathrm{nn}}(\cos k_x + \cos k_y)$ is the dispersion relation of square-lattice tight-binding model. Since the CDW order is driven by the Hartree term, we have neglected the Fock exchange term for simplicity. We have also dropped the constant diagonal term $V\overline{n}$ which contributes only to an overall phase of the wave functions. Using the

ansatz (2.9) for the Slater determinant in Eq. (6.3), the time-dependent CDW order parameter is given by

$$\Delta(t) = \sum_{\mathbf{k}} \left(\left| \eta_{\mathbf{k}}^{A}(t) \right|^2 - \left| \eta_{\mathbf{k}}^{B}(t) \right|^2 \right) \tag{2.11}$$

The dynamical equation of the CDW state is then reduced to that of a collection of two-level systems, each associated with a wave vector $\mathbf{k}$. An intuitive description of a dynamical two-level system is given by the Anderson pseudospin approach [81]. To this end, we introduce an effective spin $\mathbf{S}_{\mathbf{k}}$ for each wave vector $\mathbf{k}$, with the following definition:

$$\begin{aligned} S_{\mathbf{k}}^{x} &= \eta_{\mathbf{k}}^{A*}\eta_{\mathbf{k}}^{B} + \eta_{\mathbf{k}}^{B*}\eta_{\mathbf{k}}^{A}, \\ S_{\mathbf{k}}^{y} &= -i\left(\eta_{\mathbf{k}}^{A*}\eta_{\mathbf{k}}^{B} - \eta_{\mathbf{k}}^{B*}\eta_{\mathbf{k}}^{A}\right), \\ S_{\mathbf{k}}^{z} &= \left|\eta_{\mathbf{k}}^{A}(t)\right|^2 - \left|\eta_{\mathbf{k}}^{B}(t)\right|^2. \end{aligned} \tag{2.12}$$

Since the A and B sublattices are related by the wave vector $\mathbf{Q} = (\pi, \pi)$, as will be shown in the next section, each pseudospin $\mathbf{S}_{\mathbf{k}}$ thus represents the dynamical degree of freedom for a fundamental particle-hole pair with momenta $\mathbf{k}$ and $\mathbf{k} + \mathbf{Q}$. The dynamics of these effective spins is governed by the Bloch equation [144],

$$\frac{d\mathbf{S}_{\mathbf{k}}}{dt} = \mathbf{B}_{\mathbf{k}}(t) \times \mathbf{S}_{\mathbf{k}}, \tag{2.13}$$

which essentially describes the Landau-Lifshitz precession dynamics with a time-dependent magnetic field

$$\mathbf{B}_{\mathbf{k}}(t) = \frac{2}{\hbar}\left(\epsilon_{\mathbf{k}},\, 0,\, -V\Delta(t)\right). \tag{2.14}$$

Note that the Bloch equations for different spins are coupled to each other through the z-component of the magnetic field. From the definition Eq. (2.11), we have $B^z(t) = -V\sum_{\mathbf{k}} S^z_{\mathbf{k}}(t)$, which shows that the magnetic field that drives the spin dynamics originates from individual pseudospins.

In the following, we apply the above coupled Bloch equations to simulate the interaction quench of the CDW order of the t-V model at half-filling. As discussed in Sec. 2.1, due to a perfect nesting of the Fermi surface at half-filling, the system is unstable against the formation of checkerboard CDW order for an arbitrarily small V. In our interaction quench simulations, the system is initially prepared in the mean-field ground state of the t-V model with the interaction fixed at an initial value V_i. At time $t = 0$, the interaction is suddenly changed to V_f. The quantum quench simulation can also be viewed as the time evolution of a system which is initialized in a CDW state stabilized by V_i at $t = 0$ and is subject to an time-independent Hamiltonian with V_f for $t > 0$.

Our simulations summarized in Fig. 2.1 show that the post-quench CDW order exhibits the three major dynamical behaviors common to order parameters of other symmetry-breaking phases discussed in Sec. 1.2. First, in the phase-locked regime

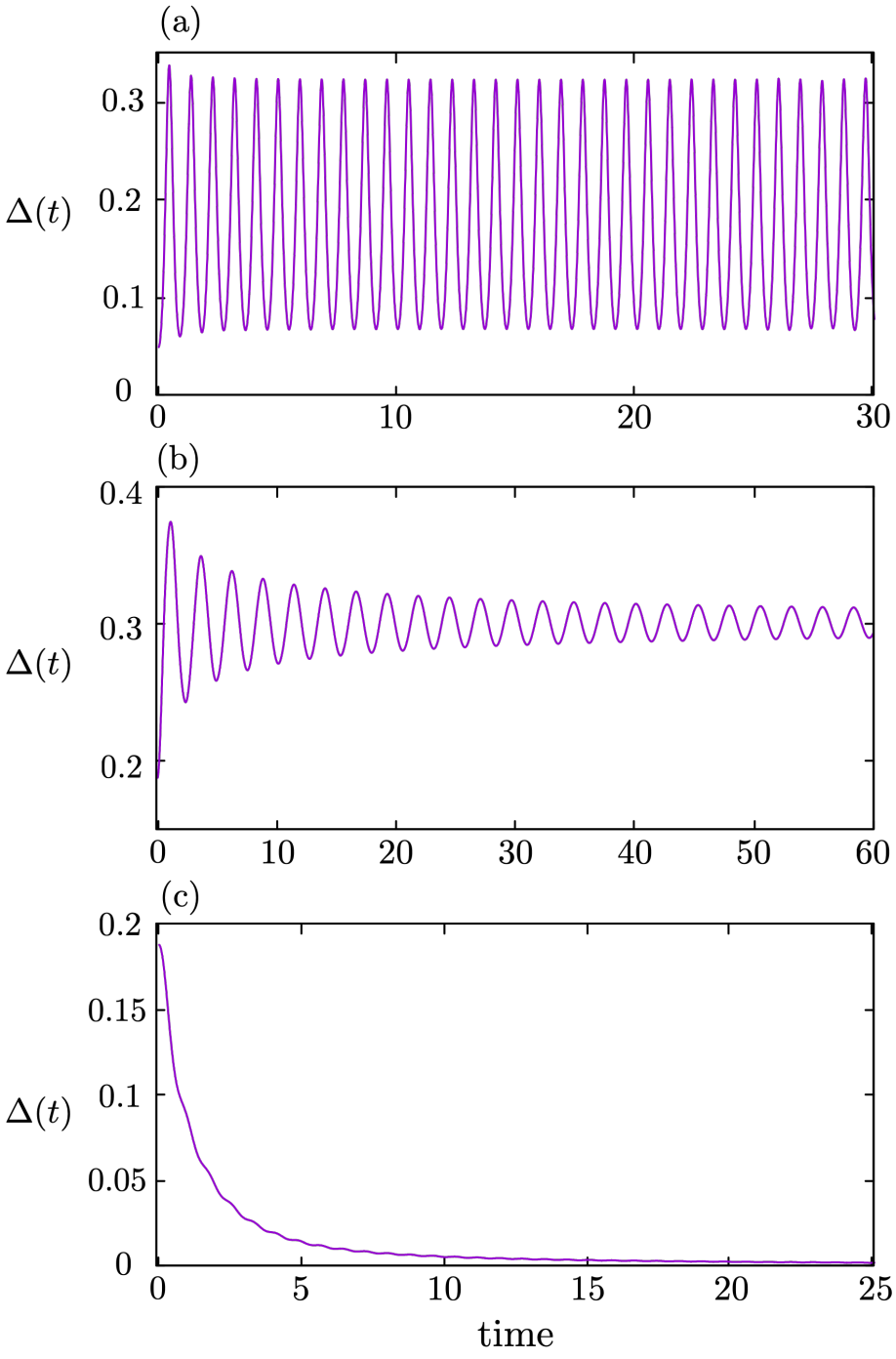

Figure 2.1: The time dependence of the CDW order parameter $\Delta(t)$ shows three main dynamical regimes of a quantum quench: (a) phase-locked regime with persistent oscillation ($V_i = 0.2$, $V_f = 5.0$), (b) Landau-damping regime ($V_i = 0.5$, $V_f = 1.0$), and (c) over-damped regime with a dynamical vanishing of the order parameter ($V_i = 0.5$, $V_f = 0.1$), obtained from pseudospin simulations similar to [1].

corresponding to a strong quench with $V_f/V_i \gg 1$, the CDW order parameter exhibits a persistent oscillation after a short transient period, as shown in Fig. 2.1(a). In this regime, the precessional dynamics of individual pseudospins synchronizes with one another to produce an oscillating B-field that drives their own oscillatory dynamics self-consistently. Physically, this describes a synchronized oscillation of the collective CDW order parameter and individual particle-hole pairs.

For intermediate quenches such that the static CDW order parameters before and after the quench are similar $\Delta_f \sim \Delta_i$, the sudden change of interaction again results in an oscillation of the CDW order parameter. Yet, the amplitude of the oscillation decreases with time and the CDW order gradually settles to a different value at large time; see Fig. 2.1(b). More specifically, the decay of the oscillation amplitude follows a $1/\sqrt{t}$ power law, as in the interaction quench of BCS superconductor and SDW. This dynamical behavior is similar to the Landau-damping phenomena in plasma physics and numerous other physical systems. The decaying oscillation of the order parameter results from a dissipationless energy transfer from the collective modes to quasiparticle excitations [1, 145]. This damping can also be understood as a result of the increasingly incoherent precessional motions of pseudospins which fail to produce a self-sustaining driving force.

Finally, for quenches toward to a much smaller interaction, $V_f \ll V_i$, the post-quench state exhibits a dynamical vanishing of the CDW order as shown in Fig. 2.1(c). In this regime, the magnetic field in Eq. (2.14) is dominated by the kinetic energy

term. As the precession dynamics of individual particle-hole pairs resorts to their respective natural frequencies, the resultant dephasing leads to an overdamping of the CDW order. It is worth noting that here the quenched system relaxes to a state with a vanishing CDW, despite the fact that a finite CDW order is expected to exist for a nonzero $V_f > 0$ due to the Fermi-surface nesting instability discussed above. Although the system cannot really thermalize under the TDHF evolution, the vanishing CDW order can be intuitively understood as a result of the system being in a quasi-equilibrium state of a temperature that is higher than the critical T_c of V_f. Inclusion of dissipative mechanisms in the post-quench evolution is thus expected to bring the CDW order back to the static Δ_f.

We also note that, instead of an exponential decay as in the case of quench dynamics of BCS pairing, the decline of the CDW order, which sometimes is accompanied by a small oscillation, follows a $1/t$ power-law, similar to the case of SDW order in the quantum quench of square lattice Hubbard model [73]. This algebraic decay could be attributed to the non-analyticity of the density of states of the square-lattice tight-binding model at half-filling [73].

Chapter 3

Quench-induced pattern formation in CDW states in t-V model

In this chapter, we demonstrate quench-induced pattern formations in a system with a broken Z_2 symmetry, which is perhaps one of the simplest symmetry-breaking phases, of a fermionic system. Specifically, we present extensive simulations on the interaction quench of the square lattice t-V model, which exhibits a checkerboard CDW order at half-filling. As the checkerboard charge modulation breaks the sublattice symmetry of the square lattice, the resultant CDW order is characterized by a Z_2 Ising order parameter. A time-dependent mean-field approach is employed to describe the coherent dynamics of the perturbed t-V model. Assuming homogeneous CDW order throughout the quench process, the coherent dynamics of the post-quench CDW states can be modeled by an Anderson pseudospin theory as discussed in Chapter 2, similar to the ones used for quench dynamics of BCS superconductors [1, 63, 81]. To incorporate dynamical inhomogeneities into the quench simulations, we further develop a real-space nonlinear von Neumann equation formulation that allows for efficient

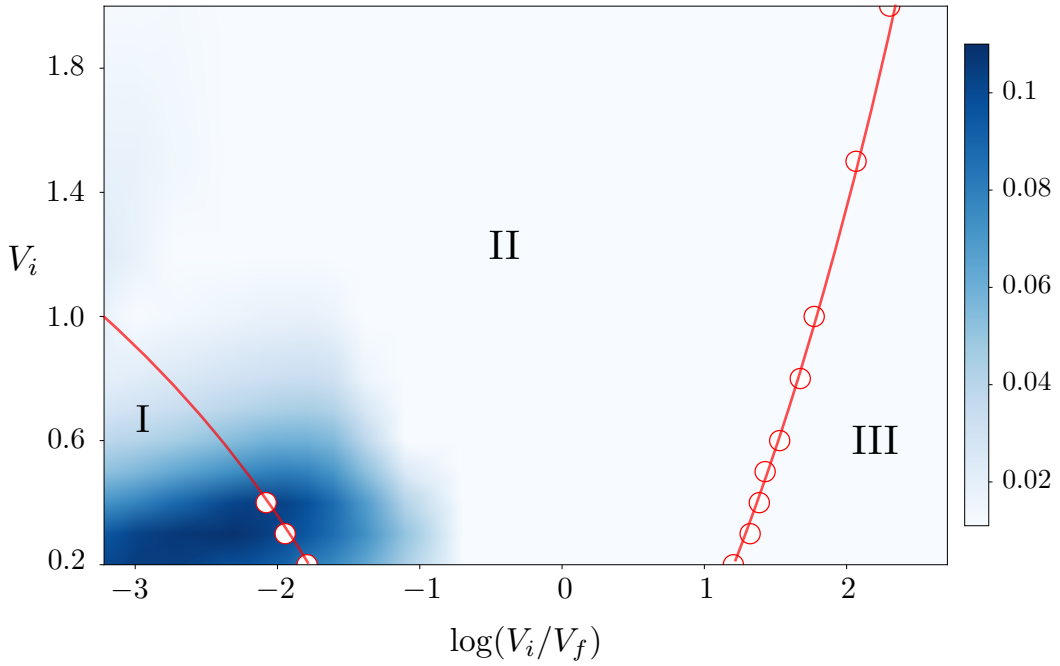

Figure 3.1: Phase diagram of post-quench CDW states of the square-lattice t-V model. V_i and V_f denote the density-density repulsion before and after the sudden quench. The three dynamical phases are: (I) phase-locked persistent oscillation, (II) Landau-damped oscillation, (III) over-damped oscillation with a vanishing CDW order. The data points are obtained from the Anderson pseudospin method based on the assumption that a homogeneous CDW order persists in the post-quench states. Large-scale quench simulations based on the real-space von Neumann equation are used to study quench-induced dynamical inhomogeneity. The color intensity indicates the spatial inhomogeneity of density-modulation in the post-quench states.

large-scale simulations.

3.1 Real-space von Neumann equation

The Anderson pseudospin approaches discussed in the previous section are widely used in the study of quantum quenches of various symmetry-breaking phases including superconductivity and spin-density waves. As the pseudospin methods assume the persistence of a perfect long-range order after the quench, these previous works thus

preclude any spatial inhomogeneity in the post-quench states. To go beyond the pseudospin methods and allow for spatial fluctuations after a quantum quench, here we discuss an efficient real-space formulation of TDHF in terms of correlation function $\rho_{ij} = \langle \hat{c}_j^\dagger \hat{c}_i \rangle$, also known as the single-particle density matrix. From the definition of the Slater determinant in Eqs. (2.3) and (2.4), the density matrix is related to the time-dependent single-particle wave functions as

$$\rho_{ij}(t) = \langle \Psi(t) | c_j^\dagger c_i | \Psi(t) \rangle = \sum_\mu \phi_i^\mu(t) \phi_j^{\mu *}(t), \tag{3.1}$$

Compared with time-dependent Schrödinger equation (2.6) for the effective wave functions, the density matrix approach has the advantage that ρ_{ij} is directly related to observables and the corresponding equation of motion is amenable to efficient numerical simulations.

The pseudospins $\mathbf{S_k}$ in Sec. 2.3 actually correspond to the Fourier transform of the density matrix elements, which are given by

$$\rho_{\mathbf{q}',\mathbf{q}} = \left\langle \hat{c}_{\mathbf{q}'}^\dagger \hat{c}_{\mathbf{q}} \right\rangle, \tag{3.2}$$

where $\hat{c}_{\mathbf{q}} = (1/\sqrt{N}) \sum_i \hat{c}_i e^{-i\mathbf{q}\cdot\mathbf{r}_i}$ denotes the fermion operator in momentum space. In the presence of a perfect CDW order, the only nonzero matrix elements are $\rho_{\mathbf{k},\mathbf{k}}$ and $\rho_{\mathbf{k},\mathbf{k}\pm\mathbf{Q}}$, where wave vectors $\mathbf{k}$ are now restricted to the reduced Brillouin zone. The effective spins are then given by

$$S_{\mathbf{k}}^x = \frac{1}{2} \left(\rho_{\mathbf{k},\mathbf{k}} - \rho_{\mathbf{k}+\mathbf{Q},\mathbf{k}+\mathbf{Q}} \right), \tag{3.3}$$

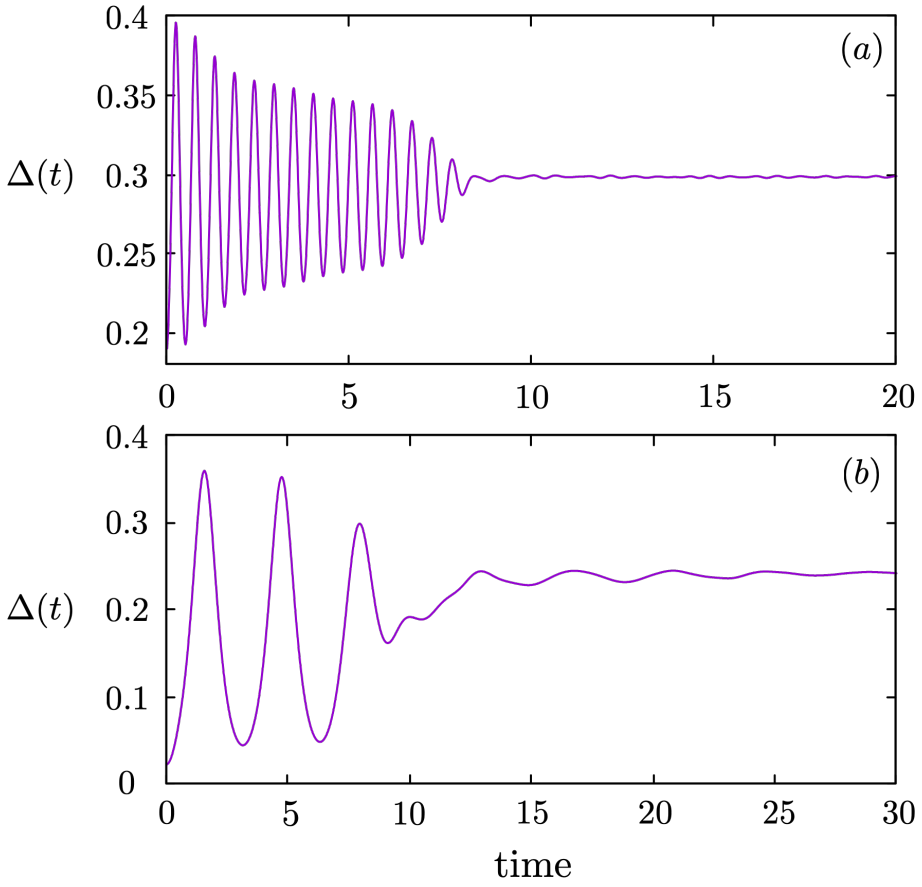

Figure 3.2: The overall CDW order parameter $\Delta(t)$ as a function of time in the regime of spatially inhomogeneous post-quench states. The quench parameters are: (a) $V_i = 0.5$ to $V_f = 5.0$, and (b) $V_i = 0.1$ to $V_f = 1.5$. Snapshots of the emergent patterns are shown in Fig. 3.3 and 3.4.

$$S^y_{\mathbf{k}} = -\mathrm{Im}\,\rho_{\mathbf{k},\mathbf{k}+\mathbf{Q}}, \qquad S^z_{\mathbf{k}} = \mathrm{Re}\,\rho_{\mathbf{k},\mathbf{k}+\mathbf{Q}}.$$

This simple analysis further highlights the fact that the pseudospin approach precludes inhomogeneous post-quench states. The onset of spatial fluctuations thus corresponds to the emergence of nonzero matrix elements $\rho_{\mathbf{k},\mathbf{k}+\mathbf{q}}$ with incommensurate wave vectors $\mathbf{q} \neq \mathbf{Q}$.

The dynamical equation that governs the time dependence of ρ_{ij} can be directly obtained from the time-dependent Schrödinger equation (2.6). An alternative, which

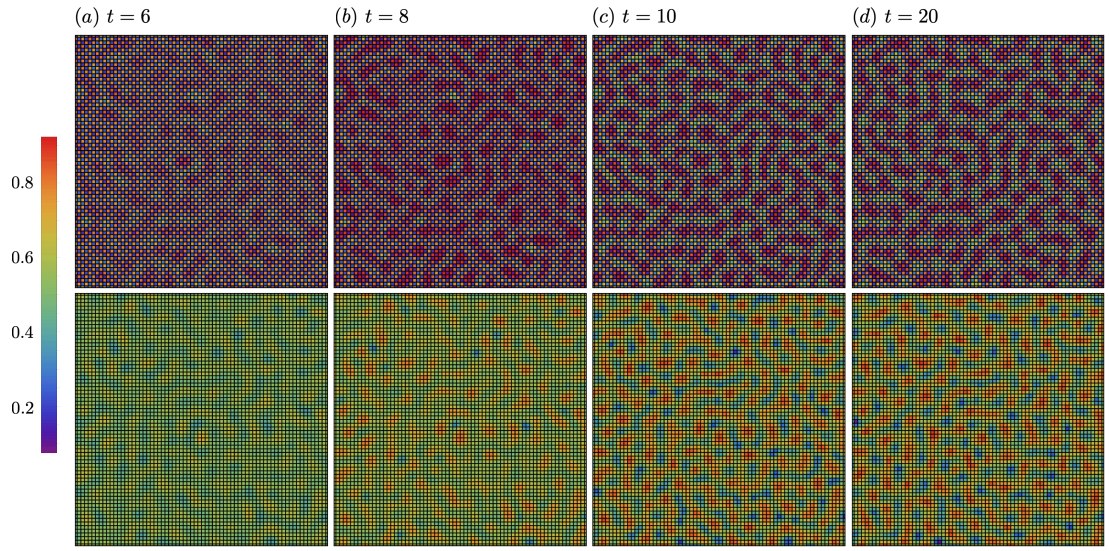

Figure 3.3: Snapshots of particle density $n_i = \rho_{ii}$ distributions (top) and local CDW order parameter ϕ_i (bottom) at different time steps after a quantum quench from $V_i = 0.5$ to $V_f = 5.0$. The corresponding checkerboard CDW order as a function of time is shown in Fig. 3.2(a). Note that the Ising order parameter field, while exhibiting complex patterns, remains positive throughout the relaxation process.

is physically more intuitive, is to use the "first-quantized" formulation of the mean-field Hamiltonian. To this end, we note that from the standard mean-field decoupling for the interaction term: $\hat{n}_i\hat{n}_j \to \langle\hat{n}_i\rangle\hat{n}_j + \hat{n}_i\langle\hat{n}_j\rangle = \rho_{ii}\hat{n}_j + \rho_{jj}\hat{n}_i$, one can define a time-depndent mean-field Hamiltonian

$$\hat{\mathcal{H}}_{\rm MF}(t) = \sum_{ij} \hat{c}_i^\dagger \, H_{ij}[\rho(t)] \, \hat{c}_j, \tag{3.4}$$

where the first-quantized Hamiltonian has a simple form

$$H_{ij} = -t_{ij} + \delta_{ij} \, v_i(t). \tag{3.5}$$

The first term represents the kinetic energy, and the second term denotes an effective

on-site potential

$$v_i(t) = V \sum_j{}' \rho_{jj}(t) \tag{3.6}$$

where $\sum_j{}'$ indicates summation over sites j that are nearest neighbors to i. This Hamiltonian can also be read directly from the form of the time-dependent Schrödinger equation in Eq. (2.6). The single-particle density matrix then satisfies a self-consistent nonlinear von Neumann equation,

$$-i\hbar \frac{d\rho}{dt} = [\rho, H(\rho)], \tag{3.7}$$

where ρ and H denote the $N \times N$ matrix of the density matrix and the first-quantized Hamiltonian, respectively. Using Eq. (3.5), the explicit von Neumann equation for the density matrix is

$$-i\hbar \frac{d\rho_{ij}}{dt} = (v_j - v_i)\rho_{ij} + \sum_k \left(t_{ik}\rho_{kj} - \rho_{ik}t_{kj}\right). \tag{3.8}$$

The CDW order parameter in Eq. (2.7) can be straightforwardly computed from the diagonal matrix elements

$$\Delta(t) = \frac{1}{N} \sum_i \rho_{ii}(t) e^{i\mathbf{Q}\cdot\mathbf{r}_i}. \tag{3.9}$$

It is worth noting that for a system of N sites, there are $N/2$ pseudospins, each indexed by a wave vector $\mathbf{k}$ in the reduced Brillouin zone. The computational complexity of solving the coupled Bloch equations is thus of order $O(N)$. On the other hand, the number of independent matrix elements of ρ scales as N^2 for general Slater determi-

nant states with potential spatial inhomogeneity. Integration of the von Neumann equation using a naive matrix-matrix multiplication method would lead to a $O(N^3)$ complexity. The von Neumann equation formulation allows one to take advantage of efficient sparse matrix multiplication algorithms, thus improving the computational efficiency. It is worth noting that even though the TDHF approach essentially reduces the many-body problem to an effective single-particle one, additional complexity is required for evolving a density matrix or equivalently a Slater determinant in order to account for the quantum statistics of identical fermions.

Applying the von Neumann equation method to simulate quantum quenches of the t-V model up to $N = 70 \times 70$ systems, we first confirm that, for the same system sizes, the real-space approach exactly reproduces the Landau-damped and over-damped oscillations when the V_i, V_f parameters are set to those used in Fig. 2.1. Yet, for most of the strong quench regime where phase-locked oscillation is expected, our large-scale simulations observe a CDW dynamics that is distinctly different from the three dynamical regimes discussed above; two such examples are shown in Fig. 3.2. In both cases, the interaction is quenched from a small V_i to a much larger V_f. As discussed in Sec. 2.2, the pseudospin simulations for such strong quench regime predicts a persistent oscillation of the CDW order parameter in the post-quench states. Instead, the CDW time traces shown in Fig. 3.2 exhibit damped oscillations and a finite asymptotic value, similar to the Landau-damping behavior.

However, contrary to the algebraic $1/\sqrt{t}$ decay characteristic of the Landau-

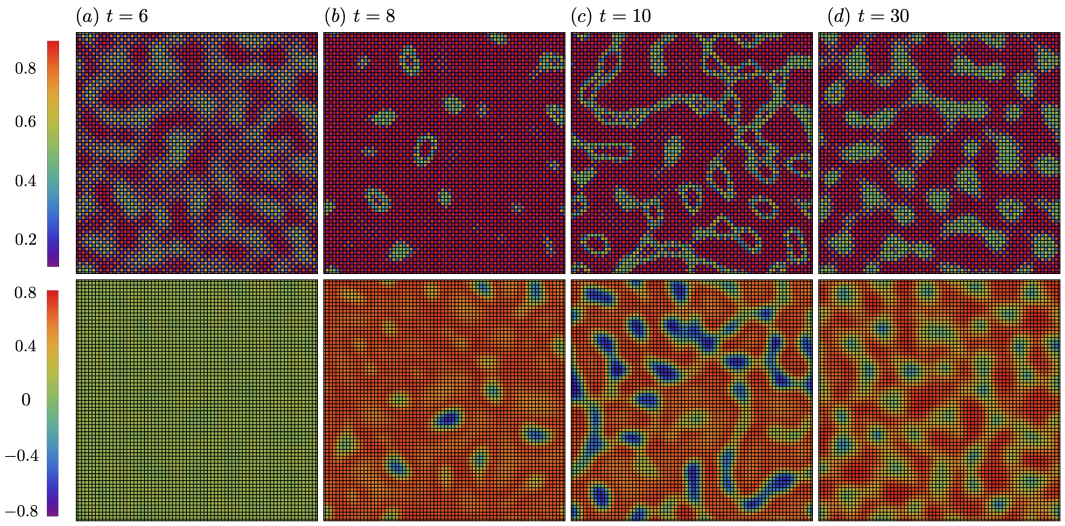

Figure 3.4: Snapshots of particle density $n_i = \rho_{ii}$ distributions (top) and local CDW order parameter ϕ_i (bottom) at different time steps after a quantum quench from $V_i = 0.1$ to $V_f = 1.5$. The corresponding checkerboard CDW order as a function of time is shown in Fig. 3.2(b). The interfaces that separate CDW domains of opposite signs correspond to the finite green lines with a nearly constant fermion density of $\rho_{ii} \sim 0.5$ in the top panels.

damping regime, here we observe a much faster decay of the oscillation amplitudes. In fact, the decline of the oscillation is even accelerated before the CDW order eventually collapses to a nearly constant value. This seemingly complex dynamical behaviors in time domain are not caused by a complex order parameter as in some previous studies. Instead, as we show in the next section, the collapsed oscillation of the CDW order is due to the emergence of inhomogeneous post-quench states.

3.2 Dynamical inhomogeneity and pattern formation

The CDW order parameter $\Delta(t)$ computed in Eq. (3.9) only represents the overall difference of particles in the two sublattices, $\Delta(t) = \big(N_A^e(t) - N_B^e(t)\big)/N$, yet gives no information about the spatial distribution of particles within the sublattices. The

unusual damped oscillations in the strong quench regime, as shown in Fig. 3.2, thus could be caused by the onset of spatial inhomogeneity. To examine this scenario, the top panels in Fig. 3.3 and 3.4 show the snapshots of on-site particle number $n_i(t) = \rho_{ii}(t)$ at different times after the quench for the two settings in Fig. 3.2(a) and (b), respectively. As clearly shown in these snapshots, highly complex patterns develop in the post-quench states.

Careful examinations show that the quench-induced inhomogeneity mostly is in the form of longer wavelength density modulations on top of the checkerboard CDW order. To better characterize such super modulations of particle density, it is convenient to introduce a scalar order parameter field for the local CDW order

$$\phi(\mathbf{r}_i) = \left(n_i - \frac{1}{4}\sum_j{}' n_j\right) \exp\left(i\mathbf{Q}\cdot\mathbf{r}_i\right), \tag{3.10}$$

where the prime in the second term again indicates that the summation is restricted to the nearest neighbors of site-i. This local parameter essentially measures the difference of the particle number at a given site and that of its nearest neighbors. A nonzero ϕ_i thus indicates the presence of local particle modulation around site-i. The phase factor $\exp(i\mathbf{Q}_i\cdot\mathbf{r}_i) = \pm 1$ is introduced to account for the short-distance checkerboard modulation within a CDW domain. In a perfect checkerboard CDW state, this local order parameter becomes site-independent and is given by the overall CDW order parameter $\Delta(t)$ defined in Eq. (3.9).

Snapshots of this scalar order parameter ϕ_i corresponding to the particle density

profiles at the top row of Fig. 3.3 and 3.4 are shown in the respective bottom panels. These results highlight a super-modulation of particle density, as demonstrated by the quasi-periodic square-like patterns in the ϕ_i field, which itself represents a ultrashort-period checkerboard density modulation.

In the first case where the interaction is quenched from $V_i = 0.5$ to $V_f = 5.0$, the local CDW order parameter ϕ_i remains positive throughout the whole system as shown in Fig. 3.3. This overall positive ϕ-field indicates that a long-range coherence of the initial checkerboard CDW is preserved in the strong quench process. The complex patterns observed in our real-space simulations thus correspond to additional long-wavelength density modulations within a coherent checkerboard domain inherent from the initial CDW state before the quench. This underlying coherent checkerboard order is also consistent with the nearly constant CDW order parameter after the collapse of the oscillations shown in Fig. 3.2. If we use the discrete Ising variable $\sigma_i = \operatorname{sign} \phi_i$ to characterize such post-quench states, they would be very different from configurations observed in thermal quenches from a random state to the low-temperature phase of a broken Z_2 symmetry [146, 147]. Due to the locality of thermal relaxations, a temperature quenches typically results in multiple Ising domains of *both* signs $\sigma = \pm 1$ that coexist in a heterogeneous state.

On the other hand, for quenches starting from a much smaller V_i as demonstrated in the bottom panels of Fig. 3.4, Ising domains of opposite signs indeed emerge in the post-quench states. In this case, the initial state before the quench exhibits a

homogeneous CDW order with a small positive value $\phi \sim 10^{-2}$. Immediately after the quench, the collapse of the coherent oscillation gives rise to a heterogeneous state where multiple CDW domains with $\sigma_i = \text{sign}\,\phi_i = -1$ are embedded in a background of positive CDW order parameter ϕ; see Fig. 3.4(b) and (c). The interfaces that separate Ising domains of opposite signs are of a finite width with a nearly constant particle density of $\rho_{ii} \sim 0.5$. As the system further relaxes, those Ising domains with a negative ϕ gradually revert back to the positive sign, yet with a rather small particle modulation as shown in Fig. 3.4(d).

To further characterize the emergent density patterns, we compute the corresponding structure factor

$$S(\mathbf{q}, t) = |\tilde{n}(\mathbf{q}, t)|^2, \tag{3.11}$$

where $\tilde{n}(\mathbf{q}, t)$ is the Fourier transform of the time-dependent particle density $n_i(t) = \rho_{ii}(t)$. In terms of the momentum-space density matrix introduced in Eq. (3.2), the amplitude of density modulation at wave vector $\mathbf{q}$ is

$$\tilde{n}(\mathbf{q}, t) = \frac{1}{\sqrt{N}} \sum_{\mathbf{k}} \rho_{\mathbf{k},\mathbf{k}+\mathbf{q}}(t). \tag{3.12}$$

Fig. 3.5 shows the structure factors of the post-quench states at a few selected times after a quench from $V_i = 0.5$ to $V_f = 5$. These figures are obtained by averaging over 90 independent von Neumann dynamics simulations on a $N = 70 \times 70$ system. In the early stage of the post-quench relaxation, the coherent oscillation of a spatially homogeneous CDW order gives rise to a delta-function peak in the structure factor shown

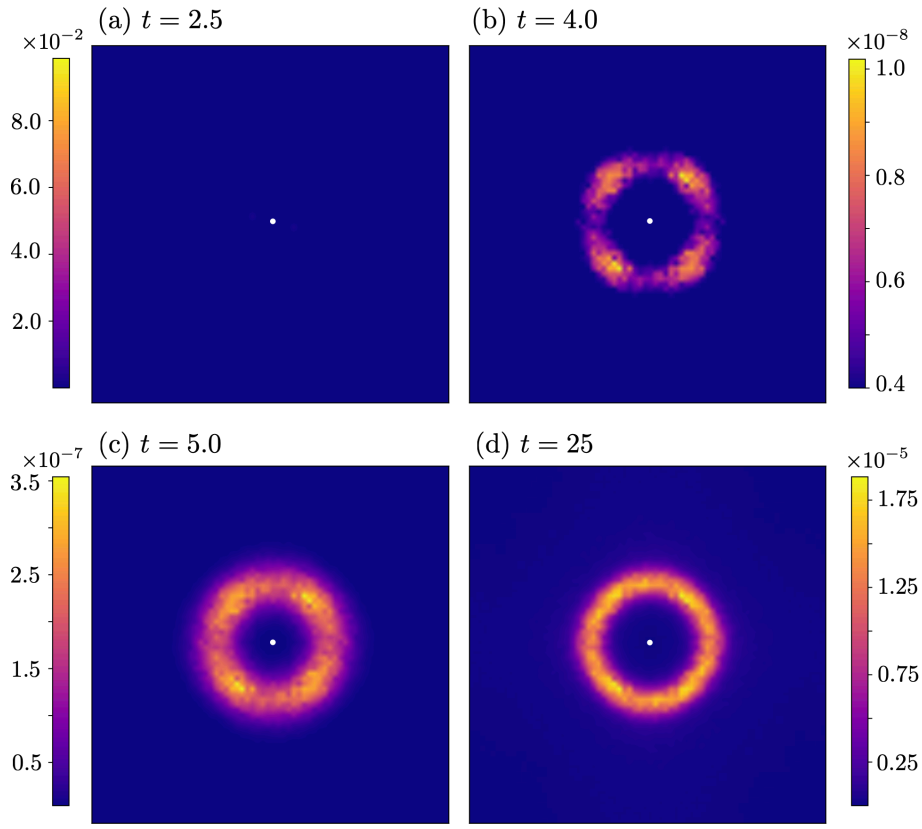

Figure 3.5: Structure factors $S(\mathbf{k}, t)$ at various time steps after a quantum quench from $V_i = 0.5$ to $V_f = 5.0$ at time $t = 0$. The simulated system size is $N = 70 \times 70$. The results are obtained by averaging over 90 independent von Neumann dynamics simulations. The white dot at $\mathbf{Q} = (\pi, \pi)$ corresponds to a dominant checkerboard CDW order. The scale of the color bars in panels (b)–(d) is chosen to highlight the emergent unstable modes.

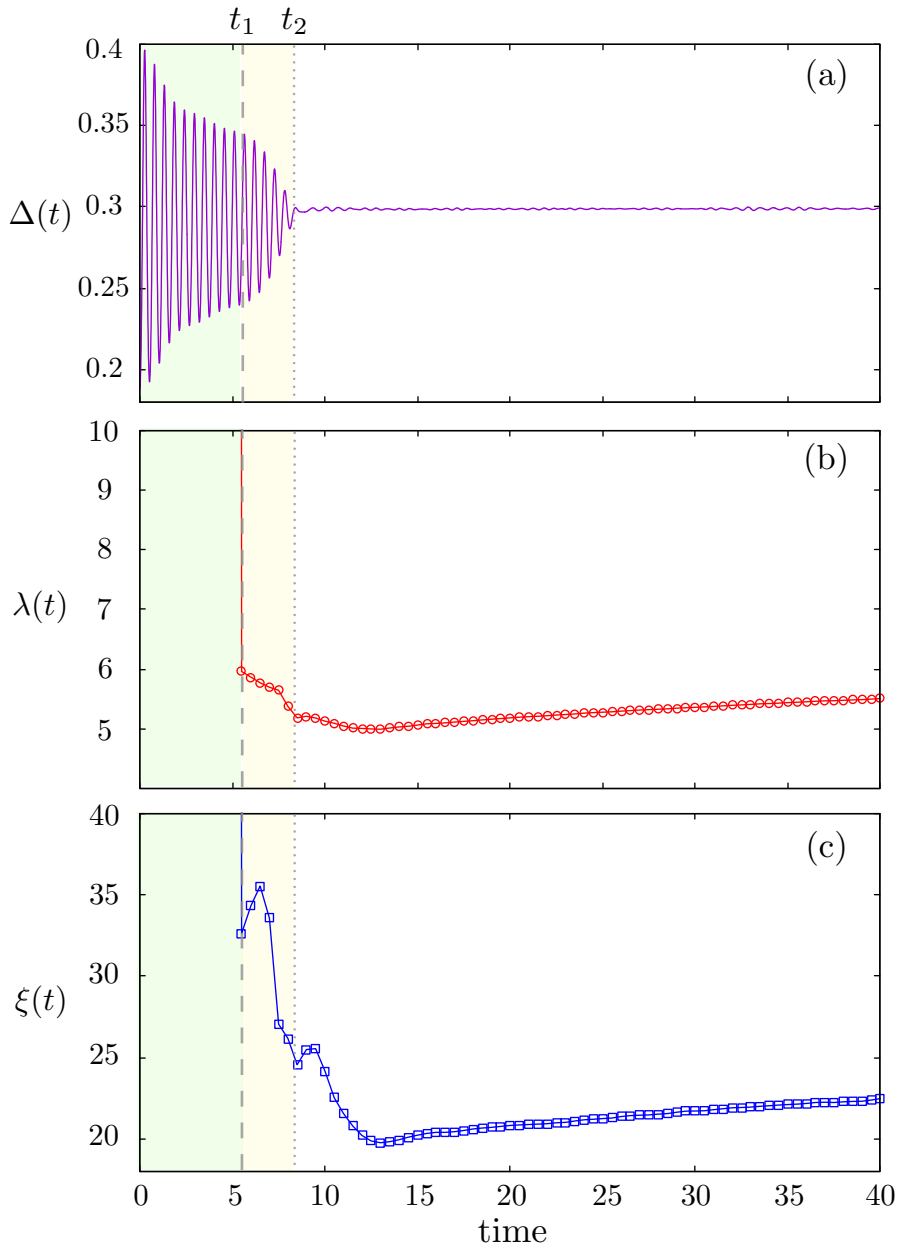

Figure 3.6: Post-quench dynamics in the regime with emergent pattern formation for a quench from $V_i = 0.5$ to $V_f = 5.0$: (a) time dependence of the CDW order parameter $\Delta(t)$, (b) Modulation length $\lambda(t)$, and (c) correlation length versus time. The two characteristic times t_1 and t_2 mark the onset of spatial inhomogeneity and the collapse of coherent oscillations, respectively.

in Fig. 3.5(a). As the system further relaxes, the emergence of spatial inhomogeneity corresponds to the gradual growth of a ring-like feature around the delta-peak, as shown in Figs. 3.5(b)–(d). The higher intensity points on the ring correspond to the unstable modes that lead to the pattern formation. The ring-like feature is also characteristic of the labyrinthine structures observed in many pattern-forming systems. Labyrinths are spatial structures where local stripe orders with random orientations fail to develop into a long-range order [148, 149].

In our case, the super modulations of particle densities shown in Fig. 3.3 seem to be a combination of local stripe and local checkerboard patterns. A domain of local stripe modulation on top of the ultrashort period checkerboard CDW is represented by a pair of wave vectors $\mathbf{Q} \pm \eta\hat{\mathbf{n}}$, where η denotes the modulation wave number and $\hat{\mathbf{n}}$ is a unit vector indicating the orientation of the stripe. Similarly a domain of checkerboard super-modulation on top of the (π, π) CDW order is characterized by a quadrupole of wave vectors $\mathbf{Q} \pm \eta\hat{\mathbf{n}}_1$ and $\mathbf{Q} \pm \eta\hat{\mathbf{n}}_2$, where $\hat{\mathbf{n}}_1$ and $\hat{\mathbf{n}}_2$ are a pair of orthogonal unit vectors. The inhomogeneous CDW states obtained in our real-space simulations can be viewed as consisting of multiple domains with random unit vectors $\hat{\mathbf{n}}$. The lack of long-range orientational order thus leads to the formation of a ring centered at $\mathbf{Q}$ as shown in Fig. 3.5(d).

The modulations of the local CDW order parameter can be characterized by two length scales: the modulation period λ of the superstructure (stripes or checkerboard) and the correlation length ξ, or characteristic size of superstructure domains. These

two length scales are related to the ring feature in the structure factor $S(\mathbf{q})$ discussed above. The modulation length is given by the inverse of the radius η, while the correlation length is proportional to the inverse of the width of the ring. Specifically, the modulation period can be computed as $\lambda = 2\pi/\langle|\mathbf{q}-\mathbf{Q}|\rangle$, where the angle bracket indicates average using the structure factor $S(\mathbf{q})$ as the weighting factor. A similar formula for the averaged width of the ring can be used to compute the correlation length.

The evolution of these two length scales after a quench from $V_i = 0.5$ to $V_f = 5.0$ is shown in Fig. 3.6. Two characteristic times t_1 and t_2 are introduced to characterize the initial relaxation of the post-quench states. As a homogeneous CDW order is preserved in the initial oscillation period, the correlation length is of the order of the system size and the modulation period is ill-defined. The onset of inhomogeneity is signaled by a sudden drop of the correlation length at time t_1. We also note that the super-modulation patterns corresponding to a finite λ emerges immediately at the onset of inhomogeneity at t_1. This indicates that the pattern formation here is generated by a quick growth of the unstable modes that becomes significant at t_1. The emergence of spatial inhomogeneity also accelerates the decline of the oscillation amplitude, and the CDW order Δ settles to a constant at time t_2, although small fluctuations can still be seen afterward.

We also note that both length scales λ and ξ of the quasi-steady states at late stage of the relaxation depend on the depth V_f/V_i of the interaction quench. This

is demonstrated by the snapshots, shown in Figs. 3.7(a)–(d), of the late-stage local CDW order parameter ϕ_i for four different final V_f with the same initial interaction $V_i = 0.5$. Long-wavelength super modulations can be clearly seen in an otherwise overall positive ϕ_i field. As discussed above, this overall positive CDW order indicates that a coherent (π, π) checkerboard density modulation persists in the background for these quench parameters. The modulation period and coherent length of these superstructures versus the final V_f are shown in Fig. 3.7(e) at time $t \sim 200$ after the quench. Both length scales decrease with an increasing V_f. Overall, the post-quench system exhibits a higher level of inhomogeneity with a stronger quench. The dependence of the modulation period on V_f is related to the instability mechanism for the pattern formation, which will be left in future work. On the other hand, the reduced correlation length ξ in the presence of a stronger quench is likely due to the locality of the pattern formation process in a scenario similar to the Kibble-Zurek mechanism.

3.3 Conclusion

To summarize, we have presented a comprehensive study of quantum quench dynamics of CDW states in the t-V model. For the square-lattice model at half-filling, the checkerboard CDW order can be well described by a self-consistent mean-field theory, which can be generalized to include dynamics via the time-dependent variational principle. This approach essentially describes the evolution of a Slater determinant CDW state and is equivalent to the well-known time-dependent Hartree-Fock (TDHF)

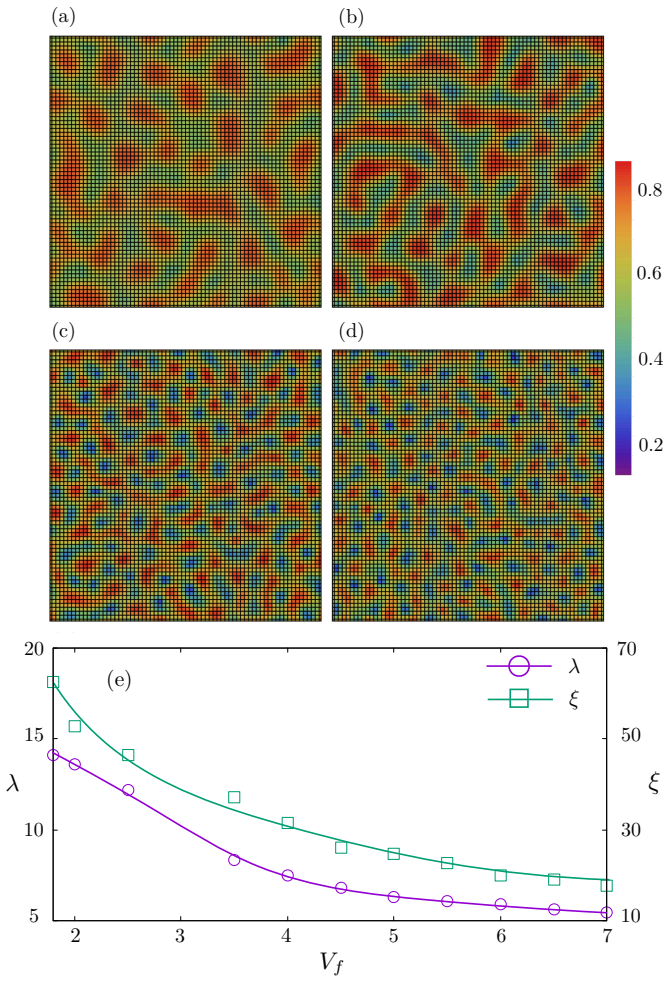

Figure 3.7: Local CDW order parameter field at late stage of the quantum quench for (a) $V_f = 2.0$, (b) $V_f = 2.5$, (c) $V_f = 4.0$, and (d) $V_f = 5.0$ with the initial interaction set at $V_i = 0.5$. (e) The modulation length λ, and the correlation length ξ versus V_f with a fixed initial $V_i = 0.5$.

theory. Assuming that a homogeneous CDW state is maintained throughout the interaction quench, we show that the TDHF is reduced to an Anderson pseudospin theory, which is widely used for the coherent dynamics of order parameter field in the collisionless limit. Our extensive quench simulations produce three dynamical behaviors of the CDW order, namely, the phase-locked persistent oscillation, Landau-damped oscillation, and dynamical vanishing of the order parameter. These are consistent with previously reported dynamical phases induced by interaction quenches of symmetry-breaking phases.

To incorporate spatial inhomogeneity into the quench dynamics, an efficient nonlinear von Neumann equation is obtained from the real-space TDHF theory to describe the evolution of the post-quench CDW state. For strong quenches starting from a relatively small initial interaction, our large-scale real-space simulations uncover complex pattern formation in the post-quench CDW states. The onset of spatial inhomogeneity effectively introduces a dephasing mechanism, leading to the collapse of the otherwise phase-locked oscillations of the CDW order parameter. The quench-induced spatial patterns are characterized by domains of super modulations of the particle density in the form of stripes or checkerboards on top of the original ultrashort-period CDW order. However, the lack of orientational coherence between different domains leads to overall disordered patterns similar to the labyrinthine structures observed in many pattern-forming systems. The resultant structure factor is characterized by a ring-like feature centered at the checkerboard wave vector $\mathbf{Q} = (\pi, \pi)$. The inverse radius and

width of the ring correspond to the super modulation period and coherent length, respectively, of the inhomogeneous CDW state.

The emergence of the super modulation patterns on top of the CDW order is caused by unstable modes with wave vectors $\mathbf{q} = \mathbf{Q} + (2\pi/\lambda)\hat{\mathbf{n}}$, where λ is the modulation period. A common mechanism for pattern formation is the parametric instability where a pair of unstable modes grow spontaneously from the decay of an initial driver mode through nonlinear interactions. Indeed, the parametric instability has been shown to result in the decay of a uniform oscillating pairing order parameter and the emergence of an inhomogeneous Cooper pair turbulence state. A possible scenario for pattern formation of the quenched t-V model is the decay of the checkerboard CDW order parameter into a pair of such unstable modes $\mathbf{q}_1$ and $\mathbf{q}_2$ through the parametric instability mechanism. However, for general modulation period λ, the momentum is not conserved in this process $\mathbf{q}_1 + \mathbf{q}_2 \neq \mathbf{Q}$. This consideration thus rules out the instability as the direct decay of the phase-locked oscillation of the CDW order. On the other hand, detailed examinations of the initial relaxation after a quench show that the unstable modes indeed appear in pairs, suggesting a modified version of the parametric instability. A detailed study of the instability mechanism will be presented elsewhere.

Our work underscores the importance of dynamical inhomogeneity in quantum quench dynamics of many-body systems. Indeed, here we demonstrate that the post-quench dynamics of a many-fermion system with a simple broken Z_2 symmetry is

susceptible to pattern-formation instability, even in the collisionless limit. The emergence of complex patterns in this limit is entirely due to the nonlinear dynamics of order parameter fields. Our results indicate that pattern formation is likely to be a generic feature of quantum quenches with more complex order parameters. It is worth noting that while pattern formation in classical physics is a well-studied subject, quench-induced spatial inhomogeneity in quantum many-body systems is a relatively unexplored area of research. In addition to the nonlinearity originating from the many-body interactions, the quantum fermionic statistics could play a crucial role in the instability mechanisms. For symmetry-breaking phases characterized by complex ordering structures, the associated pattern formation and mechanisms might be closely related to the topological defects of the corresponding order parameter fields. Finally, inclusion of incoherent processes, such as quantum fluctuations, quasiparticle scattering, and energy dissipation, are expected to produce even richer spatiotemporal dynamical behaviors of the post-quench states.

Chapter 4

Pseudospin formular for Holstein model

4.1 Introduction

To explore post-quench dynamics in the symmetry-breaking phase while avoiding the artifacts and constraints of mean-field theory, we propose to study the time evolution of the CDW state in the Holstein model following a interaction quench. The Holstein model [150, 151] describes the coupling between electronic charge and lattice vibrations, which represent local structural distortions. The vibrational degrees of freedom are akin to the dispersionless phonons in Einstein's model. In a bipartite lattice in 2D and 3D at half-filling, the system is rendered to forming a checkerboard modulation of local electron density, i.e., the CDW order, accompanied by a staggered arrangement of lattice distortions, due to Fermi surface nesting. As the checkerboard charge modulation breaks the sublattice symmetry of the square lattice, the resultant CDW order is characterized by a Z_2 Ising order parameter, which is perhaps the simplest symmetry-breaking phase in fermionic system. The Holstein model has been

extensively used to investigate phenomena related to electron-lattice coupling, such as polaron dynamics and superconductivity [152–157], making it a canonical model for studying CDW physics. Notably, the CDW state remains robust even in the classical limit of the phonons [158]. The Holstein model is numerically exactly solvable when treating the lattice degrees of freedom classically, and thus, providing a framework for studying CDW physics without the limitations of mean-field theory.

The Anderson pseudospin approach [81] has found widespread application in studying the post-quench dynamics of order parameter fields in various symmetry-breaking phases, including superconductivity and spin-density-wave states [1, 63–66]. For example, the dynamical equation of BCS pairings can be packed into the Bloch's equation in the pseudospin formulation, which effectively describes a spin precessing in a magnetic field [1, 63]. A pseudospin formalism for CDW states in the t-V model has been established in Section 2.3, suggesting the potential derivation of a similar pseudospin formalism for CDW states in the Holstein model.

Unlike superconducting pairing in the BCS model or CDW states in the t-V model, which are solely based on electronic degrees of freedom, the Holstein model incorporates electron-lattice couplings. Therefore, one anticipates reproducing dynamical regimes for CDW states analogous to the three main dynamical regimes in the t-V model, however, with additional equations accounting for lattice distortions and momenta alongside the CDW equations. Of particular interest is the evolution of CDW in the non-adiabatic limit, where lattice distortions exhibit a checkerboard

modulation following the electron modulation. In this limit, the dynamical equations governing lattice distortion and its corresponding momentum, combined with the pseudospin formalism of CDW states, constitute the dynamics of CDW states in electron-lattice coupled systems. Interestingly, in the over-damped regime of CDW dynamics, finite lattice oscillations persist even when CDW is oscillating around zero with a small amplitude, indicating the emergence of coherent phonons. Therefore, it is expected that the dynamical behaviors of the CDW order parameter and lattice distortions go beyond those in pure electronic models.

In this chapter, we demonstrate quench-induced time-evolution of CDW states in a system with a broken Z_2 symmetry of a fermionic system using Holstein model. We reproduce the three dynamical regimes, i.e., phase-locked oscillation, Landau-like damping and over-damped regimes in both electronic and lattice degrees of freedom. Specifically, we present the renormalization of the natural frequency of the lattice degrees of freedom, induced by the electron-lattice couplings, which is absent in the pure electronic system.

The rest of the chapter is organized as follows. In Section 4.2, we derive the pseudospin formalisms for the CDW states, and the dynamical equations for lattice degrees of freedom, both based on the assumption that the system is under checkerboard modulation. Due to the redundancy of the parameters in the system, we perform a dimensional analysis and transform the equations to dimensionless to facilitate parameter selection. We then discuss the dynamical behaviors in electronic and

lattice degrees of freedom in Section 4.3. More characterizations of the dynamical behaviors and physical discussions are analyzed in detail in Section 4.4.

4.2 Model and Methods

A simplified Holstein model [159] which describes half-filled spinless fermions on a square lattice interacting with lattice degrees of freedom can be written as:

$$\hat{\mathcal{H}} = \hat{\mathcal{H}}_{\mathrm{e}} + \hat{\mathcal{H}}_{\mathrm{L}} + \hat{\mathcal{H}}_{\mathrm{eL}}. \tag{4.1}$$

The Hamiltonian is devided into three parts: the electronic kinetic term, the lattice degrees of freedom, and the electron-lattice coupling term. The first term, $\hat{\mathcal{H}}_{\mathrm{e}}$, contains the hopping of electrons between nearest neiboring sites

$$\hat{\mathcal{H}}_{\mathrm{e}} = -t_{nn} \sum_{\langle ij \rangle} \left(c_i^{\dagger} c_j + c_j^{\dagger} c_i \right), \tag{4.2}$$

The second term describes the lattice vibrations,

$$\hat{\mathcal{H}}_{\mathrm{L}} = \sum_i \left(\frac{1}{2m} P_i^2 + \frac{1}{2} m \Omega^2 Q_i^2 \right) \tag{4.3}$$

where m is the mass of a phonon, and $K \equiv m\Omega^2$ is the force constant. There exists an on-site coupling between the electronic and lattice degrees of freedom

$$\hat{\mathcal{H}}_{\mathrm{eL}} = -g \sum_i \left(c_i^{\dagger} c_i - \frac{1}{2} \right) Q_i \tag{4.4}$$

Assuming that the quantum state of the Holstein model is represented as a direct product state: $|\Gamma(t)\rangle = |\Phi(t)\rangle \otimes |\Psi(t)\rangle$, where $|\Phi(t)\rangle$ and $|\Psi(t)\rangle$ denote the phonon

and electron wave-functions, respectively. The phonon wave-function can be written as a direct product of single-site phonon states, denoted as $|\Phi(t)\rangle = \prod_i |\phi_i(t)\rangle$. This assumption aligns with the mean-field approximation of the phonons. Consequently, the expectation values of position and momentum operators can be expressed as $Q_i = \langle\phi_i|\,\hat{Q}_i\,|\phi_i\rangle$ and $P_i = \langle\phi_i|\,\hat{P}_i\,|\phi_i\rangle$. To derive the dynamical equation of the phonon, we employ the Heisenberg equation of motion, $d\hat{Q}_i/dt = -i\langle[\hat{Q}_i, \hat{\mathcal{H}}]\rangle/\hbar$, where $\langle ...\rangle$ is the expectation value computed using the full wave-function $|\Gamma(t)\rangle$. The dynamical equations for Q_i and P_i can be simplified as

$$\begin{aligned} \frac{dQ_i}{dt} &= \frac{P_i}{m}, \\ \frac{dP_i}{dt} &= gn_i - m\Omega^2 Q_i, \end{aligned} \tag{4.5}$$

which are exactly the Newton's equations of motion for position and momentum.

For the electron wave-function, given that the Holstein Hamiltonian is bilinear in fermion operators, the many-body electron wave-function manifests as a time-dependent single Slater determinant state. This state persists if the system is initially prepared in such a configuration [160]. However, due to the complexity of integrating the Slater determinant wave-function, a method that has primarily been employed in small-scale systems [161, 162], we opt to define the single-particle density matrix utilizing the Slater determinant wave-function as:

$$\rho_{ij}(t) = \langle\Psi(t)|\,\hat{c}_j^\dagger \hat{c}_i\,|\Psi(t)\rangle\,. \tag{4.6}$$

Given that the dynamical equation governing the density matrix is influenced by the

segment of the Hamiltonian involving the electronic degrees of freedom, specifically $\hat{\mathcal{H}}_{\mathrm{e}}$ and $\hat{\mathcal{H}}_{\mathrm{eL}}$, their first quantized formulations can be readily expressed as:

$$\hat{\mathcal{H}}_{\mathrm{e}}(t) + \hat{\mathcal{H}}_{\mathrm{eL}}(t) = \sum_{ij} \hat{c}_i^{\dagger} \, H_{ij} \, \hat{c}_j, \tag{4.7}$$

To derive the equation of motion for the single-particle density matrix, ρ_{ij}, we commence with the Heisenberg equation of motion for the electron operator,$d\hat{c}_i/dt = -i[\hat{c}_i, \hat{\mathcal{H}}]/\hbar$. The resultant equation corresponds to the von Neumann equation, employing the first quantized Hamiltonian formulation as depicted in Eq. 4.7, and can be written as:

$$i\hbar \frac{d\rho_{ij}}{dt} = \sum_{k} \left(\rho_{ik} t_{kj} - t_{ik} \rho_{kj}\right) + g \left(Q_j - Q_i\right) \rho_{ij}. \tag{4.8}$$

The von Neumann equation in reciprocal space can be written as

$$\begin{aligned} \frac{d\rho_{\mathbf{p},\mathbf{q}}}{dt} = \frac{i}{\hbar} \big[& \left(\epsilon(\mathbf{q}) - \epsilon(\mathbf{p})\right) \rho_{\mathbf{p},\mathbf{q}} \\ & + g Q(\mathbf{K}) \left(\rho_{\mathbf{p}-\mathbf{K},\mathbf{q}} - \rho_{p,\mathbf{q}+\mathbf{K}}\right) \big] \end{aligned} \tag{4.9}$$

where we have assumed that the Fourier component of Q_i has only one dominant term, $Q(\mathbf{K})$ at $\mathbf{K} = (\pi, \pi)$. $\epsilon(\mathbf{k}) \equiv -2t_{nn}(\cos(k_x) + \cos(ky))$ is the kinetic energy term. The Hamiltonian in reciprocal space reads:

$$\begin{aligned} \hat{\mathcal{H}}(\mathbf{k}) = \sum_{\mathbf{k}} \epsilon(\mathbf{k}) \left(c_{\mathbf{k}}^{\dagger} c_{\mathbf{k}} - c_{\mathbf{k}+\mathbf{K}}^{\dagger} c_{\mathbf{k}+\mathbf{K}}\right) - g Q(\mathbf{K}) \sum_{\mathbf{k}} \left(c_{\mathbf{k}}^{\dagger} c_{\mathbf{k}+\mathbf{K}} + c_{\mathbf{k}+\mathbf{K}}^{\dagger} c_{\mathbf{k}}\right) \\ + \frac{P^2(\mathbf{K})}{2m} + \frac{K Q^2(\mathbf{K})}{2} \end{aligned} \tag{4.10}$$

Define $\mathbf{S}(\mathbf{p}) \equiv (S^x(\mathbf{p}), S^y(\mathbf{p}), S^z(\mathbf{p}))$, where $S^x(\mathbf{p}) \equiv \Re(\rho_{\mathbf{p},\mathbf{p}+\mathbf{K}})$, $S^y(\mathbf{p}) = \Im(\rho_{\mathbf{p},\mathbf{p}+\mathbf{K}})$, and $S^z(\mathbf{p}) \equiv (\rho_{\mathbf{p},\mathbf{p}} - \rho_{\mathbf{p}+\mathbf{K},\mathbf{p}+\mathbf{K}})/2$. Then following Eq. (4.9), the dynamical equations

of the three pseudospin components can be written as

$$\frac{dS^z(\mathbf{p})}{dt} = 2gQ(\mathbf{K})S^y(\mathbf{p}) \tag{4.11}$$

$$\frac{dS^x(\mathbf{p})}{dt} = 2\epsilon(\mathbf{p})S^y(\mathbf{p}) \tag{4.12}$$

$$\frac{dS^y(\mathbf{p})}{dt} = -2\epsilon(\mathbf{p})S^x(\mathbf{p}) - 2gQ(\mathbf{K})\Re(S^z(\mathbf{p})) \tag{4.13}$$

Then the above equations can be packed into Bloch equation as

$$\frac{d\mathbf{S}(\mathbf{p})}{dt} = \mathbf{S}(\mathbf{p}) \times \mathbf{B} \tag{4.14}$$

where $\mathbf{B} = (2gQ(\mathbf{K}), 0, -2\epsilon(\mathbf{p}))$.

The Newtonian equations, Eq. (4.5), in reciprocal space can be written as

$$\frac{dQ(\mathbf{K})}{dt} = \frac{P(\mathbf{K})}{m} \tag{4.15}$$

$$\frac{dP(\mathbf{K})}{dt} = gn(\mathbf{K}) - m\Omega^2 Q(\mathbf{K}) \tag{4.16}$$

where $n(\mathbf{K}) = \sum_{\mathbf{p}} \rho_{\mathbf{p},\mathbf{p}+\mathbf{K}}/N$. Therefore, Eqs. (4.14)-(4.16) are combined to form closed equations to describe the dynamics of electronic and lattice degrees of freedom.

To facilitate parameter selection for dynamical simulations, we aim to render the equations dimensionless. We note that there are two time (energy) scales in Eq. (4.5) and (4.8). To conduct the simulations effectively, we introduce a characteristic time,

$\tau = \hbar/t_{nn}$, such that the dimensionless time can be defined as $\tilde{t} = t/\tau$. Next, we define the characteristic position Q_0 and its corresponding characteristic momentum $P_0 = m\Omega Q_0$. Then the dimensionless hopping amplitude is naturally set to one, which establishes the energy scale for the electronic degrees of freedom. By ensuring that $d\tilde{t}$ is the same for both the von Neumann equation and Newtonian's equations, we define the energy scales for the dynamics of electronic and lattice degrees of freedom. The dimensionless coupling constant and the spring constant are then expressed as $\tilde{g} = gQ_0/t_{nn}$ and $\tilde{K} = KQ_0^2/t_{nn}$ respectively. The derivations of the dynamical equations with dimensionless quantities, as well as the choice of parameters, are detailed in Appendix A. Our dynamical simulations are conducted based on the dimensionless parameters defined above.

4.3 Results

The ground state of the system exhibits a checkerboard modulation of local electron density, i.e., the checkerboard CDW state. We initialize the system in this ground state using a single Slater determinant state, which remains persistent throughout the dynamics, as discussed in Sec. 4.2. In the following, we apply the coupled Bloch equations for pseudospin and Newton's equations for lattice degrees of freedom to simulate the interaction quench of the CDW order of the Holstein model at half-filling. Initially, the system is prepared in the ground state at an initial coupling constant g_i. At time $t = 0$, the coupling is suddenly switched to g_f, and the time evolution of the initial ground state is subjected to a time-independent Hamiltonian

at g_f in the following.

The CDW order parameter is defined as $\Delta(t) = \sum_{\mathbf{p}} \rho_{\mathbf{p},\mathbf{p}+\mathbf{K}}$. The simulation results are summarized in Fig. 4.1 and 4.2, for CDW order parameter $\Delta(t)$ and lattice distortions $Q(\mathbf{K})$ respectively. The post-quench CDW order parameter exhibits three main dynamical behaviors that are overall similar to order parameters in other symmetry-breaking phase. However, in the phase-locked regime, the peak of the oscillation contains the overlap of small oscilation with higher frequency, leading to a deviation from sinusoidal function. In the Landau-like damping regime, we observe the decay of the oscillation amplitude. However, the oscillation does not disappear even after a long simulation time before the finite-size effect comes into play. This can be understood as the non-thermal nature of the Holstein model. The Slater-determinant state remains throughout the time evolution, which prevents the system from being thermalized, resulting a possible persistent oscillation of the order parameter. In the over-damped regime, the order parameter oscillates with an average value approximately to zero. Higher frequency oscillations sits on top of the main oscillation can be observed from the small peaks atop the sinusoidal function. The deviation of non-adiabatic post-quench dynamics of CDW order parameter in Holstein model from other symmetry-breaking phase results from the electron-lattice coupling and the classical limit of the lattice degrees of freedom.

For the dynamical behaviors of lattice distortions $Q(\mathbf{K})$, a sinusoidal persistent oscillation is observed in the phase-locked regime. In the Landau-like damping regime,

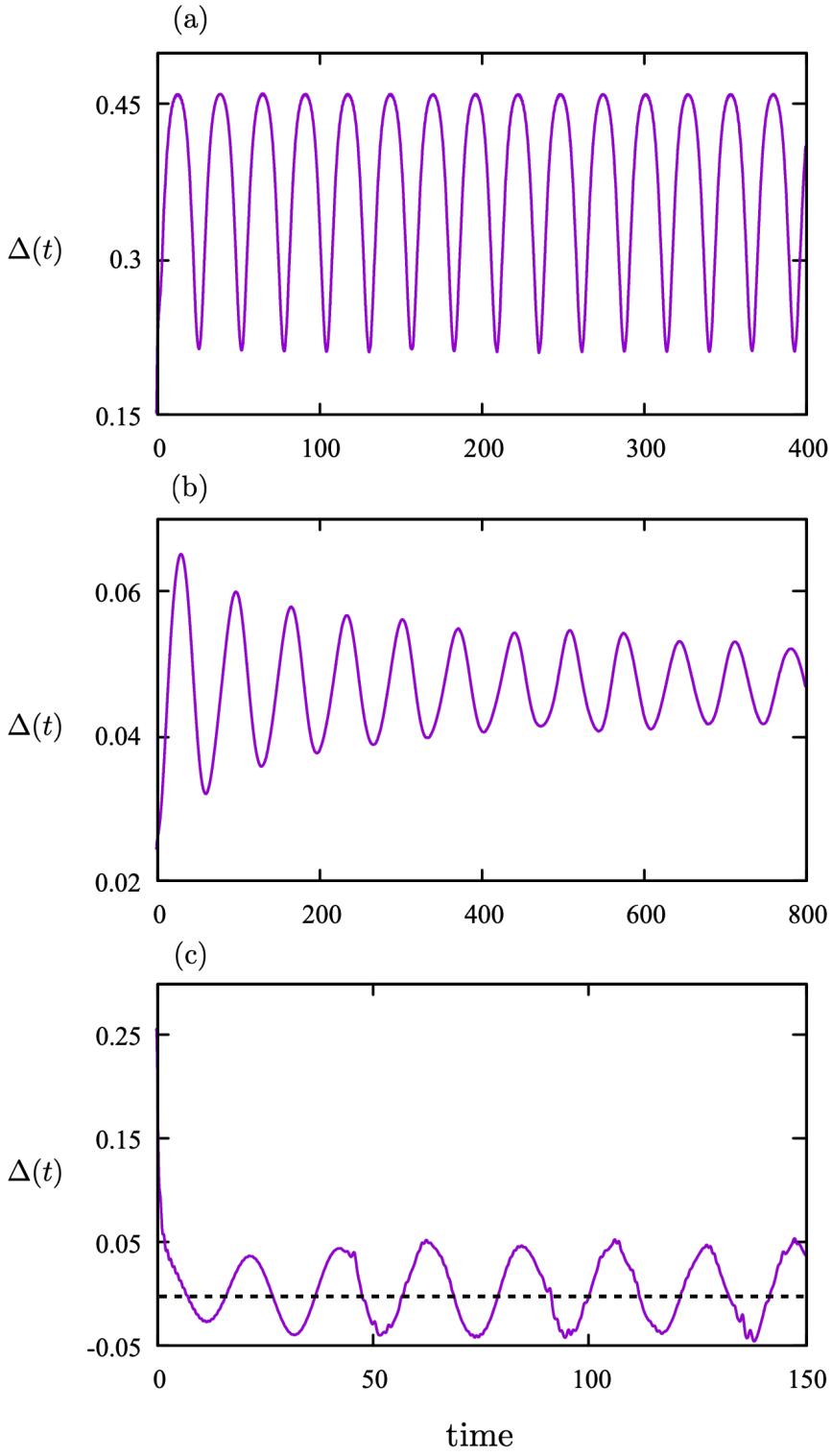

Figure 4.1: The time dependence of the CDW order parameter $\Delta(t)$ in the three main dynamical regimes of a quantum quench: (a) phase-locked regime with persistent oscillation ($g_i = 0.8$, $g_f = 1.6$), (b) Landau-damping regime ($g_i = 0.5$, $g_f = 0.6$), and (c) dynamical vanishing of the order parameter ($g_i = 1.0$, $g_f = 0.1$).

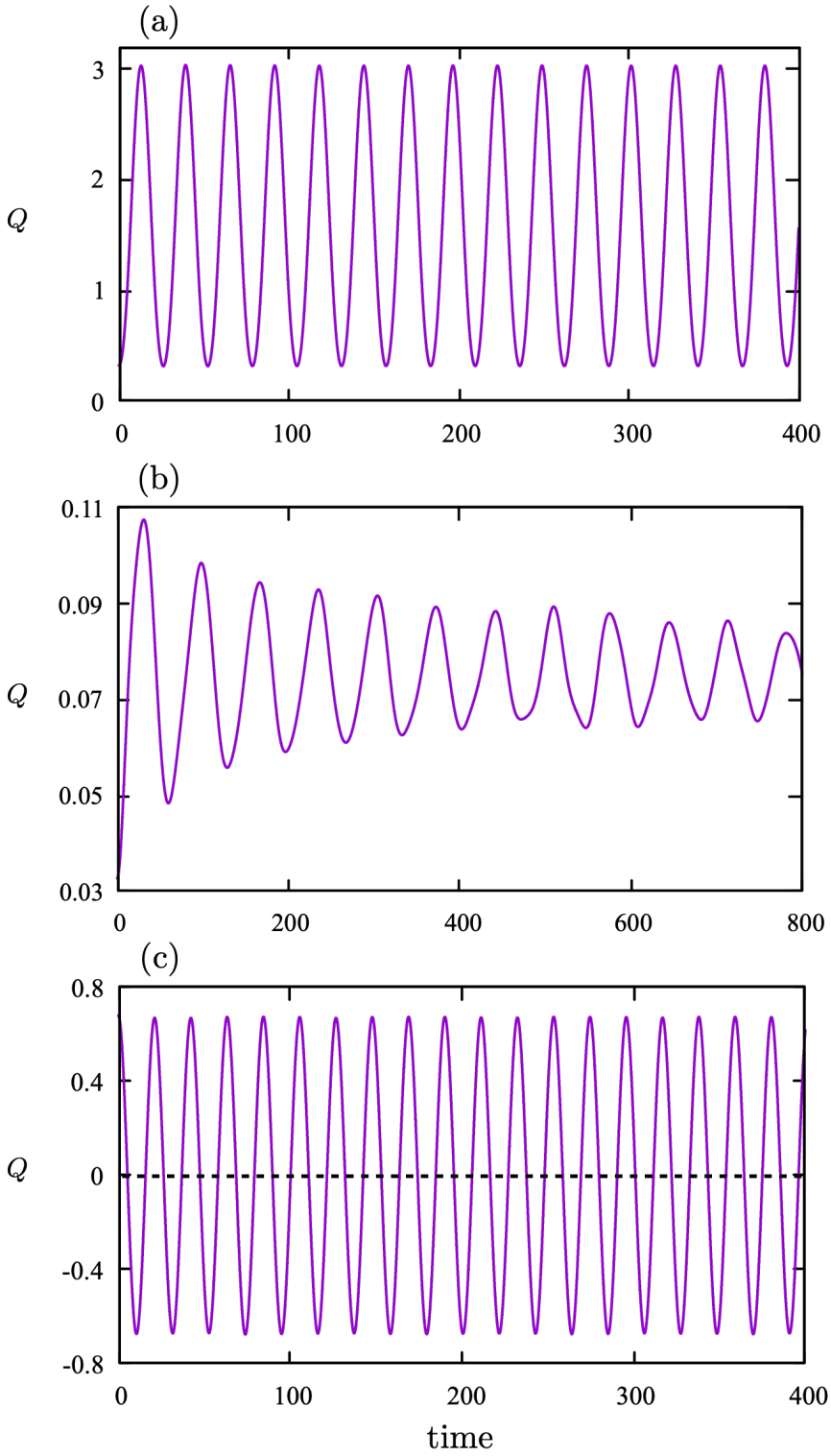

Figure 4.2: The time dependence of the $Q_{\mathbf{K}}(t)$ in the three main dynamical regimes of a quantum quench: (a) phase-locked regime with persistent oscillation ($g_i = 0.5$, $g_f = 3.0$), (b) Landau-damping regime ($g_i = 0.8$, $g_f = 0.9$), and (c) dynamical vanishing of the order parameter ($g_i = 0.8$, $g_f = 0.1$).

the dynamics of $Q(\mathbf{K})$ mirrors that of the CDW order parameter. The dynamical behaviors of these two regimes are shown in Fig. 4.1 (a)-(b) respectively. Interestingly, in the over-damped regime, although the CDW order parameter is quickly damped to an average value around zero, as shown in Fig. 4.1(c), the lattice distortion exhibits persistent oscillation with a finite amplitude. This indicates the emergence of coherent phonons. The generation of coherent phonons is unique to systems involving lattice vibrations. Since the damping of the CDW order parameter, defined as $\Delta(t) = n_{\mathbf{K}}$, occurs rapidly, the driving term on the right-hand side of Eq. 4.16 vanishes early in the dynamics, resulting in the maintenance of the checkerboard modulation of the lattice distortions.

To obtain more details in the post-quench dynamics of charge and lattice degrees of freedom, we can calculate the time evolution of electronic energy, kinetic and potential energies, of the lattice degrees of freedom, labelled by E_e, E_k, and E_p respectively. The definition of the three energies can be written as:

$$\begin{aligned} E_e &= \sum_{\mathbf{p}} \epsilon(\mathbf{p})\rho_{\mathbf{p},\mathbf{p}} - gQ(\mathbf{K})\rho_{\mathbf{p},\mathbf{p}+\mathbf{K}}, \\ E_k &= \frac{1}{2m}P^2(\mathbf{K}), \\ E_p &= \frac{1}{2}KQ^2(\mathbf{K}). \end{aligned} \tag{4.17}$$

The time evolution of the three energies (averaged over the total number of sampled wave vectors) in different dynamical regimes is plotted in Fig. 4.3. In the phase-locked regime, the three energies oscillate persistently, indicating the exchange of energy

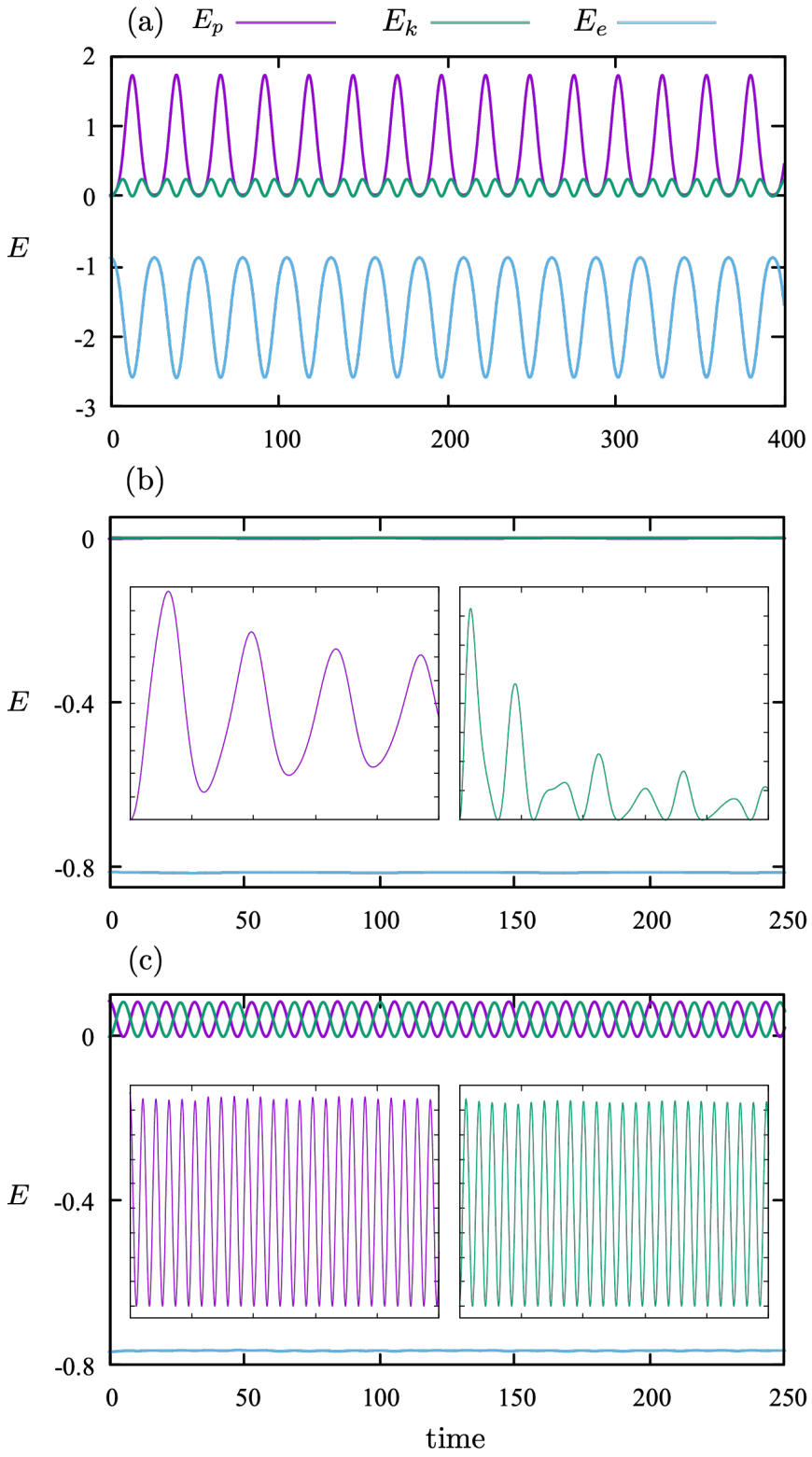

Figure 4.3: The time dependence of the potential energy E_p (purple curves), kinetic energy E_k (green curves), and electronic energy E_e (blue curves) in (a) phase-locked, (b) Landau-like damping, and (c) over-damped regimes respectively.The inner panels in (b) and (c) are potential energy E_p and kinetic energy E_k.

between different degrees of freedom without decay. In the Landau-like damping regime, the kinetic and potential energies decay over time, suggesting a reduction in the oscillation amplitude of lattice distortions. Finally, in the over-damped regime, the kinetic and potential energies exhibit a time evolution characteristic of a harmonic oscillator, consistent with the observation of coherent phonons.

To conclude this section, we summarize that our simulations reproduce the three dynamical regimes found in the post-quench dynamics of symetry-breaking phase in pure electronic systems. On top of that, we also study the dynamical behaviors of the lattice distortion $Q(\mathbf{K})$. The dynamical behaviors of lattice distortion are similar to CDW order parameter in phase-locked and Landau-like damping regimes. However, in the over-damped regime, lattice distortion exhibits persistent oscillation even after the CDW order is damped to nearly zero. This indicates the emergence of coherent phonons. The frequency of the lattice degrees of freedom and the electron-lattice coupling play important roles in the dynamics of the CDW order parameter and lattice distortion. How does such coupling affects the oscillation frequency and dynamical behaviors of CDW order parameter and lattice distortion? The detailed analysis is presented in the next section.

4.4 Discussion

As proposed at the end of Sec. 4.3, we need to study how the electron-lattice coupling affects the dynamical behaviors of the CDW order parameter and lattice distortion. A characteristic Q_0 for lattice distortions can be estimated from the balance of elastic

energy and electron-phonon coupling: $KQ_0^2 \sim g\langle n\rangle Q_0$. Assuming electron number $\langle n\rangle \sim 1$, we obtain $Q_0 \sim g/K$. Based on this characteristic scale, the value of $Q(\mathbf{K})$ in ground state is the same, as determined by the self-consistent condition $d\langle\mathcal{H}(\mathbf{k})\rangle/dQ(\mathbf{K}) = 0$, where the expectation value is found using the direct product state of the electron and phonon wave-functions. If we fixed the values of initial and final coupling constants, g_i and g_f respectively, we can determine the initial and final self-consistent lattice distortions, $Q_i(\mathbf{K})$ and $Q_f(\mathbf{K})$. Therefore, the value of $Q_i(\mathbf{K})$ and $Q_f(\mathbf{K})$ is unchanged if Ω varies. Here we show the time evolution of lattice distortions quenching from $g_i = 1.0$ to $g_f = 4.0$ at various Ω in Fig. 4.4. For small Ω, the lattice distortions exhibits persistent oscillation without decay in amplitude. However, as Ω increases, the oscillatory amplitude decays to a smaller finite values in later stage of the time evolution. We can calculate the oscillation amplitude, ΔQ, of the lattice distortion at each Ω, and the relation between ΔQ and Ω is shown in Fig. 4.5(a). The simulations suggest that the oscillation amplitudes decreases when the Ω increases. It is important to clarify that the oscillation frequency of the lattice distortion after quantum quench, $\tilde{\Omega}$, is different from the natural frequency Ω for the classical degrees of freedom. The oscillation frequency of the lattice distortion can be calculated through the Fourier transformation in time domain, and its relation with Ω is shown in Fig. 4.5(b). The actual oscillation frequency is smaller than the natural frequency due to the renormalization by the electron-lattice coupling.

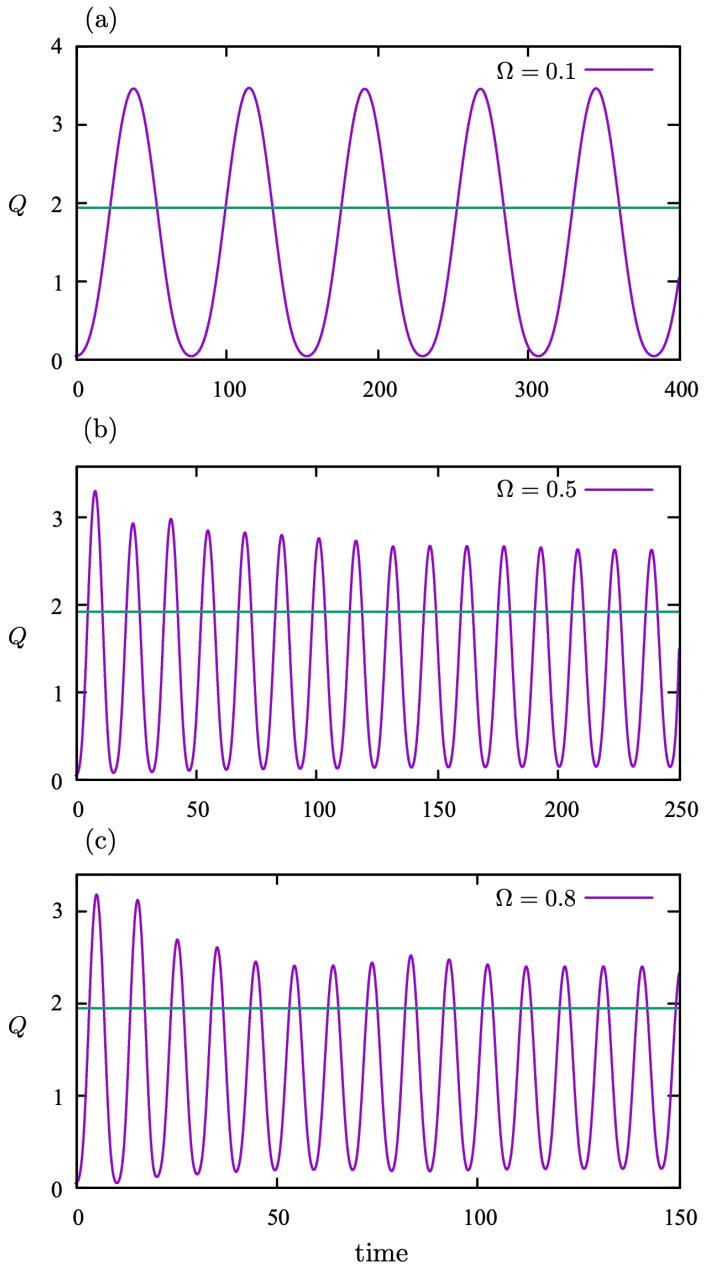

Figure 4.4: Post-quench dynamics of lattice distortions Q from $g_i = 1.0$ to $g_f = 4.0$, in which $Q_i(\mathbf{K}) \simeq 0.06$ and $Q_f(\mathbf{K}) \simeq 1.94$, at various frequencies for classical degrees of freedom, (a) $\Omega = 0.1$, (b) $\Omega = 0.5$, and (c) $\Omega = 0.8$. $Q_f(\mathbf{K})$ is labelled with a green line.

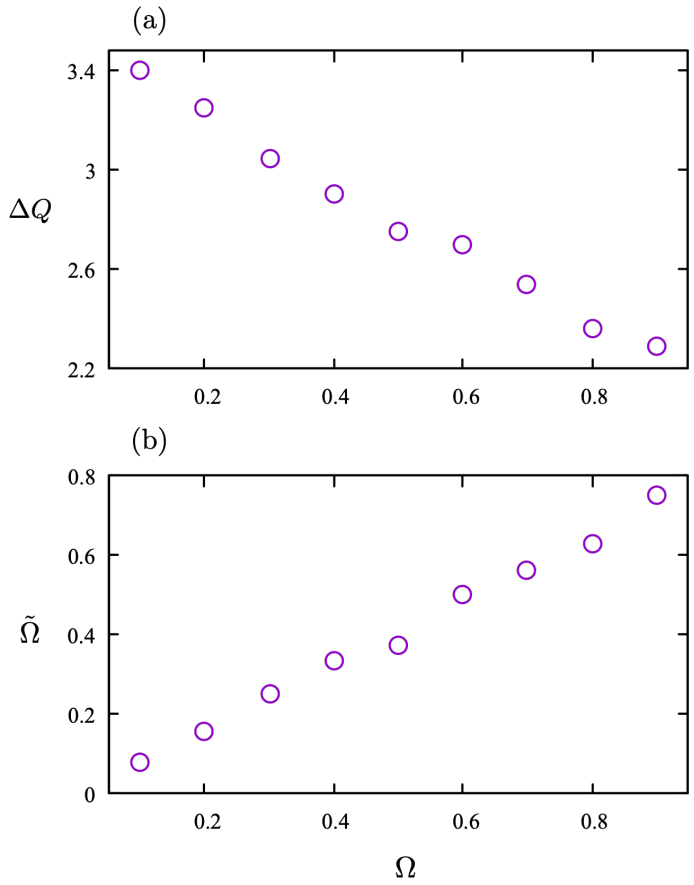

Figure 4.5: (a) The relation between the oscillation amplitude of the lattice distortions and the natural frequency of the classical degrees of freedom; (b) The relation between the oscillation frequency of the lattice distortions and the natural frequency of the classical degrees of freedom.

Chapter 5

Possible anomalous coarsening and spontaneous glassy in CDW states

5.1 Introduction

In this chapter, we investigate the post-quench dynamics of CDW states in Holstein model that goes beyond the pseudospin method and allows spatial fluctuations after the quantum quench. The efficient formulation of Newton and von Neumann equations, Eqs. 4.5 and 4.8 outlined in Section 4.2, are adopted for the real-space simulations. There are two quench scenarios we would like to investigate. In the first scanario, the initial state is prepared when the electron-lattice couplings vanish, so as the lattice distortions and momenta. In other words, the initial state is a non-interacting fermion system. If the Hamiltonian is quenched to finite electron-lattice coupling, it is expected that CDW order states emerged during the post-quench time evolution. Our simulations indicate that, when the final coupling constant $g_f < 0.6$, there is no significant CDW order emerged. However, if $g_f \in [0.6, 1.4]$, there exists an anomalous coarsening in CDW domains. Finally, if $g_f > 1.4$, the system exhibits

spontaneous glassy states. In the second scenario, instead of zero electron-lattice coupling, the initial state is prepared in the checkerboard modulated CDW state at a finite coupling g_i. When the system quenched to another finite coupling g_f, the emergent modes can be understood with mechanism of the parametric instability. The systematic numerical and theoretical study of the second scenario are in progress. We will only present the numerical results in this dissertation.

5.2 Anomalous coarsening of CDW states

We first investigate the post-quench dynamics of starting from a state with vanishing electron-lattice coupling. The main results of our extensive quench simulations are summarized in a schematic phase diagram of dynamical regimes shown in Fig. 5.1. In the first regime in Fig. 5.1(a), quenching to a small final g_f gives no CDW order states. However, if the system is quenched to an intermediate g_f, where g_f is roughly in $[0.6, 1.4]$, the system exhibits coarsening of CDW domains as shown in Fig. 5.1(b). If the system is quenched to a even larger g_f, say $g_f \geq 1.5$, the system relaxes to a glassy states, as shown in Fig. 5.1(c).

As we learn from the spatial inhomogeneity and patter formation observed in t-V model in Section 3.2, the quench-induced inhomogeneity mostly is in the form of longer wavelength density modulations on top of the checkerboard CDW order. Therefore, it is convenient to use the local lattice distortion order parameter, Φ_i,

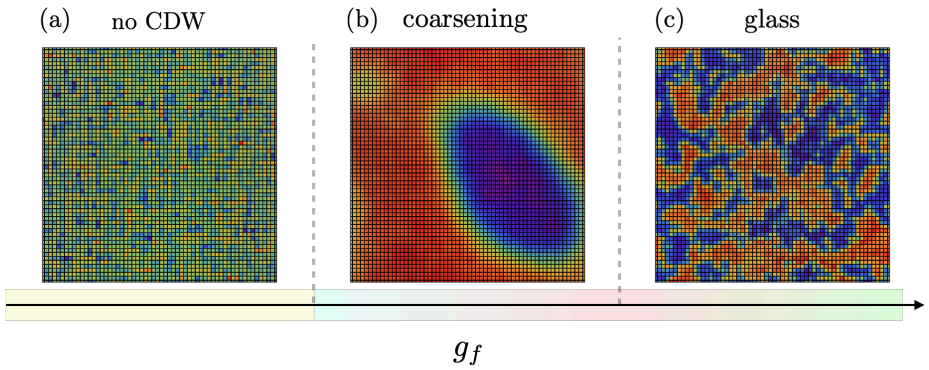

Figure 5.1: Phase diagram of post-quench CDW states of the square-lattice Holstein model. g_f denotes the strength of electron-lattice coupling constant after interaction quench. The three dynamical phases are: $((a))$ small final g_f in which no significant CDW order states emerged, (b) coarsening of CDW domains after quenching to intermediate g_f, and (c) spontaneous glassy states with large g_f.

defined as

$$\Phi(\mathbf{r}_i) = \left(Q_i - \frac{1}{4}\sum_j{}' Q_j\right) \exp\left(i\mathbf{K}\cdot\mathbf{r}_i\right), \tag{5.1}$$

to characterize the super modulation. This scalar order parameter is similar to its electronic counterpart defined in Eq. 3.10. Snapshots of this local CDW order parameter Φ_i corresponding to the lattice distortion profiles of the coarsening and glassy regimes are shown by top and bottom row of Fig. 5.2 respectively. These results highlight a super-modulation of lattice distortions, as demonstrated by the quasi-periodic square-like patterns in the Φ_i field, which itself represents a ultrashort-period checkerboard density modulation. We can again use the discrete Ising variable $\sigma_i = \text{sign}(\Phi_i)$ to characterize such post-quench state. In the snapshots in Fig. 5.2 (a)-(d), multiple positive and negative Ising domains emerged, and those domains tend to merge and form larger domains during the relaxation. In Fig. 5.2 (e)-(h), although the multiple

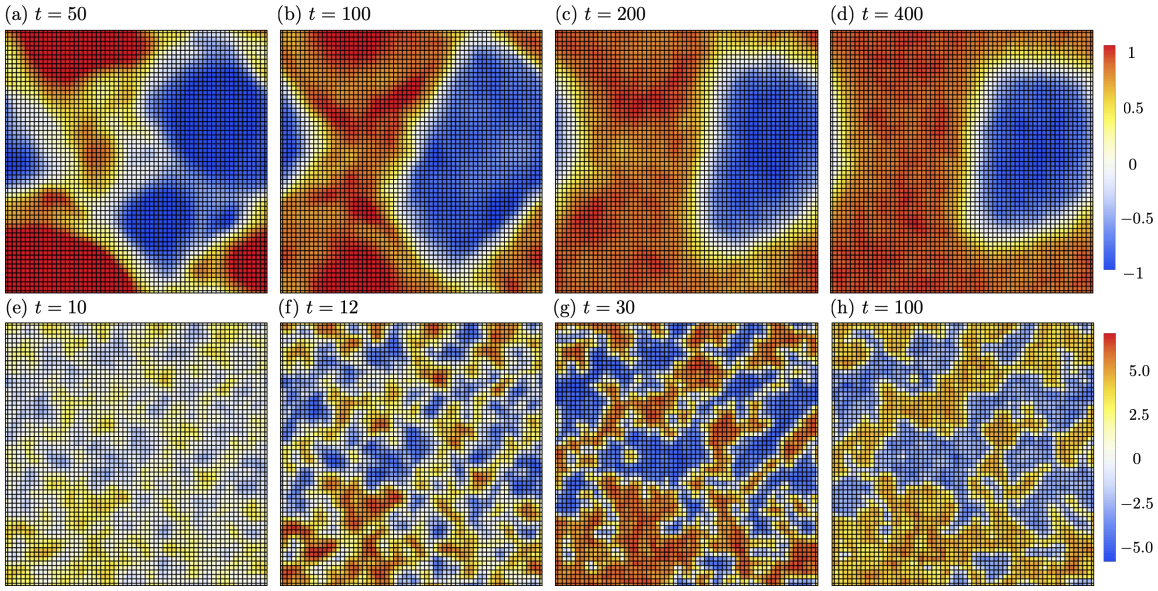

Figure 5.2: Snapshots of Φ_i at various time steps for system quenching from $g_i = 0$ to (a)-(d): $g_f = 0.8$, where coarsening of CDW domains is observed; and (e)-(h): $g_f = 1.5$, in which a spontaneous glassy state is emerged.

domains are merging to form larger domains in the early stage, this process renders to the formation of relatively steady patterns with multiple positive and negative Ising domains, which can be understood as a spontaneous glassy state. Notice that the interfaces that separate Ising domains of opposite signs are of a finite width with a nearly vanishing lattice distortions.

To further characterize the coarsening and glassy state, one can we compute the corresponding structure factor

$$S_Q(\mathbf{q}, t) = |\tilde{Q}(\mathbf{q}, t)|^2, \tag{5.2}$$

where $\tilde{Q}(\mathbf{q}, t)$ is the Fourier transform of the time-dependent lattice distortions $Q_i(t)$,

$$\tilde{Q}(\mathbf{q}, t) = \frac{1}{\sqrt{N}} \sum_i \left(Q_i(t) - \bar{Q}\right) \exp^{i\mathbf{k}\cdot\mathbf{r}_i}. \tag{5.3}$$

If the lattice distortions exhibit checkerboard modulated pattern, it corresponds to a peak at wave vector $\mathbf{K} = (\pi, \pi)$. However, as shown in Fig. 5.3 (a)-(c), the quenched state exhibits a broad diffusive peak around $\mathbf{K}$ due to the existence of multiple CDW domains with opposite signs in the early stage of the time evolution. The width of the diffusive peak thus provides an estimation of the typical size of the CDW domains, defined as $L(t) = 2\pi/\langle|\mathbf{q} - \mathbf{K}|\rangle$, where the angle bracket indicates average using the structure factor $S(\mathbf{q})$ as the weighting factor. In the coarsening regime, the emerged CDW domains tend to merge and form larger domains, which indicates that $L(t)$ becomes larger, as shown in Fig. 5.3(d). Similar oscillatory behavior accompanying the coarsening in the time evolution of $L(t)$, is reported in coarsening in quench dynamics of ferromagnetic spinor Bose gas [163], As the system becomes more ordered in the later stage as only two CDW domains remain, the width of the diffusive peak in the structure factor becomes smaller in the later stage of the dynamics.

It is important to examine whether the coarsening of CDW domains, characterized by the characteristic length $L(t)$ according to the kinetics of phase ordering, follows the well-established power law growth rate [164]. Kinetic Monte Carlo simulations [165,166] of the nearest-neighbor ferromagnetic Ising model on different lattice systems find that the power-law domain growth satisfies the following expression,

$$L(t) \sim t^{1/z}, \tag{5.4}$$

where z is universal, independent from the lattice geometry and dimensionality. Since

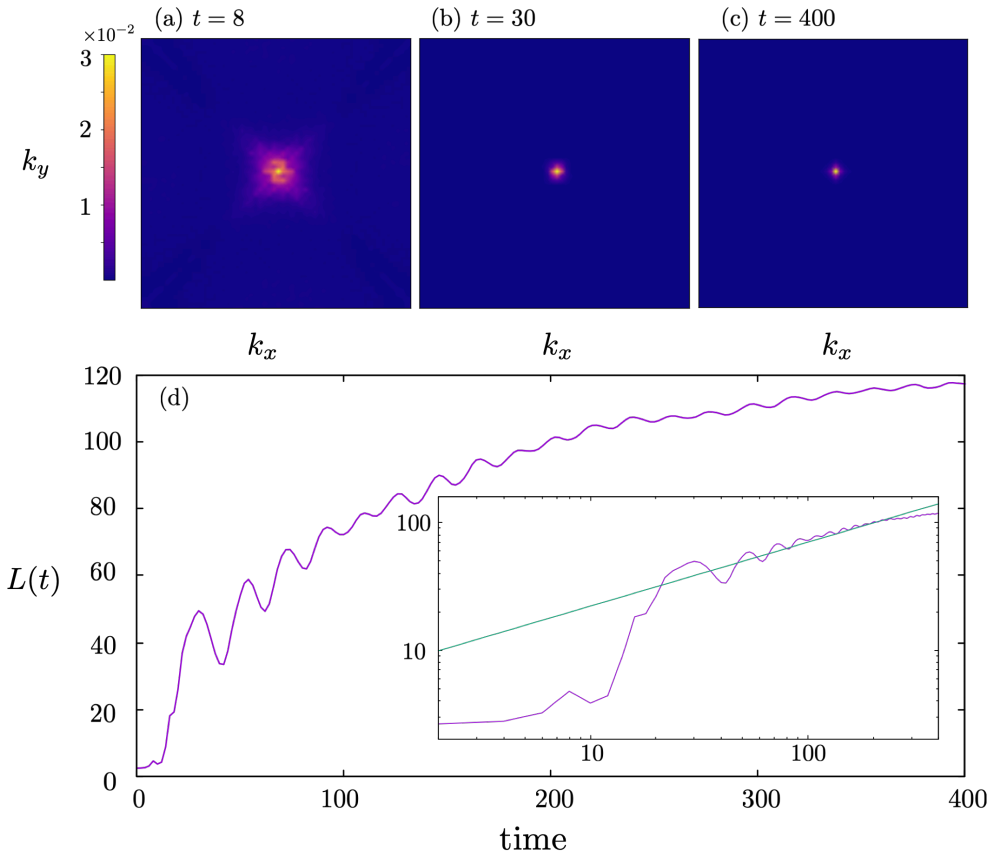

Figure 5.3: (a)-(c): structure factors at various time steps for systems quenched to $g_f = 0.8$; (d) the time dependence of characteristic length, $L(t)$, of CDW domains; inner panel: log-log scale of $L(t)$, with a power-law growth characterized by an exponent $1/z = 0.55$.

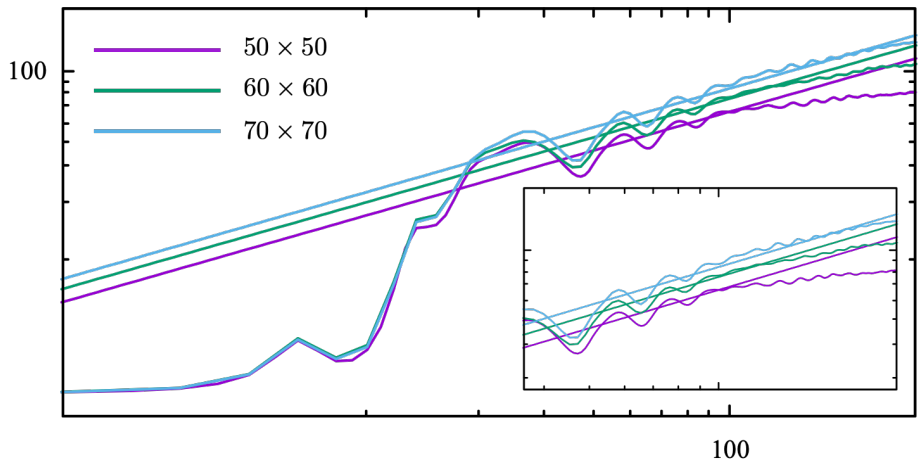

Figure 5.4: The power-law growth for the coarsening of CDW domains are characterized by exponent $1/z = 0.55$ for different dimensinalities of 50×50, 60×60, and 70×70. The deviation of $L(t)$ from the power-law growth occurs at a later stage when system size becomes larger, which indicate that such deviation is likely due to the finite size effect.

the CDW transition belongs to the Ising universality class, the CDW is expected to have similar coarsening behavior as that in Ising system. In dynamics with non-conserving Ising order parameter, as in our CDW coarsening dynamics, the power-law growth obeys the Allen-Cahn law with exponent $z = 2$. Based on the above analysis, we fit the power-law growth of $L(t)$ and the exponent is roughly $1/z \sim 0.55$, indicating a non-Allen-Cahn law growth. The deviation of $L(t)$ from this power-law growth is possibly due to the finite size effect. To verify this, we conduct simulations for sizes from 50×50 to 70×70. The characteristic lengths calculated from different system sizes are plotted and fit in Fig. 5.4. The power-law growth for the coarsening of CDW domains are characterized by exponent $1/z = 0.55$ for different dimensinalities. The deviation of $L(t)$ from the power-law growth occurs at a later stage if the system size becomes larger, indicating that such deviation is likely due to the finite size effect.

In conclusion, the coarsening of CDW domains in such post-quench dynamics is not following the Allen-Cahn law with $1/z = 0.5$, which indicates that it is an anomalous coarsening behaviors. The finite size effect of our simulation is address by comparing the power-law growth of different $L(t)$ computed from various system sizes. Quantitative method for determining the exponent can be achieved by the data collapse method [167] in the future study.

5.3 Spontaneous glassy states

The bottom row in Fig. 5.2 for quenching to large electron-lattice coupling indicates a different dynamical behavior from coarsening. The CDW pattern becomes relatively stable at late stage, indicating a spontaneous glassy state. To verify this, we can calculate the structure factor $S_Q(\mathbf{q}, t)$ and $L(t)$ for $g_f = 1.5$. The structure factor at various time steps are shown in Fig. 5.5 (a)-(c). As the system exhibits multiple CDW domains with different signs, the structure factor exhibits a diffusive peak surrounding $\mathbf{K} = (\pi, \pi)$. The fluctuations of the local lattice distortion order parameter Φ_i in each domain causes the increase and decrease in the modes other than $\mathbf{K}$. However, the diffusive peak is maintained in late stage, suggesting the formation of glassy state and the characteristic length is approaching a finite value, as shown in Fig. 5.5(d).

We label the characteristic length in glassy regime in late stage as ξ. To see the relation between g_f and ξ can be obtained by calculating the characteristic length in late stage at various g_f. The results are shown in Fig. 5.6. The value of ξ becomes smaller for larger g_f, suggesting that the CDW domains are not able to merge to

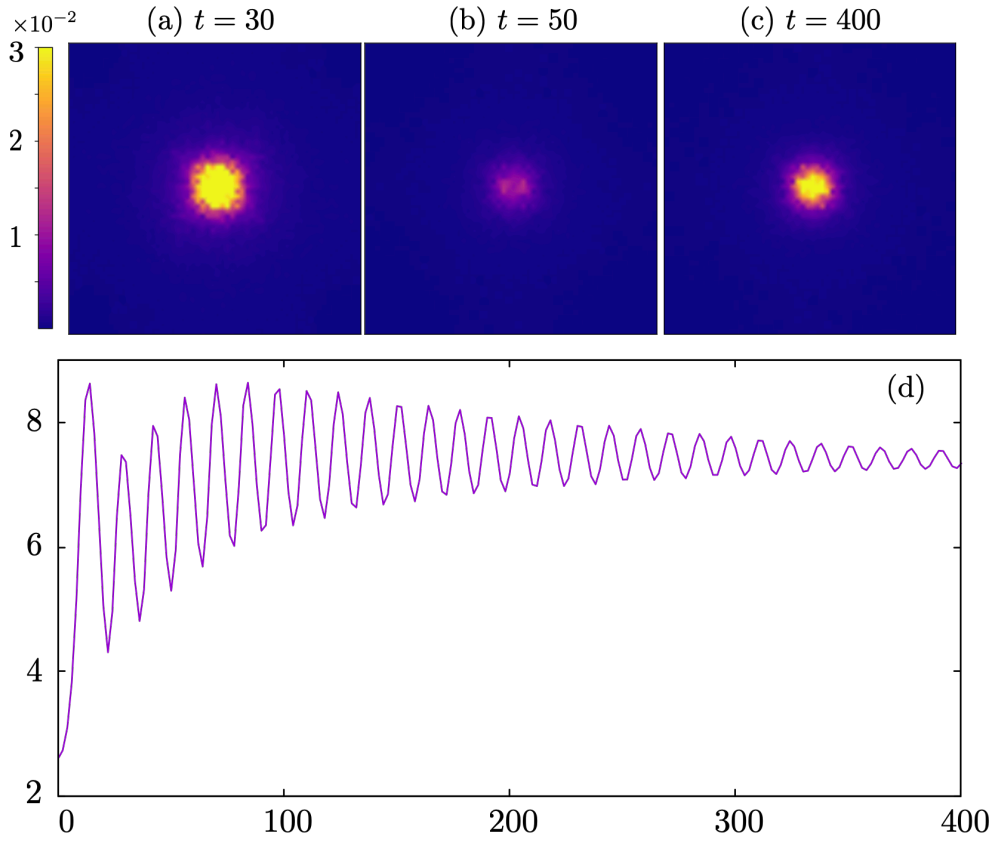

Figure 5.5: (a)-(c): structure factors at various time steps for systems quenched to $V_f = 1.5$; (d) the time dependent CDW characteristic length.

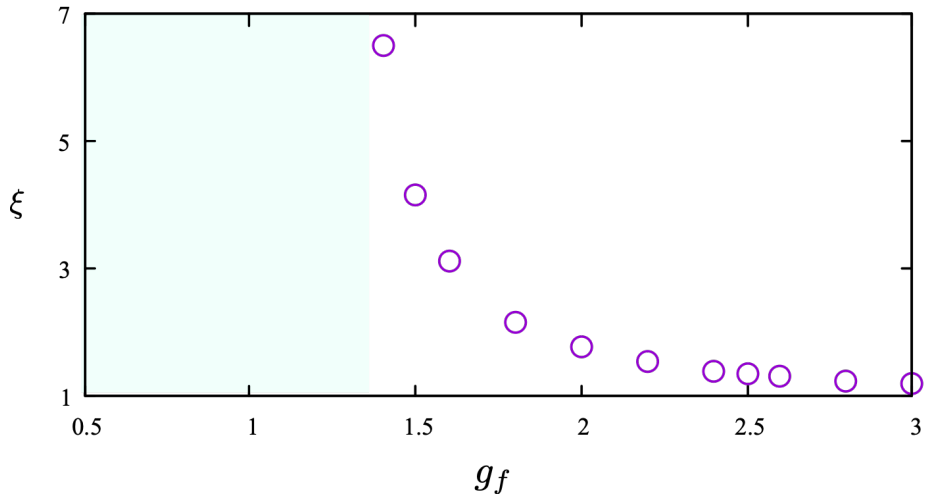

Figure 5.6: The g_f dependence of characteristic length in late stage in glassy regime. The light blue region indicates the range of g_f without glassy state.

form larger domains for quenching to large g_f. However, with the increase of g_f, the decrease of ξ becomes smaller and finally asymtotically approaching a finite value of ξ.

5.4 Conclusion and outlook

To conclude this chapter, we briefly discuss the scenarios when the system is prepared in the ground state with finite electron-lattice coupling. In this case, the ground state is the checkerboard modulation of charge density and lattice distortion, and only a peak at $\mathbf{K} = (\pi, \pi)$ is observed. When the system is quenched to a larger g_f, modes other than $\mathbf{K}$ emerged during the post-quench dynamics. In the structure factor of a quench simulation from $g_i = 0.5$ to $g_f = 5.0$, we find that the first modes other than $\mathbf{K}$ emerged around $\mathbf{k}_1 = (\pi, 0)$ and $\mathbf{k}_2 = (0, \pi)$, as shwon in Fig 5.7. This can be understood as a decay from mode at $\mathbf{K}$ to modes at $\mathbf{k}_1$ and $\mathbf{k}_2$.

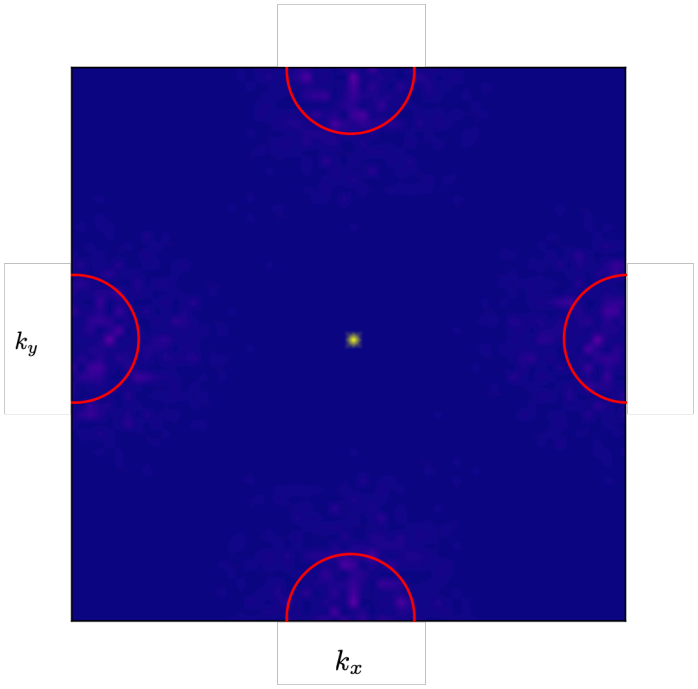

Figure 5.7: The initial state has only one mode at $\mathbf{K} = (\pi, \pi)$. In the post-quench dynamics, modes at $\mathbf{k}_1 = (\pi, 0)$ and $\mathbf{k}_2 = (0, \pi)$, which suggests a parametric instability mechanism for the emergence of spatial inhomogeneity.

Such a process obeys the conservation of energy and momentum, and thus is likely a process of parametric instability [90]. Theoretical understanding of such parametric instability process can be derived from the Bloch equation and Newton equations using pseudospin formalism, and the Fermi statistics is possibly playing an important role in this mechanism. The relevant investigation is in progress.

Chapter 6

Photo-induced pattern formation in CDW states

6.1 Introduction

In this chapter, we present large-scale real-space simulations of photo-induced ultrafast CDW dynamics in a 2D semi-classical Holstein model [159]. This model is a prototypical system for studying phenomena related to electron-phonon coupling, such as phonon-mediated superconductivity [168, 169], polaron dynamics [170, 171], and in particular CDW physics [172–175]. Also notably, CDW orders in Holstein model are intimately related to lattice distortion, thus providing a platform for investigating the interplay between collective CDW behaviors and lattice dynamics. To account for dynamical inhomogeneities induced by laser pulses, an efficient real-space methods is developed by combining the von Neumann equation for electron density matrix with the Newton equation for lattice distortions.

We find that while the CDW order is reduced due to the injected energy, the ultrafast photoexcitation also generates a coherent oscillation of both the CDW order

and lattice distortion. The melting of the CDW order depends critically on the amplitude as well as the frequency of the laser pulse. Our large-scale simulations show that the melting process proceeds through the breakup of the initial uniform CDW domain into a highly inhomogeneous state with finite CDW order locally. Intriguingly, we find that while an overall CDW order survives for slightly sub-critical excitations, the system exhibits stripe modulations of the CDW amplitude. This initial stripe pattern then breaks into more complex patterns at later times.

The rest of the chapter is organized as follows. In Sec. 6.2, we briefly review the Holstein model and the Peierls substitution for modeling the laser pulse excitation. We also discuss the governing equations of the CDW state in the semi-classical Holstein model and the efficient implementation of the real-space method. The ultrafast dynamics of photo-induced CDW states is summarized in Sec. 6.3. A systematic analysis of the CDW order on the fluence and frequency of the pump pulse is also presented. Detailed descriptions of the pattern formation and its structures in some specific frequency are summarized in Sec. 6.4. Finally, we conclude the paper with a summary and outlook in Sec. 6.5.

6.2 Model and Methods

We consider a Holstein model [159] with spinless fermions on a square lattice, and the Hamiltonian is listed in Eq. (4.1)-(4.4). The Newton equations for lattice degrees of freedom, and von Neumann equation for electronic degrees of freedom are derived in Chapter 4 in Eqs. (4.5) and (4.8).

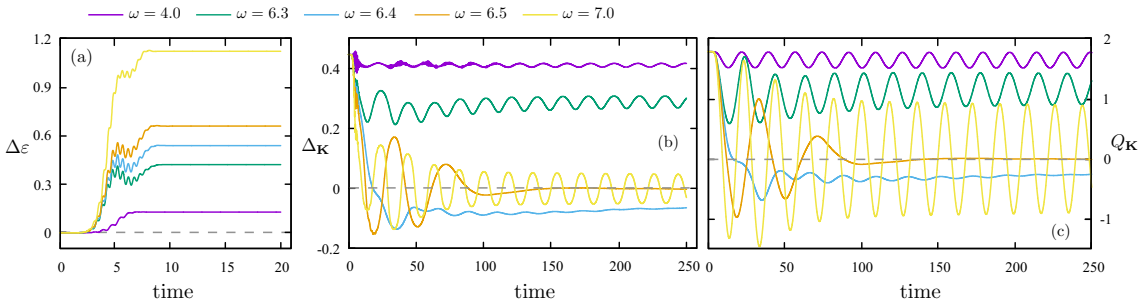

Figure 6.1: Time evoulution of (a) the injected energy per site $\Delta\varepsilon(t) = [E(t) - E_0]/N$, (b) the CDW order parameter $\Delta_{\mathbf{K}}(t)$, and (c) amplitude of staggered distortion $Q_{\mathbf{K}}(t)$, for laser pulse excitation with different center frequencies. The width of the laser pulse is fixed at $\sigma = 2$, the peak time is at $t_0 = 5$, and the amplitude is $\mathcal{A} = 0.5$.

In order to model the laser excitation, the Peierls substitution is employed to incorporate the coupling to the electric field of a laser pulse. Consider a uniform linearly polarized electric field $\mathbf{E}(t) = -\partial\mathbf{A}/\partial t$, where $\mathbf{A}(t) = \hat{\mathbf{p}}A(t)$ is the time-varying vector potential, and $\hat{\mathbf{e}}$ is the polarization vector. In the presence of an electric field, the electron hopping integral acquires a phase factor

$$t_{ij}c_i^\dagger c_j \to t_{ij}e^{i\mathbf{A}(t)\cdot(\mathbf{r}_i-\mathbf{r}_j)}c_i^\dagger c_j. \tag{6.1}$$

In our simulations below, we assume a Gaussian function for the laser pulse

$$A(t) = \mathcal{A}\exp\left[(t-t_0)^2/\sigma^2\right]\cos\left[\omega(t-t_0)\right], \tag{6.2}$$

where $\mathcal{A}$ represents the amplitude of the pulse, t_0 is the peak time, σ is the pulse width, and ω is the center frequency of the pulse.

There are two characteristic time scales for the dynamics of the Holstein model. First, from the bandwidth of the electron tight-binding model $W = 8t_{\rm nn}$, one can

define a time scale $\tau_e = \hbar/t_{nn}$ for the electron dynamics. On the other hand, the natural frequency Ω of the Einstein phonons gives a characteristic time $\tau_L = 1/\Omega$ for the lattice dynamics. The dimensionless adiabatic parameter is defined as the ratio $r = \tau_e/\tau_L = \hbar\Omega/t_{nn}$. which characterizes the relative time scales of the two subsystems. A characteristic Q_0 for lattice distortions can be estimated from the balance of elastic energy and electron-phonon coupling: $KQ_0^2 \sim g\langle n\rangle Q_0$. Assuming electron number $\langle n\rangle \sim 1$, we obtain $Q_0 \sim g/K$. A momentum scale $P^* = m\Omega Q_0$ can be obtained from Eq. (4.5). Based on this characteristic scale, the electron-phonon coupling can be characterized by a dimensionless parameter $\lambda = gQ_0/W = g^2/WK$. For all simulations discussed below, the two dimensionless parameters are set to $r = 0.4$ and $\lambda = 1$, the simulation time is measured in unit of τ_e, and the lattice distortion is expressed in terms of Q_0.

6.3 Photo-induced Melting of CDW order

The method discussed in Sec. 6.2, namely the real-space von Neumann equation (4.8) coupled with Newton equation (4.5), is applied to simulate the photo-induced ultrafast CDW dynamics in a pump-probe setup. In all simulations below, we consider a polarization along the symmetric diagonal direction $\hat{\mathbf{e}} = (\hat{\mathbf{x}} + \hat{\mathbf{y}})/\sqrt{2}$, and a system size of 60×60. The system is initially prepared in a ground state with a homogeneous CDW order and a concomitant checkerboard lattice distortion. This initial CDW state is then subject to a short laser pulse of the wave form (6.2). It is worth noting that the square-lattice tight-binding model exhibits a divergent Lindhard susceptibility at

half-filling due to a perfect nesting of the Fermi surface. As a result, the system is unstable against the formation of a staggered lattice distortion $Q_i = \mathcal{Q}\exp(i\mathbf{K}\cdot\mathbf{r}_i)$, where $\mathbf{K} = (\pi, \pi)$ is the ordering wave vector of the checkerboard pattern and $\mathcal{Q}$ is the distortion amplitude. As detailed in App. B, the staggered distortion induces a concomitant charge modulation and opens a spectral gap $\varepsilon_{\text{gap}} = 2g\mathcal{Q}$, rendering the system a CDW insulator. The energy gap is determined by the competition between the gain of electronic energy through gap opening and the cost of elastic energy; details can be found in App. B.

The finite spectral gap also means that electron-hole pairs cannot be excited by photon energies less than the CDW band gap. This implies a threshold frequency $\hbar\omega_{\text{th}} = \epsilon_{\text{gap}} = 2g\mathcal{Q}$ for continuous wave excitations. Yet, instead of a sharp threshold transition as a function of frequency, a crossover behavior is expected due to a combination of nonlinear effects and finite width of the pump pulse. A laser pulse of width σ comprises photons of energies in a finite range $\hbar(\omega \pm \delta\omega)$ around the center frequency, where the bandwidth $\delta\omega \sim \sigma^{-1}$. Consequently, for a pulse with a sub-threshold center frequency, photons in the higher energy end of the pulse spectrum could exceed the CDW gap and excite electron-hole pairs, a process that is further enhanced by nonlinear effects with a large laser fluence.

A quantitative measure of the above-gap photoexcitation is the average energy (per site) $\Delta\varepsilon$ deposited to the system by the laser pulse. Fig. 6.1(a) shows the injected energy $\Delta\varepsilon(t)$ as a function of time for various center frequencies. The pulse width is

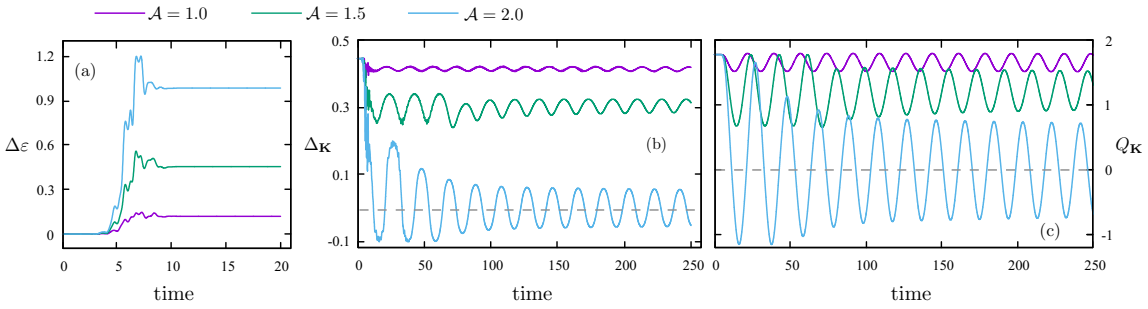

Figure 6.2: Time evoulution of (a) the injected energy per site $\Delta\varepsilon(t) = [E(t) - E_0]/N$, (b) the CDW order parameter $\Delta_{\mathbf{K}}(t)$, and (c) amplitude of staggered distortion $Q_{\mathbf{K}}(t)$, for laser pulse excitation with different amplitude $\mathcal{A}$. The width of the laser pulse is fixed at $\sigma = 2$, the peak time is at $t_0 = 5$. The center frequency of the laser pulse is set at $\omega = 3$, which is well below the threshold $\omega_{\rm th} = 7.142$.

fixed at $\sigma = 2$, and the peak time is at $t_0 = 5$. Most of the energy injection occurs during the pulses width. The total energy remains nearly a constant after the pulse excitation, indicating a closed-system evolution under the coupled von Neumann and Newton dynamics. Importantly, although the threshold frequency from the initial condition is $\hbar\omega_{\rm th} = 2g\mathcal{Q} = 7.142$, significant energy transfer takes place already at $\hbar\omega \sim 3$. The overall energy deposition increases with the center frequency.

To quantify the dynamics of the nonequilibrium CDW state, we introduce time-dependent order parameters for the checkerboard density modulation

$$\Delta_{\mathbf{K}}(t) = \frac{1}{N}\sum_i \langle\Psi(t)|\hat{n}_i|\Psi(t)\rangle e^{i\mathbf{K}\cdot\mathbf{r}_i}, \tag{6.3}$$

where $|\Psi(t)\rangle$ is the single Slater determinant state, and the phase factor $\exp(i\mathbf{K}\cdot\mathbf{r}_i) = +1$ and -1 for sites in the A and B sublattice, respectively. Fig. 6.1(b) shows the CDW order versus time for laser pulses of varying center frequencies. The photoinduced

nonequilibrium CDW states exhibit complex dynamics. Importantly, for most cases the laser pulse induces a prominent coherent oscillation of the CDW order which persists for a long time. This oscillation is accompanied by a lattice dynamics as shown in Fig. 6.1(c), where we plot the time dependence of the order parameter $Q_{\mathbf{K}}(t)$ that characterizes the overall staggered distortion

$$Q_{\mathbf{K}}(t) = \frac{1}{N} \sum_i Q_i(t)\, e^{i\mathbf{K}\cdot\mathbf{r}_i}. \tag{6.4}$$

The time evolution of the staggered lattice mode closely follows that of the CDW order parameter.

As discussed above, sub-threshold excitation results in the reduction of CDW order already for frequencies as low as $\hbar\omega = 4$, which is well below the threshold $\hbar\omega_{\text{th}} = 7.142$. Upon increasing the center frequency of laser pulses, more energy is injected into the CDW state, giving rise to a reduced average CDW order. The photoexcitation with a sub-threshold center frequency is further enhanced by an increasing laser intensity due to the nonlinear effects. For example, Fig. 6.2 summarizes simulation results of laser excitations with a sub-threshold frequency $\hbar\omega = 3$ and varying intensities $\mathcal{A}$. Upon increasing the laser intensity, more energy is deposited onto the system, which in turn results in a reduced average CDW order and an enhanced coherent oscillation. For laser excitations with large enough fluence, e.g. $\mathcal{A} = 2.0$, even a pulse with sub-threshold frequency can completely melts the CDW order, as shown in the case of $\mathcal{A} = 2.0$ in Fig. 6.2(b) and (c).

The mechanism of photoinduced suppression and melting of the checkerboard CDW order and the emergence of coherent oscillation can be understood as follows. Assuming negligible momentum of the incoming photons, the laser pulse excites a quasi-particle from the filled valence band $E^-_{\mathbf{q}}$ to the empty conduction band $E^+_{\mathbf{q}}$ of the initial CDW state, i.e. $|\pm\mathbf{q}\rangle \propto \hat{\gamma}^\dagger_{+,\mathbf{q}}\hat{\gamma}_{-,\mathbf{q}}|\mathrm{CDW}_0\rangle$, where $\hat{\gamma}_{\pm,\mathbf{q}}$ are the quasi-particle operators. The characteristic frequency of a pair of quasi-particle and quasi-hole is $\hbar\nu_{\mathbf{q}} = E^+_{\mathbf{q}} - E^-_{-\mathbf{q}} = 2\sqrt{\varepsilon^2_{\mathbf{q}} + (g\mathcal{Q})^2}$. In the absence of electron-electron scattering, the dynamics of a quasi particle-hole pair is an oscillatory motion with their natural frequency. Importantly, the photoexcited quasi-particles will modify the density matrix in Fourier space $\rho_{\mathbf{q},\mathbf{q}+\mathbf{K}}$, which in turn contributes to the CDW order parameter

$$\begin{aligned}\Delta_{\mathbf{K}}(t) &= \sum_{\mathbf{q}} \rho_{\mathbf{q},\mathbf{q}+\mathbf{K}}(t) \\ &= \sum_{\mathbf{q},\mu\nu=\pm} C^{\mu\nu}_{\mathbf{q}} \langle\Psi(t)|\gamma^\dagger_{\mu,\mathbf{q}}\gamma_{\nu,\mathbf{q}}|\Psi(t)\rangle.\end{aligned} \tag{6.5}$$

Here $\rho_{\mathbf{q},\mathbf{q}+\mathbf{K}}(t) = \langle\Psi(t)|\hat{c}^\dagger_{\mathbf{q}+\mathbf{K}}\hat{c}_{\mathbf{q}}|\Psi(t)\rangle$ describes the correlation of a particle-hole pair with a momentum difference $\mathbf{K} = (\pi,\pi)$ that characterizes the checkerboard charge modulation, and $C^{\pm,\pm}_{\mathbf{q}}$ are determined by coefficients that relate the quasiparticle operators to the electron operators; see App. B for details. The independent oscillations of different pairs with their respective natural frequencies give rise to a reduced CDW order due to destructive interferences in the summation of Eq. (6.5).

Through the electron-phonon coupling, the oscillations of electron-hole pairs also initiate an oscillation of the checkerboard lattice distortion $Q_{\mathbf{K}}$ through the displacive

excitation mechanism. Indeed, from the Fourier transform of Eq. (4.5), the equation of motion for the staggered distortion is that of a simple Harmonic oscillator driven by an external force that is proportional to the CDW order parameter

$$\frac{d^2Q_{\mathbf{K}}}{dt^2} + \Omega^2 Q_{\mathbf{K}} = \frac{g}{m}\Delta_{\mathbf{K}} \tag{6.6}$$

In equilibrium, a nonzero CDW order gives rise to a lattice distortion $Q_{\mathbf{K}} = (g/K)\Delta_{\mathbf{K}}$. As the CDW order is reduced from its initial value by the pulse excitation, the sudden shift to a new equilibrium results in the coherent phonon oscillation. The oscillation of the checkerboard lattice mode in turn drives the dynamics of electron-hole pairs $\rho_{\mathbf{q},\mathbf{q}+\mathbf{K}}(t)$ which follows the dynamical equation

$$i\hbar\frac{d\rho_{\mathbf{q},\mathbf{q}+\mathbf{K}}}{dt} = 2\epsilon_{\mathbf{q}}\rho_{\mathbf{q},\mathbf{q}+\mathbf{K}} + gQ_{\mathbf{K}}\left(\rho_{\mathbf{q},\mathbf{q}} - \rho_{\mathbf{q}+\mathbf{K},\mathbf{q}+\mathbf{K}}\right). \tag{6.7}$$

Although the oscillation of different electron-hole pairs favor their own natural frequencies, the dynamical coupling to a common checkerboard lattice oscillation promotes partial coherence among the various electron-hole modes and locks them into a coherent oscillation of the CDW order that lasts for a long time.

Depending on laser fluences, the oscillation amplitude can be seen to decay with time, although in most of the cases shown here the decay is rather slow. Since the system is isolated from any reservoir other than the short pulse excitation in our simulations, the damped oscillations of the CDW or staggered distortion are not caused by energy dissipations. Such dissipationless damping could result from a mechanism known as Landau damping where the energy of the collective mode,

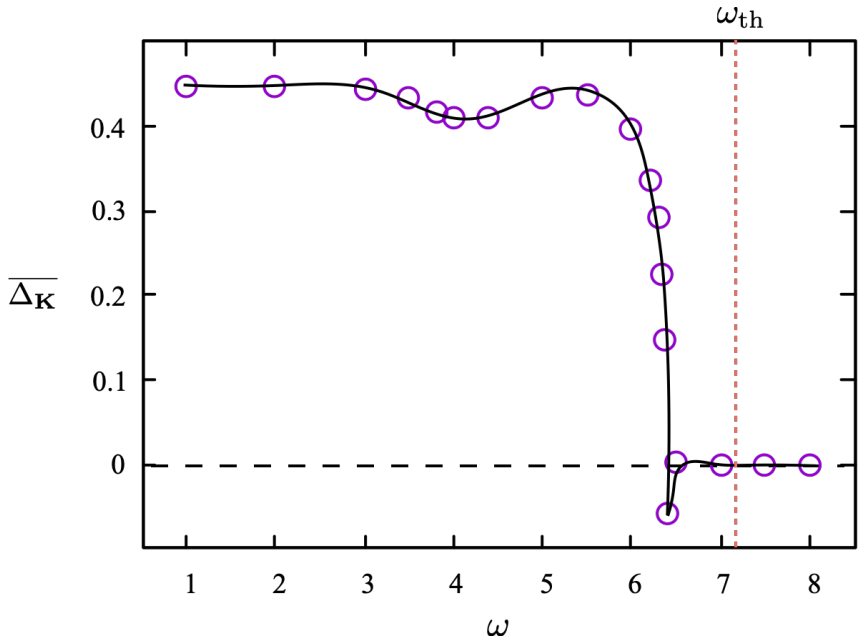

Figure 6.3: The late-stage CDW order parameter $\overline{\Delta}_{\mathbf{K}}$ averaged over several oscillation period versus the center frequency ω of the laser pulse. The dashed line indicates the threshold frequency $\omega_{\rm th} = 2g\mathcal{Q} = 7.142$ determined from the energy gap of the initial CDW state.

such as CDW order, is transferred to individual quasi-particle excitations. Indeed, Landau damping of coherent oscillations have been reported in quench dynamics of various symmetry-breaking phases including superconductivity and CDW [176]. Detailed analysis of the coherent CDW oscillatory dynamics and their damping will be discussed elsewhere.

The photo-induced melting of CDW order as a dynamical phase transition is summarized in Fig. 6.3 which shows the late-stage CDW order $\overline{\Delta}_{\mathbf{K}}$, averaged over several oscillation period, as a function of the center frequency ω. Complete melting of CDW order occurs for frequencies $\hbar\omega \gtrsim 6.5$, which is below the threshold frequency $\hbar\omega_{\rm th} = 7.142$. Yet, the dependence of the quasi-steady CDW order $\overline{\Delta}_{\mathbf{K}}$ is neither a

sharp transition nor a smooth crossover. Immediately before the complete melting, the perturbed CDW state exhibits an intriguing charge-order inversion, indicated by a sharp dip at frequency $\hbar\omega \sim 6.4$ in the $\overline{\Delta}_{\mathbf{k}}$ versus ω curve shown in Fig. 6.3. The corresponding time dependence of the CDW order $\Delta_{\mathbf{K}}(t)$ and the associated staggered distortion are shown in Fig. 6.1(b) and (c); see the curves of $\hbar\omega = 6.4$. After the short pulse excitation, the CDW order quickly decays to zero, seemingly indicating a complete melting. However, instead of staying at zero, the CDW order flips sign and slowly grows to a steady state with a small oscillation around the average value.

Similar photo-induced charge-order inversion phenomena were reported in previous theoretical studies of Z_2 type CDW/lattice order [177–179]. Experimentally, a laser-induced ultrafast reversal of combined excitonic order and lattice distortion has been observed in phonon coupled excitonic insulator Ta_2NiSe_5 [179, 180]. In general, the reversal occurs when the laser fluence is just large enough to induce a complete melting of CDW order (or the excitonic order). The physical picture of the charge-order reversal is as follows. The dephasing effect from different photoexcited electron-hole pairs quickly reduces the CDW order to zero when the pulse excitation is over. Through the electron-phonon coupling, the lattice distortion follows the vanishing CDW order with a decreasing amplitude. Yet, when the CDW order is partially recovered, a nonzero lattice momentum carries the system across the zero and toward a state that is characterized by a CDW order of opposite sign.

Another interesting feature of the photo-induced dynamical transition in Fig. 6.3

is a broad dip at the mid-gap frequency $\omega_r \sim \omega_{\rm th}/2$. The reduced CDW order at this sub-threshold frequency indicates an enhanced photo-excitation. A similar intensified photo-induced dynamics was also reported in the CDW state of the 1D t-V model [181] and BCS superconductors [20, 182]. Since there is no in-gap state in the initial homogenous CDW insulator, this mid-gap dip cannot be ascribed to a linear resonant absorption. On the other hand, as the resonant frequency is roughly half the CDW band gap, photo-excitations of quasi-particles can be achieved through a nonlinear two-photon process with $2\hbar\omega_r \sim \epsilon_{\rm gap}$. Moreover, since the electron DOS exhibits a divergence at the band edge $\varrho(E) \sim E/\sqrt{E^2-(\epsilon_{\rm gap}/2)^2}$, the resonance at the mid-gap ω_r results from the intensified two-photon absorption assisted by an enhanced electron density of states at the edge of the CDW band gap.

6.4 Dynamical Inhomogeneity and Pattern Formation

Interestingly, for the cases immediate preceding the complete melting, e.g. $\omega \sim 6.4$ or 6.5, the coherent oscillation amplitudes exhibit a significant damping. Yet, for laser frequency above the threshold such as $\omega = 7.0$, the complete melting of the CDW order is followed by a pronounced coherent oscillation that lasts for a long time. Although damped oscillations can be understood as arising from the Landau damping mechanism discussed above, the strong damping of the CDW order at excitation frequencies near the threshold is related to the emergence of spatial inhomogeneity.

The real-space simulations discussed in Sec. 6.2 can provide information about

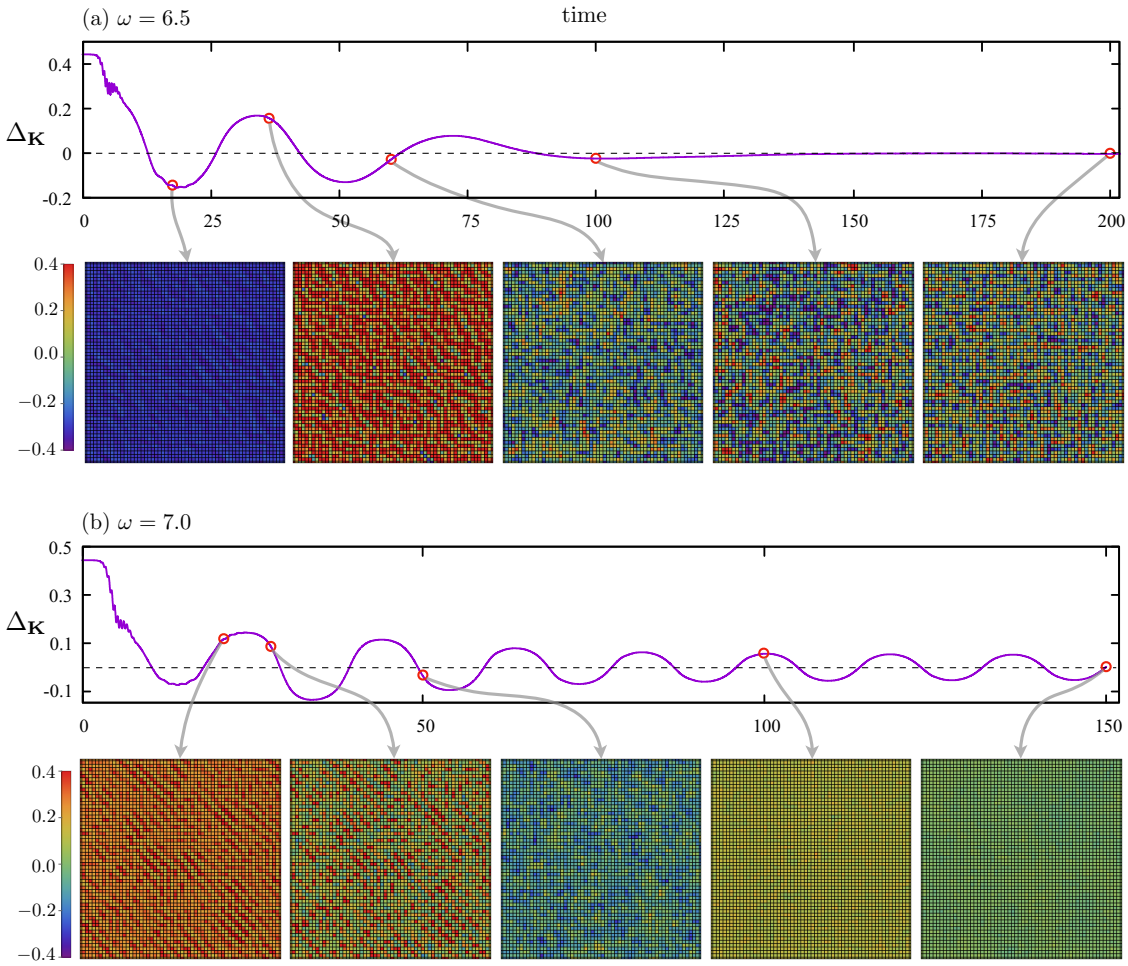

Figure 6.4: The time dependence of global CDW order $\Delta_{\mathbf{K}}(t)$ and representative CDW configurations during the photo-excitation process for laser pulses with a frequency of (a) $\hbar\omega = 6.5$ and (b) $\hbar\omega = 7.0$.

the spatial inhomogeneity. In particular, to characterize the emergence of nonuniform CDW states, we define the following local CDW order parameter

$$\phi(\mathbf{r}_i) = \left(n_i - \frac{1}{4}\sum_j{}' n_j\right) \exp\left(i\mathbf{K}\cdot\mathbf{r}_i\right). \tag{6.8}$$

Here, the prime indicates that the summation is restricted to the four nearest neighbors of site-i. This quantity measures the difference in electron density between a

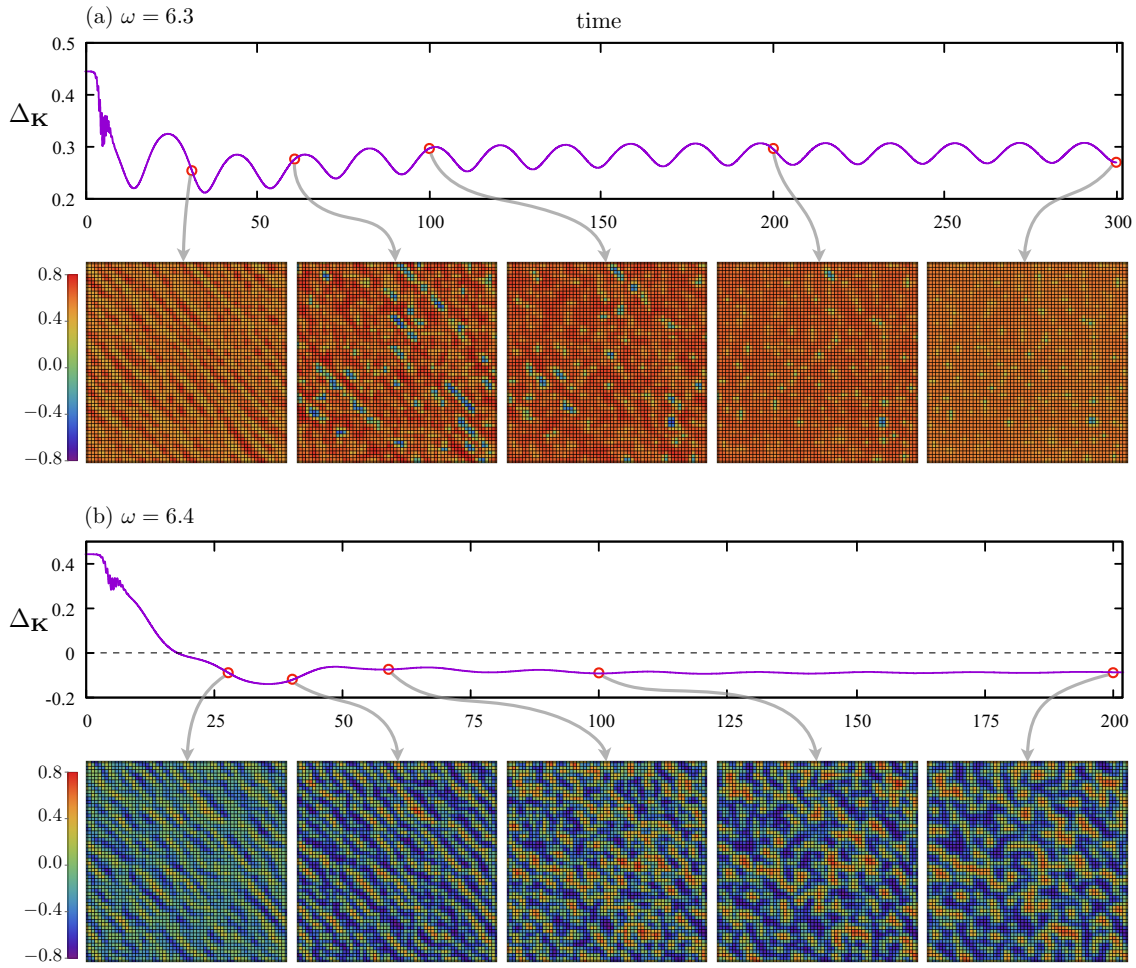

Figure 6.5: The time dependence of global CDW order $\Delta_{\mathbf{K}}(t)$ and representative CDW configurations during the photo-excitation process for laser pulses with a frequency of (a) $\hbar\omega = 6.3$ and (b) $\hbar\omega = 6.4$.

given site and its nearest neighbors. The phase factor, $\exp(i\mathbf{K}\cdot\mathbf{r}_i) = \pm 1$, is introduced to account for the ultra-short range checkerboard modulation within a CDW domain. A homogeneous CDW state is thus described by a constant local order parameter, and any inhomogeneity is manifested as a spatially varying $\phi(\mathbf{r})$ field.

First we compare the two cases where laser excitations result in complete melting of the CDW order. Fig. 6.4 shows the time dependence of the global CDW order

parameter $\Delta_{\mathbf{K}}(t)$ and the real-space configuration of the local CDW order $\phi(\mathbf{r}, t)$ at various times for frequencies $\hbar\omega = 6.5$ and 7.0. In the former case, the global CDW order exhibits a damped oscillation with the oscillation amplitude decays to zero at late times; see Fig. 6.4(a). As the snapshot at $t = 18$ shows, the CDW order parameter $\phi(\mathbf{r})$ remains roughly homogeneous when $\Delta_{\mathbf{K}}$ changes to the negative sign. Yet, when the global CDW order bounces back to the positive side at $t = 35$, significant inhomogeneity has developed in the CDW state. As the damped oscillation reaches a steady state with nearly vanishing global CDW order $\Delta_{\mathbf{K}} \approx 0$ at times $t \gtrsim 125$, the system stays in a highly inhomogeneous state with a standard deviation of the local CDW as high as $\sigma_\phi \sim 0.3$. It is worth noting that, since the snapshot shows the spatial configuration of the local order-parameter field $\phi(\mathbf{r})$ (instead of the charge density itself), the observed inhomogeneity corresponds to a super-modulation of charge density on top of the underlying checkerboard (π, π) charge modulation.

For laser excitation with a center frequency $\hbar\omega = 7.0$, the snapshots at times $t = 22$ and 28 also exhibit noticeable inhomogeneity; see Fig. 6.4(b). In particular, the inhomogeneous CDW states at $t = 22$ clearly shows a pattern of stripes running along the $y = -x$ diagonal direction, which is perpendicular to the direction of electric field of the laser pulse. The initial CDW state is melted down in the sense that the time-averaged global CDW order tends to zero at late times. However, a pronounced coherent oscillation remains. Moreover, in stark contrast to the previous melting scenario which ends with a rather disordered CDW state, the CDW order

in this dynamical regime is found to be rather homogeneous, as demonstrated in the snapshots of $t = 100$ and 150 in Fig. 6.4(b).

The emergence of this dynamical regime in the $\hbar\omega = 7.0$ case can be understood as follows. The pump pulse with a larger center frequency produces electron-hole pairs at higher energies. While such excitations quickly leads to the destruction of the static CDW order, a coherent phonon oscillation $Q_{\mathbf{K}}$ with a larger amplitude is also generated. The incoherent dynamics of photo-excited quasi-particles manifests itself not only in the time domain, as described by the Landau-damping mechanism, but also in the spatial dimension which leads to the inhomogeneous CDW states in the early stage of the melting process. Yet, the enhanced oscillations of the phonons reinforce the coherence of the electron-hole pairs both in temporal and spatial domains, giving rise to a sustained oscillation of CDW order in a relatively homogeneous state. Indeed, although there is no static global CDW order after averaging over time, the relatively homogeneous CDW state shown in Fig. 6.4(b), sustained by a coherent phonon oscillation, can be viewed as a dynamical counterpart of the conventional CDW state.

As discussed in Sec. 6.3, the photo-excited electron-hole pairs have a relative momentum $\mathbf{K} = (\pi, \pi)$, which contribute to the initial checkerboard CDW pattern. The incoherence of the electron-hole pairs only reduces the amplitude of checkerboard CDW, which is expected to remain spatially homogeneous. A spatial modulation of the particle density with a wave vector $\mathbf{q}$ requires electron-hole correlations with the

same relative momentum, i.e.

$$\Delta_{\mathbf{p}}(t) = \sum_i \rho_{ii}(t)\, e^{i\mathbf{p}\cdot\mathbf{r}_i} = \sum_{\mathbf{k}} \rho_{\mathbf{k},\mathbf{k}+\mathbf{p}}(t). \tag{6.9}$$

Consequently, the emergence of spatial inhomogeneity indicates the spontaneous generation of electron-hole pairs $\rho_{\mathbf{q},\mathbf{q}+\mathbf{p}} = \langle c^\dagger_{\mathbf{q}+\mathbf{p}} c_{\mathbf{q}} \rangle$ with a relative momentum $\mathbf{p} \neq \mathbf{K}$, i.e. different from the initial checkerboard $\mathbf{K}$. The generation of such additional density modulations is often achieved through a pattern formation instability mechanism. More precisely, the spatial patterns arise from the amplification of initial infinitesimal density fluctuations of certain wave vectors through nonlinear effects of the dynamical evolution.

This scenario is illustrated in the two cases shown in Fig. 6.5. For the first case, the initial CDW order is reduced by the laser pulse with $\hbar\omega = 6.3$, yet a finite static time-averaged global CDW order parameter $\overline{\Delta}_{\mathbf{K}} \sim 0.28$ remains at late times. Importantly, a spatially inhomogeneous CDW state with stripes running along the $y = -x$ diagonal can be seen at $t = 30$. Interestingly, such stripe pattern is similar to those observed in Fig. 6.4 with larger laser frequencies. The additional density modulations $\Delta_{\mathbf{p}}$ are characterized by wave vectors $\mathbf{p} \parallel \mathbf{E}$, parallel to the electric field direction. Indeed, at time $t = 60$ in Fig. 6.5(a), there are several diagonal streaks where the local CDW order parameter ϕ_i changes sign. As the system settles into a self-sustained coherent oscillation with the phonons, the diagonal patterns are gradually suppressed. This is another example of restoration of partial homogeneity by the coherent dynamics.

However, a small residual inhomogeneity remains even at late times.

The nonequilibrium CDW state induced by a laser pulse with $\hbar\omega = 6.4$ not only shows the phenomenon of charge-order reversal, but also exhibits the a pronounced pattern formation as shown in Fig. 6.5(b). Contrary to the previous $\hbar\omega = 6.3$ case, the global CDW order $\Delta_{\mathbf{K}}(t)$ shows nearly indiscernible oscillations and quickly settles to a steady-state value (with a sign opposite to the initial CDW state). This lack of late-time coherent oscillation is also intimately related to the emergent dynamical inhomogeneity. Indeed, stripe modulations of the local CDW order can be seen at times as early as $t = 28$ and 40 in the charge-inverted state. As the system further evolves, more complicated patterns emerge with an even stronger modulation in the ϕ-field.

It is worth noting that, in terms of the on-site electron numbers ρ_{ii}, these stripe patterns correspond to a super modulation of charge density on top of an underlying ultrashort range checkerboard charge pattern. The more complicated patterns at late times, e.g. $t = 200$, seem to originate from the breaking up of the original stripes. To further characterize this inhomogeneous state, we compute the structure factor of the charge density

$$S(\mathbf{p}, t) = |\Delta_{\mathbf{p}}(t)|^2 , \tag{6.10}$$

where $\Delta_{\mathbf{p}}(t)$ is the density modulation defined in Eq. (6.9). The structure factor, as depicted in of the states with pattern formation is shown in Fig. 6.6, has been derived

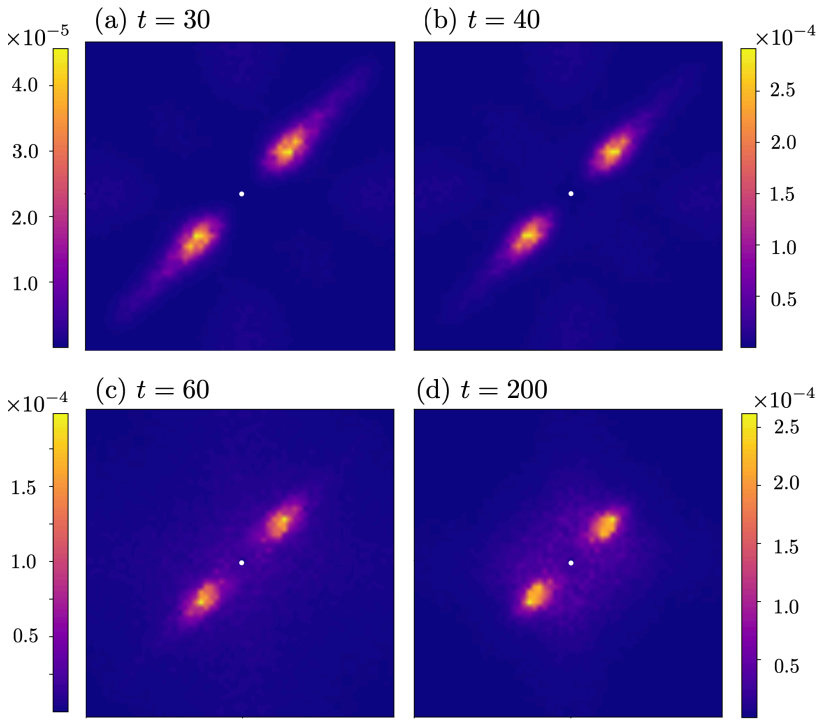

Figure 6.6: Structure factors $S(\mathbf{p}, t)$ at various time steps after the pump-probe excitations at $\omega = 6.4$. The simulated system size is $N = 60 \times 60$. The results are obtained by averaging over 20 independent von Neumann dynamics simulations. The white dot at $\mathbf{K} = (\pi, \pi)$ corresponds to a dominant checkerboard CDW order. The scale of the color bars in all panels are chosen to highlight the emergent unstable modes.

from averaging results over 20 independent von Neumann dynamical simulations. Initially, the ground state of the Holstein model reveals a prominent delta-peak at the wavevector $\mathbf{K} = (\pi, \pi)$, indicative of coherent oscillations in the CDW order parameter right after the injection of laser pulse. As the system evolves, we observe a shift in dominant modes away from $\mathbf{K}$ towards the diagonal of the Brillouin zone. These emergent modes correspond to stripe-like structures evident in the early stages of the $\phi(\mathbf{r}_i)$ distributions, as expected due to set up of the direction of the vector potential (along $(\hat{x}+\hat{y})$ direction). Subsequently, in later stages of the time evolution, we observe additional modes surrounding the $\mathbf{K}$ point, such that the peak at (π, π) becomes diffusive. This is consistent with the emergence of super-modulations atop the checkerboard and off-diagonal stripe-like patterns.

6.5 Conclusion and Outlook

In summary, we have conducted a comprehensive investigation into the dynamics of CDW states following a pump-probe excitation within the framework of the Holstein model. For the square-lattice model at half-filling, the ground state of the Holstein model exhibits checkerboard CDW order. Given the bilinear nature of the Holstein Hamiltonian in fermion operators, the quantum state of the system adopts the form of a Slater determinant CDW state, presumed to persist throughout the temporal evolution. To examine the correlation between CDW dynamics and the amplitude and frequency of the light pulse, we derived an efficient nonlinear von Neumann equation governing the evolution of the CDW state, along with Newtonian's equations

governing the classical degrees of freedom, from the Heisenberg equation of motion. Our extensive dynamical simulations successfully replicate the observed breakdown of CDW order in one- [183, 184] and two-dimensional systems [177].

Our extensive simulations on the dynamics of CDW order after pump-probe experiments are summarized in the phase diagram depicted in Fig. 6.7. The initial state of the Holstein model corresponds to its ground state, characterized by checkerboard charge density modulations and lattice distortions. Upon applying a laser pulse with sufficient frequency or amplitude, the CDW order can be suppressed due to the excitation by the injection of energy and formation of electron-hole pairs. Consequently, an abrupt decline in the CDW order parameter is observed in the early stages of the time evolution. Subsequently, the CDW order parameter may either exhibit persistent oscillations or experience regrowth after several oscillation periods. In the case of persistent oscillations, defined as Phase I, the system maintains its checkerboard-modulated CDW order. Notably, in scenarios characterized by CDW order regrowth, denoted as Phase II, the system tends to form CDW domains with distinct discretized Ising variable σ_i. Furthermore, instances of CDW order inversion are observed, wherein CDW domains with $\sigma_i = -1$ is larger in size than those with $\sigma_i = 1$. Upon further increasing the frequency or amplitude of the light pulse, the CDW order parameter exhibits small oscillations around zero following the initial rapid decline. This scenario, labeled as Phase III, indicates near-complete melting of the CDW order, with on-site charge density approaching half-filling and the local

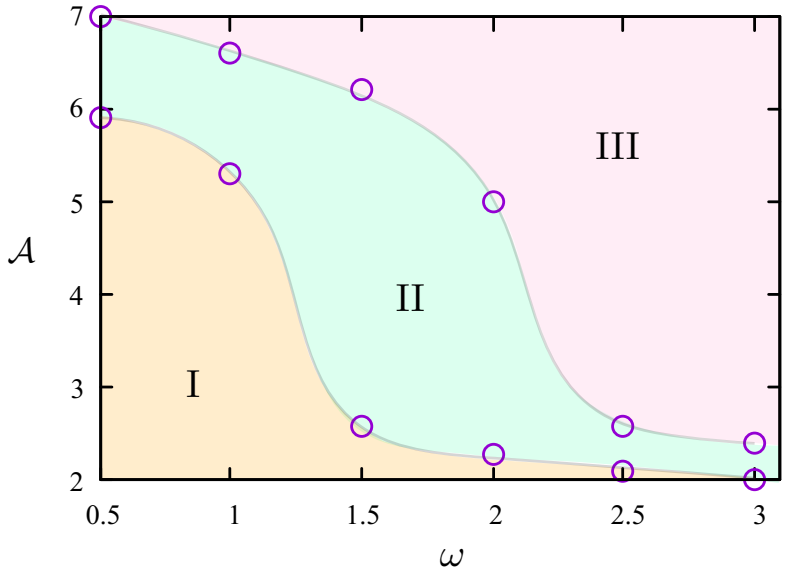

Figure 6.7: Phase diagram that schematically shows the boundary between coherent oscillating $\Delta(t)$ (Phase I) and pattern formation (Phase II), the boundary between pattern formation and CDW melt down (Phase III).

CDW order parameter nearing zero.

For high-frequency light pulses, whose energy approaches the gap of the Holstein model, the CDW order parameter weakens to a finite value without exhibiting oscillations in the later stages of time evolution. Through extensive real-space simulations, we have unveiled the emergence of complex pattern formations within the CDW states. In the ealy stage of the time evolution, the system presents a striped phase on top of the checkerboard initial CDW state, due to the predominant vector potential aligning along the $\hat{x} + \hat{y}$ direction. As the CDW state evolves, additional modes arise surrounding the $\mathbf{K} = (\pi, \pi)$ point, causing the peak at $\mathbf{K}$ to become diffuse, indicative of complex pattern formation. These spatial patterns are characterized by domains featuring super modulations of particle density in the form of stripes or

checkerboards atop the original ultrashort-period CDW order. The diagonal orientation between different domains, induced by the orientation of the overall vector potential, gives rise to an overall striped pattern. However, the lack of orientational coherence among the modes emerging in the later stages suggests the formation of disordered patterns long after the effects of the light pulse have dissipated. Analysis of the resultant structure factor indicates a competition between the striped phase induced by the orientational vector potential and the disordered patterns induced by time evolution. It's conceivable that introducing a spatially inhomogeneous light pulse into the system could lead to the formation of even more disordered patterns over time.

The emergence of super modulation patterns on top of the checkerboard and striped CDW orders is attributed to unstable modes surrounding $\mathbf{K}$. A common mechanism driving pattern formation is parametric instability, where a pair of unstable modes spontaneously grows from the decay of an initial driver mode through nonlinear interactions. Indeed, parametric instability has been demonstrated to lead to the decay of a uniform oscillating pairing order parameter and the emergence of an inhomogeneous Cooper pair turbulence state. In the context of our pump-probe excitation scenario, a plausible mechanism for pattern formation involves the decay of the checkerboard and striped CDW order parameters, mixing into a pair of such unstable modes $\mathbf{q}_1$ and $\mathbf{q}_2$ through the parametric instability mechanism. However, in the general modulation observed in our case, momentum conservation does not hold

for either the decay from the checkerboard CDW order or the decay from the striped CDW order. Hence, our results suggest a modified version of parametric instability, which presents an intriguing avenue for future exploration.

Our work underscores the importance of dynamical inhomogeneity in the dynamics of many-body systems after a pump-probe excitation. The emergence of complex patterns is entirely due to the nonlinear dynamics of order parameter fields. Our results indicate that pattern formation is likely to be a generic feature of pump-probe with more complex order parameters. In addition to the nonlinearity originating from the many-body interactions, the quantum fermionic statistics could play a crucial role in the instability mechanisms. For symmetry-breaking phases characterized by complex ordering structures, the associated pattern formation and mechanisms might be closely related to the topological defects of the corresponding order parameter fields. Finally, inclusion of incoherent processes, such as quantum fluctuations, quasiparticle scattering, and energy dissipation, are expected to produce even richer spatiotemporal dynamical behaviors of the post-quench states.

Appendix

Appendix A

Derivations of dimensionless von Neumann and Newton equations

To facilitate parameter selection for dynamical simulations, we aim to transform the dynamical equations to dimensionless formulations. To initiate this process, we introduce the characteristic time, $\tau = \hbar/t_{nn}$, and define the dimensionless time $\tilde{t} = t/\tau$. Subsequently, Eq. (4.8) can be expressed in terms of dimensionless quantities as

$$i\frac{d\rho_{ij}}{d\tilde{t}} = \frac{\sum_k \left(\rho_{ik}t_{kj} - t_{ik}\rho_{kj}\right) + g\left(Q_j - Q_i\right)\rho_{ij}}{t_{nn}}, \tag{A.1}$$

Next, we define a characteristic position Q_0 and its corresponding characteristic momentum $P_0 = m\Omega Q_0$, where $\Omega = \sqrt{K/m}$ is the oscillation frequency. We then introduce dimensionless position and momentum variables as $\tilde{Q}_i = Q_i/Q_0$ and $\tilde{P}_i = P_i/P_0$. Thus, Eq. (A.1) can be expressed as

$$i\frac{d\rho_{ij}}{d\tilde{t}} = \sum_k \left(\rho_{ik}\tilde{t}_{kj} - \tilde{t}_{ik}\rho_{kj}\right) + \tilde{g}\left(\tilde{Q}_j - \tilde{Q}_i\right)\rho_{ij}, \tag{A.2}$$

where $\tilde{t}_{kj} = t_{kj}/t_{nn}$ and $\tilde{g} = gQ_0/t_{nn}$. Similarly, the Newtonian's equations can be expressed as

$$\begin{aligned} \frac{d\tilde{Q}_i}{d\tilde{t}} &= \Omega\tau\tilde{P}_i, \\ \frac{d\tilde{P}_i}{d\tilde{t}} &= \eta\tilde{g}n_i - \Omega\tau\tilde{Q}_i, \end{aligned} \tag{A.3}$$

where $\Omega\tau$ represents the ratio of typical phonon energy to bandwidth, and $\eta = \hbar\Omega/KQ_0^2$ quantifies the ratio of phonon energy to the characteristic energy of lattice vibration. Therefore, for our dynamical simulations of a semi-classical system, we choose $\tilde{t} = 1$ if it corresponds to the nearest neighbor hopping, $\tilde{g} = 2.0$, $\Omega\tau = 0.4$, and $\eta = 0.8$. These parameter choices ensure that our results are comparable to experimental observations. The initial state, i.e., the ground state of the Holstein model, can be found by solving $dE/dQ_i = 0$, where $E = \langle\Phi(0)|\,\tilde{\hat{\mathcal{H}}}\,|\Phi(0)\rangle$, and $\tilde{\hat{\mathcal{H}}}$ is the dimensionless Hamiltonian renormalized with respect to t_{nn}.

Appendix B

Quasiparticles and energy gap of a charge density wave state

We consider a staggered lattice distortion described by

$$Q_i = \mathcal{Q} \exp(i\mathbf{K} \cdot \mathbf{r}_i), \tag{B.1}$$

where $\mathcal{Q}$ is the amplitude of lattice distortion and $\mathbf{K} = (\pi, \pi)$ is the wave vector of the checkerboard pattern. By introducing electron creation/annihilation operators in momentum space, e.g. $\hat{c}^\dagger_{\mathbf{q}} = \frac{1}{\sqrt{N}} \sum_i \hat{c}^\dagger_i \, e^{i\mathbf{q}\cdot\mathbf{r}_i}$, the electron Hamiltonian $\hat{\mathcal{H}}_{\rm e} + \hat{\mathcal{H}}_{\rm eL}$ can be expressed as

$$\hat{\mathcal{H}}_{\rm CDW} = \sum_{\mathbf{q}} \hat{\boldsymbol{c}}^\dagger_{\mathbf{q}} H(\mathbf{q}) \hat{\boldsymbol{c}}_{\mathbf{q}}, \tag{B.2}$$

where the summation is restricted to the reduced Brillouin zone, $\hat{\boldsymbol{c}}_{\mathbf{q}} = (\hat{c}_{\mathbf{q}}, \, \hat{c}_{\mathbf{q}+\mathbf{K}})^t$ is a column vector of the electron operators, and $H(\mathbf{k})$ is the one-particle Hamiltonian

given by

$$H(\mathbf{q}) = \begin{pmatrix} \epsilon_{\mathbf{q}} & -g\mathcal{Q} \\ -g\mathcal{Q} & -\epsilon_{\mathbf{q}} \end{pmatrix}. \tag{B.3}$$

The diagonal elements are given by the dispersion relation of the square-lattice tight-binding model

$$\epsilon_{\mathbf{q}} = -2t_{\mathrm{nn}}(\cos q_x + \cos q_y), \tag{B.4}$$

and we have used the relation $\epsilon_{\mathbf{q}+\mathbf{K}} = -\epsilon_{\mathbf{q}}$ in the matrix equation for H. The CDW Hamiltonian can be straightforwardly diagonalized by the Bogoliubov transformation. To this end, we introduce quasi-particle operators

$$\hat{\gamma}^{\dagger}_{+,\mathbf{q}} = u_{\mathbf{q}}\hat{c}^{\dagger}_{\mathbf{q}} - v_{\mathbf{q}}\hat{c}^{\dagger}_{\mathbf{q}+\mathbf{K}}, \quad \hat{\gamma}^{\dagger}_{-,\mathbf{q}} = v_{\mathbf{q}}\hat{c}^{\dagger}_{\mathbf{q}} + u_{\mathbf{q}}\hat{c}^{\dagger}_{\mathbf{q}+\mathbf{K}}, \tag{B.5}$$

where the transformation coefficients are given by

$$\begin{aligned} u_{\mathbf{q}} &= \frac{1}{\sqrt{2}}\left(1 + \frac{\epsilon_{\mathbf{q}}}{\sqrt{\epsilon^2_{\mathbf{q}} + (g\mathcal{Q})^2}}\right)^{1/2}, \\ v_{\mathbf{q}} &= \frac{1}{\sqrt{2}}\left(1 - \frac{\epsilon_{\mathbf{q}}}{\sqrt{\epsilon^2_{\mathbf{q}} + (g\mathcal{Q})^2}}\right)^{1/2}. \end{aligned} \tag{B.6}$$

The diagonalized Hamiltonian becomes

$$\hat{\mathcal{H}}_{\mathrm{CDW}} = \sum_{\mathbf{q}}\sum_{\mu=\pm} E^{\mu}_{\mathbf{q}}\hat{\gamma}^{\dagger}_{\mu,\mathbf{q}}\hat{\gamma}_{\mu,\mathbf{q}}. \tag{B.7}$$

where the quasi-particle energies are

$$E_{\mathbf{q}}^{\pm} = \pm\sqrt{\epsilon_{\mathbf{q}}^2 + (g\mathcal{Q})^2} \tag{B.8}$$

A spectral gap $\epsilon_{\text{gap}} = 2g\mathcal{Q}$ is opened in the excitation spectrum. At half-filling, the electron energy is obtained by filling up all negative energy states, giving rise to an energy density of the CDW state

$$\varepsilon(\mathcal{Q}) = -\frac{1}{N}\sum_{\mathbf{k}}\sqrt{\epsilon_{\mathbf{k}}^2 + (g\mathcal{Q})^2} + \frac{1}{2}K\mathcal{Q}^2, \tag{B.9}$$

The order parameter of the staggered lattice distortion $\mathcal{Q}$ is determined from the minimum energy condition $\partial\varepsilon/\partial\mathcal{Q} = 0$.

The electron-hole correlation function $\rho_{\mathbf{q},\mathbf{q}+\mathbf{K}} = \langle\hat{c}_{\mathbf{q}+\mathbf{K}}^{\dagger}\hat{c}_{\mathbf{q}}\rangle$ can be expressed in terms of quasi-particle operators, as shown in Eq. (6.5), with the following expansion coefficients

$$\begin{aligned} C_{\mathbf{q}}^{+,+} &= -u_{\mathbf{q}}v_{\mathbf{q}}, \quad C_{\mathbf{q}}^{-,+} = u_{\mathbf{q}}^2, \\ C_{\mathbf{q}}^{-,-} &= u_{\mathbf{q}}v_{\mathbf{q}}, \quad C_{\mathbf{q}}^{+,-} = -v_{\mathbf{q}}^2, \end{aligned} \tag{B.10}$$

Bibliography

[1] R. A. Barankov and L. S. Levitov, "Synchronization in the bcs pairing dynamics as a critical phenomenon," *Phys. Rev. Lett.*, vol. 96, p. 230403, Jun 2006. [Online]. Available: https://link.aps.org/doi/10.1103/PhysRevLett.96.230403

[2] P. Calabrese and J. Cardy, "Quantum quenches in extended systems," *Journal of Statistical Mechanics: Theory and Experiment*, vol. 2007, no. 06, p. P06008, 2007. [Online]. Available: https://iopscience.iop.org/article/10.1088/1742-5468/2007/06/P06008/meta

[3] A. Mitra, "Quantum quench dynamics," *Annual Review of Condensed Matter Physics*, vol. 9, no. 1, pp. 245–259, 2018. [Online]. Available: https://doi.org/10.1146/annurev-conmatphys-031016-025451

[4] J. Eisert, M. Friesdorf, and C. Gogolin, "Quantum many-body systems out of equilibrium," *Nature Physics*, vol. 11, no. 2, pp. 124–130, Feb 2015. [Online]. Available: https://doi.org/10.1038/nphys3215

[5] A. Polkovnikov, K. Sengupta, A. Silva, and M. Vengalattore, "Colloquium: Nonequilibrium dynamics of closed interacting quantum systems," *Rev.*

Mod. Phys., vol. 83, pp. 863–883, Aug 2011. [Online]. Available: https://link.aps.org/doi/10.1103/RevModPhys.83.863

[6] J. Eisert, M. Friesdorf, and C. Gogolin, "Quantum many-body systems out of equilibrium," *Nature Physics*, vol. 11, no. 2, pp. 124–130, 2015. [Online]. Available: https://www.nature.com/articles/nphys3215

[7] I. Bloch, J. Dalibard, and W. Zwerger, "Many-body physics with ultracold gases," *Rev. Mod. Phys.*, vol. 80, pp. 885–964, Jul 2008. [Online]. Available: https://link.aps.org/doi/10.1103/RevModPhys.80.885

[8] M. A. Cazalilla, R. Citro, T. Giamarchi, E. Orignac, and M. Rigol, "One dimensional bosons: From condensed matter systems to ultracold gases," *Rev. Mod. Phys.*, vol. 83, pp. 1405–1466, Dec 2011. [Online]. Available: https://link.aps.org/doi/10.1103/RevModPhys.83.1405

[9] D. Fausti, R. Tobey, N. Dean, S. Kaiser, A. Dienst, M. C. Hoffmann, S. Pyon, T. Takayama, H. Takagi, and A. Cavalleri, "Light-induced superconductivity in a stripe-ordered cuprate," *science*, vol. 331, no. 6014, pp. 189–191, 2011. [Online]. Available: https://www.science.org/doi/full/10.1126/science.1197294

[10] R. Matsunaga and R. Shimano, "Nonequilibrium bcs state dynamics induced by intense terahertz pulses in a superconducting nbn film," *Phys. Rev. Lett.*, vol. 109, p. 187002, Oct 2012. [Online]. Available: https://link.aps.org/doi/10.1103/PhysRevLett.109.187002

[11] R. Matsunaga, Y. I. Hamada, K. Makise, Y. Uzawa, H. Terai, Z. Wang, and R. Shimano, "Higgs amplitude mode in the bcs superconductors $Nb_{1-x}Ti_xN$ induced by terahertz pulse excitation," *Phys. Rev. Lett.*, vol. 111, p. 057002, Jul 2013. [Online]. Available: https://link.aps.org/doi/10.1103/PhysRevLett.111.057002

[12] B. Mansart, J. Lorenzana, A. Mann, A. Odeh, M. Scarongella, M. Chergui, and F. Carbone, "Coupling of a high-energy excitation to superconducting quasiparticles in a cuprate from coherent charge fluctuation spectroscopy," *Proceedings of the National Academy of Sciences*, vol. 110, no. 12, pp. 4539–4544, 2013. [Online]. Available: https://www.pnas.org/doi/10.1073/pnas.1218742110

[13] R. Matsunaga, N. Tsuji, H. Fujita, A. Sugioka, K. Makise, Y. Uzawa, H. Terai, Z. Wang, H. Aoki, and R. Shimano, "Light-induced collective pseudospin precession resonating with higgs mode in a superconductor," *Science*, vol. 345, no. 6201, pp. 1145–1149, 2014. [Online]. Available: https://www.science.org/doi/10.1126/science.1254697

[14] M. Mitrano, A. Cantaluppi, D. Nicoletti, S. Kaiser, A. Perucchi, S. Lupi, P. Di Pietro, D. Pontiroli, M. Riccò, S. R. Clark *et al.*, "Possible light-induced superconductivity in K3C60 at high temperature," *Nature*, vol. 530, no. 7591, pp. 461–464, 2016. [Online]. Available: https://www.nature.com/articles/nature16522

[15] F. Rossi and T. Kuhn, "Theory of ultrafast phenomena in photoexcited semiconductors," *Rev. Mod. Phys.*, vol. 74, pp. 895–950, Aug 2002. [Online]. Available: https://link.aps.org/doi/10.1103/RevModPhys.74.895

[16] M. Kira and S. W. Koch, *Semiconductor Quantum Optics*. Cambridge: Cambridge University Press, 2011.

[17] R. Matsunaga and R. Shimano, "Nonequilibrium BCS state dynamics induced by intense terahertz pulses in a superconducting NbN film," *Phys. Rev. Lett.*, vol. 109, p. 187002, Oct 2012. [Online]. Available: https://link.aps.org/doi/10.1103/PhysRevLett.109.187002

[18] R. Matsunaga, Y. I. Hamada, K. Makise, Y. Uzawa, H. Terai, Z. Wang, and R. Shimano, "Higgs amplitude mode in the bcs superconductors $Nb_{1-x}Ti_xN$ induced by terahertz pulse excitation," *Phys. Rev. Lett.*, vol. 111, p. 057002, Jul 2013. [Online]. Available: https://link.aps.org/doi/10.1103/PhysRevLett.111.057002

[19] B. Mansart, J. Lorenzana, A. Mann, A. Odeh, M. Scarongella, M. Chergui, and F. Carbone, "Coupling of a high-energy excitation to superconducting quasiparticles in a cuprate from coherent charge fluctuation spectroscopy," *Proceedings of the National Academy of Sciences*, vol. 110, no. 12, pp. 4539–4544, 2013. [Online]. Available: https://www.pnas.org/doi/10.1073/pnas.1218742110

[20] R. Matsunaga, N. Tsuji, H. Fujita, A. Sugioka, K. Makise, Y. Uzawa, H. Terai, Z. Wang, H. Aoki, and R. Shimano, "Light-induced collective pseudospin precession resonating with higgs mode in a superconductor," *Science*, vol. 345, no. 6201, pp. 1145–1149, 2014. [Online]. Available: https://www.science.org/doi/10.1126/science.1254697

[21] D. Polli, M. Rini, S. Wall, R. Schoenlein, Y. Tomioka, Y. Tokura, G. Cerullo, and A. Cavalleri, "Coherent orbital waves in the photo-induced insulator–metal dynamics of a magnetoresistive manganite," *Nature Materials*, vol. 6, no. 9, pp. 643–647, 2007. [Online]. Available: https://doi.org/10.1038/nmat1979

[22] P. Beaud, A. Caviezel, S. Mariager, L. Rettig, G. Ingold, C. Dornes, S. Huang, J. Johnson, M. Radovic, T. Huber *et al.*, "A time-dependent order parameter for ultrafast photoinduced phase transitions," *Nature Materials*, vol. 13, no. 10, pp. 923–927, 2014. [Online]. Available: https://doi.org/10.1038/nmat4046

[23] H. Hashimoto, H. Matsueda, H. Seo, and S. Ishihara, "Photo-induced dynamics in charge-frustrated systems," *Journal of the Physical Society of Japan*, vol. 83, no. 12, p. 123703, 2014. [Online]. Available: https://journals.jps.jp/doi/10.7566/JPSJ.83.123703

[24] K. Nasu, Ed., *Photoinduced Phase Transitions*. Singapore: World Scientific, 2004.

[25] Y. Tokura, "Photoinduced phase transition: A tool for generating a hidden state of matter," *Journal of the Physical Society of Japan*, vol. 75, no. 1, p. 011001, 2006. [Online]. Available: https://doi.org/10.1143/JPSJ.75.011001

[26] V. Kiryukhin, D. Casa, J. Hill, B. Keimer, A. Vigliante, Y. Tomioka, and Y. Tokura, "An X-ray-induced insulator–metal transition in a magnetoresistive manganite," *Nature*, vol. 386, no. 6627, pp. 813–815, 1997. [Online]. Available: https://doi.org/10.1038/386813a0

[27] M. Chollet, L. Guerin, N. Uchida, S. Fukaya, H. Shimoda, T. Ishikawa, K. Matsuda, T. Hasegawa, A. Ota, H. Yamochi *et al.*, "Gigantic photoresponse in 1/4-filled-band organic salt $(EDO-TTF)_2PF_6$," *Science*, vol. 307, no. 5706, pp. 86–89, 2005. [Online]. Available: https://www.science.org/doi/abs/10.1126/science.1105067

[28] K. Onda, S. Ogihara, K. Yonemitsu, N. Maeshima, T. Ishikawa, Y. Okimoto, X. Shao, Y. Nakano, H. Yamochi, G. Saito, and S.-y. Koshihara, "Photoinduced change in the charge order pattern in the quarter-filled organic conductor $(EDO-TTF)_2PF_6$ with a strong electron-phonon interaction," *Phys. Rev. Lett.*, vol. 101, p. 067403, Aug 2008. [Online]. Available: https://link.aps.org/doi/10.1103/PhysRevLett.101.067403

[29] D. Fausti, R. Tobey, N. Dean, S. Kaiser, A. Dienst, M. C. Hoffmann, S. Pyon, T. Takayama, H. Takagi, and A. Cavalleri, "Light-induced superconductivity

in a stripe-ordered cuprate," *science*, vol. 331, no. 6014, pp. 189–191, 2011. [Online]. Available: https://www.science.org/doi/full/10.1126/science.1197294

[30] H. Ichikawa, S. Nozawa, T. Sato, A. Tomita, K. Ichiyanagi, M. Chollet, L. Guerin, N. Dean, A. Cavalleri, S.-i. Adachi *et al.*, "Transient photoinduced 'hidden' phase in a manganite," *Nature Materials*, vol. 10, no. 2, pp. 101–105, 2011. [Online]. Available: https://www.nature.com/articles/nmat2929

[31] L. Stojchevska, I. Vaskivskyi, T. Mertelj, P. Kusar, D. Svetin, S. Brazovskii, and D. Mihailovic, "Ultrafast switching to a stable hidden quantum state in an electronic crystal," *Science*, vol. 344, no. 6180, pp. 177–180, 2014. [Online]. Available: https://www.science.org/doi/10.1126/science.1241591

[32] J. Zhang, X. Tan, M. Liu, S. W. Teitelbaum, K. W. Post, F. Jin, K. A. Nelson, D. N. Basov, W. Wu, and R. D. Averitt, "Cooperative photoinduced metastable phase control in strained manganite films," *Nature Materials*, vol. 15, no. 9, pp. 956–960, 2016. [Online]. Available: https://www.nature.com/articles/nmat4695

[33] M. Mitrano, A. Cantaluppi, D. Nicoletti, S. Kaiser, A. Perucchi, S. Lupi, P. Di Pietro, D. Pontiroli, M. Riccò, S. R. Clark *et al.*, "Possible light-induced superconductivity in K_3C_{60} at high temperature," *Nature*, vol. 530, no. 7591, pp. 461–464, 2016. [Online]. Available: https://www.nature.com/articles/nature16522

[34] C. Giannetti, M. Capone, D. Fausti, M. Fabrizio, F. Parmigiani, and D. Mihailovic, "Ultrafast optical spectroscopy of strongly correlated materials and high-temperature superconductors: a non-equilibrium approach," *Advances in Physics*, vol. 65, no. 2, pp. 58–238, 2016. [Online]. Available: https://doi.org/10.1080/00018732.2016.1194044

[35] T. Nova, A. Disa, M. Fechner, and A. Cavalleri, "Metastable ferroelectricity in optically strained $SrTiO_3$," *Science*, vol. 364, no. 6445, pp. 1075–1079, 2019. [Online]. Available: https://www.science.org/doi/10.1126/science.aaw4911

[36] X. Li, T. Qiu, J. Zhang, E. Baldini, J. Lu, A. M. Rappe, and K. A. Nelson, "Terahertz field–induced ferroelectricity in quantum paraelectric $SrTiO_3$," *Science*, vol. 364, no. 6445, pp. 1079–1082, 2019. [Online]. Available: https://www.science.org/doi/10.1126/science.aaw4913

[37] C. Kollath, A. M. Läuchli, and E. Altman, "Quench dynamics and nonequilibrium phase diagram of the bose-hubbard model," *Phys. Rev. Lett.*, vol. 98, p. 180601, Apr 2007. [Online]. Available: https://link.aps.org/doi/10.1103/PhysRevLett.98.180601

[38] J. Berges, A. Rothkopf, and J. Schmidt, "Nonthermal fixed points: Effective weak coupling for strongly correlated systems far from equilibrium," *Phys. Rev. Lett.*, vol. 101, p. 041603, Jul 2008. [Online]. Available: https://link.aps.org/doi/10.1103/PhysRevLett.101.041603

[39] M. Cramer, C. M. Dawson, J. Eisert, and T. J. Osborne, "Exact relaxation in a class of nonequilibrium quantum lattice systems," *Phys. Rev. Lett.*, vol. 100, p. 030602, Jan 2008. [Online]. Available: https://link.aps.org/doi/10.1103/PhysRevLett.100.030602

[40] A. Flesch, M. Cramer, I. P. McCulloch, U. Schollwöck, and J. Eisert, "Probing local relaxation of cold atoms in optical superlattices," *Phys. Rev. A*, vol. 78, p. 033608, Sep 2008. [Online]. Available: https://link.aps.org/doi/10.1103/PhysRevA.78.033608

[41] M. Rigol, "Breakdown of thermalization in finite one-dimensional systems," *Phys. Rev. Lett.*, vol. 103, p. 100403, Sep 2009. [Online]. Available: https://link.aps.org/doi/10.1103/PhysRevLett.103.100403

[42] J. Dziarmaga, "Dynamics of a quantum phase transition and relaxation to a steady state," *Advances in Physics*, vol. 59, no. 6, pp. 1063–1189, 2010. [Online]. Available: https://www.tandfonline.com/doi/abs/10.1080/00018732.2010.514702

[43] C. Gogolin, M. P. Müller, and J. Eisert, "Absence of thermalization in nonintegrable systems," *Phys. Rev. Lett.*, vol. 106, p. 040401, Jan 2011. [Online]. Available: https://link.aps.org/doi/10.1103/PhysRevLett.106.040401

[44] S. Erne, R. Bücker, T. Gasenzer, J. Berges, and J. Schmiedmayer, "Universal dynamics in an isolated one-dimensional bose gas far from

equilibrium," *Nature*, vol. 563, no. 7730, pp. 225–229, 2018. [Online]. Available: https://www.nature.com/articles/s41586-018-0667-0

[45] T. Kinoshita, T. Wenger, and D. S. Weiss, "A quantum newton's cradle," *Nature*, vol. 440, no. 7086, pp. 900–903, 2006. [Online]. Available: https://www.nature.com/articles/nature04693

[46] S. Trotzky, Y.-A. Chen, A. Flesch, I. P. McCulloch, U. Schollwöck, J. Eisert, and I. Bloch, "Probing the relaxation towards equilibrium in an isolated strongly correlated one-dimensional bose gas," *Nature physics*, vol. 8, no. 4, pp. 325–330, 2012. [Online]. Available: https://www.nature.com/articles/nphys2232

[47] M. Schreiber, S. S. Hodgman, P. Bordia, H. P. Lüschen, M. H. Fischer, R. Vosk, E. Altman, U. Schneider, and I. Bloch, "Observation of many-body localization of interacting fermions in a quasirandom optical lattice," *Science*, vol. 349, no. 6250, pp. 842–845, 2015. [Online]. Available: https://www.science.org/doi/10.1126/science.aaa7432

[48] K. Mallayya and M. Rigol, "Quantum quenches and relaxation dynamics in the thermodynamic limit," *Phys. Rev. Lett.*, vol. 120, p. 070603, Feb 2018. [Online]. Available: https://link.aps.org/doi/10.1103/PhysRevLett.120.070603

[49] M. Rigol, "Fundamental asymmetry in quenches between integrable and nonintegrable systems," *Phys. Rev. Lett.*, vol. 116, p. 100601, Mar 2016. [Online]. Available: https://link.aps.org/doi/10.1103/PhysRevLett.116.100601

[50] R. Barnett, A. Polkovnikov, and M. Vengalattore, "Prethermalization in quenched spinor condensates," *Phys. Rev. A*, vol. 84, p. 023606, Aug 2011. [Online]. Available: https://link.aps.org/doi/10.1103/PhysRevA.84.023606

[51] M. Gring, M. Kuhnert, T. Langen, T. Kitagawa, B. Rauer, M. Schreitl, I. Mazets, D. A. Smith, E. Demler, and J. Schmiedmayer, "Relaxation and prethermalization in an isolated quantum system," *Science*, vol. 337, no. 6100, pp. 1318–1322, 2012. [Online]. Available: https://www.science.org/doi/abs/10.1126/science.1224953

[52] T. Langen, R. Geiger, M. Kuhnert, B. Rauer, and J. Schmiedmayer, "Local emergence of thermal correlations in an isolated quantum many-body system," *Nature Physics*, vol. 9, no. 10, pp. 640–643, Oct 2013. [Online]. Available: https://doi.org/10.1038/nphys2739

[53] M. Marcuzzi, J. Marino, A. Gambassi, and A. Silva, "Prethermalization in a nonintegrable quantum spin chain after a quench," *Phys. Rev. Lett.*, vol. 111, p. 197203, Nov 2013. [Online]. Available: https://link.aps.org/doi/10.1103/PhysRevLett.111.197203

[54] A. Mitra, "Correlation functions in the prethermalized regime after a quantum quench of a spin chain," *Phys. Rev. B*, vol. 87, p. 205109, May 2013. [Online]. Available: https://link.aps.org/doi/10.1103/PhysRevB.87.205109

[55] N. Nessi, A. Iucci, and M. A. Cazalilla, "Quantum quench and prethermalization dynamics in a two-dimensional fermi gas with long-range interactions," *Phys. Rev. Lett.*, vol. 113, p. 210402, Nov 2014. [Online]. Available: https://link.aps.org/doi/10.1103/PhysRevLett.113.210402

[56] T. Langen, S. Erne, R. Geiger, B. Rauer, T. Schweigler, M. Kuhnert, W. Rohringer, I. E. Mazets, T. Gasenzer, and J. Schmiedmayer, "Experimental observation of a generalized gibbs ensemble," *Science*, vol. 348, no. 6231, pp. 207–211, 2015, https://www.science.org/doi/pdf/10.1126/science.1257026. [Online]. Available: https://www.science.org/doi/abs/10.1126/science.1257026

[57] M. Babadi, E. Demler, and M. Knap, "Far-from-equilibrium field theory of many-body quantum spin systems: Prethermalization and relaxation of spin spiral states in three dimensions," *Phys. Rev. X*, vol. 5, p. 041005, Oct 2015. [Online]. Available: https://link.aps.org/doi/10.1103/PhysRevX.5.041005

[58] B. Bertini, F. H. L. Essler, S. Groha, and N. J. Robinson, "Prethermalization and thermalization in models with weak integrability breaking," *Phys. Rev. Lett.*, vol. 115, p. 180601, Oct 2015. [Online]. Available: https://link.aps.org/doi/10.1103/PhysRevLett.115.180601

[59] T. Langen, T. Gasenzer, and J. Schmiedmayer, "Prethermalization and universal dynamics in near-integrable quantum systems," *Journal of Statistical*

Mechanics: Theory and Experiment, vol. 2016, no. 6, p. 064009, jun 2016. [Online]. Available: https://dx.doi.org/10.1088/1742-5468/2016/06/064009

[60] M. Buchhold, M. Heyl, and S. Diehl, "Prethermalization and thermalization of a quenched interacting luttinger liquid," *Phys. Rev. A*, vol. 94, p. 013601, Jul 2016. [Online]. Available: https://link.aps.org/doi/10.1103/PhysRevA.94.013601

[61] J. Marino, M. Eckstein, M. S. Foster, and A. M. Rey, "Dynamical phase transitions in the collisionless pre-thermal states of isolated quantum systems: theory and experiments," *Reports on Progress in Physics*, vol. 85, no. 11, p. 116001, oct 2022. [Online]. Available: https://dx.doi.org/10.1088/1361-6633/ac906c

[62] M. Heyl, "Dynamical quantum phase transitions in systems with broken-symmetry phases," *Phys. Rev. Lett.*, vol. 113, p. 205701, Nov 2014. [Online]. Available: https://link.aps.org/doi/10.1103/PhysRevLett.113.205701

[63] R. A. Barankov, L. S. Levitov, and B. Z. Spivak, "Collective rabi oscillations and solitons in a time-dependent bcs pairing problem," *Phys. Rev. Lett.*, vol. 93, p. 160401, Oct 2004. [Online]. Available: https://link.aps.org/doi/10.1103/PhysRevLett.93.160401

[64] E. A. Yuzbashyan, O. Tsyplyatyev, and B. L. Altshuler, "Relaxation and persistent oscillations of the order parameter in fermionic condensates,"

Phys. Rev. Lett., vol. 96, p. 097005, Mar 2006. [Online]. Available: https://link.aps.org/doi/10.1103/PhysRevLett.96.097005

[65] E. A. Yuzbashyan and M. Dzero, "Dynamical vanishing of the order parameter in a fermionic condensate," *Phys. Rev. Lett.*, vol. 96, p. 230404, Jun 2006. [Online]. Available: https://link.aps.org/doi/10.1103/PhysRevLett.96.230404

[66] V. Gurarie, "Nonequilibrium dynamics of weakly and strongly paired superconductors," *Phys. Rev. Lett.*, vol. 103, p. 075301, Aug 2009. [Online]. Available: https://link.aps.org/doi/10.1103/PhysRevLett.103.075301

[67] M. S. Foster, M. Dzero, V. Gurarie, and E. A. Yuzbashyan, "Quantum quench in a $p + ip$ superfluid: Winding numbers and topological states far from equilibrium," *Phys. Rev. B*, vol. 88, p. 104511, Sep 2013. [Online]. Available: https://link.aps.org/doi/10.1103/PhysRevB.88.104511

[68] M. S. Foster, V. Gurarie, M. Dzero, and E. A. Yuzbashyan, "Quench-induced floquet topological p-wave superfluids," *Phys. Rev. Lett.*, vol. 113, p. 076403, Aug 2014. [Online]. Available: https://link.aps.org/doi/10.1103/PhysRevLett.113.076403

[69] N. Tsuji, M. Eckstein, and P. Werner, "Nonthermal antiferromagnetic order and nonequilibrium criticality in the hubbard model," *Phys. Rev. Lett.*, vol. 110, p. 136404, Mar 2013. [Online]. Available: https://link.aps.org/doi/10.1103/PhysRevLett.110.136404

[70] Y. Dong, L. Dong, M. Gong, and H. Pu, "Dynamical phases in quenched spin–orbit-coupled degenerate fermi gas," *Nature communications*, vol. 6, no. 1, p. 6103, 2015. [Online]. Available: https://doi.org/10.1038/ncomms7103

[71] F. Peronaci, M. Schiró, and M. Capone, "Transient dynamics of d-wave superconductors after a sudden excitation," *Phys. Rev. Lett.*, vol. 115, p. 257001, Dec 2015. [Online]. Available: https://link.aps.org/doi/10.1103/PhysRevLett.115.257001

[72] B. Dóra, M. Haque, F. Pollmann, and B. Hetényi, "Quantum quench in two dimensions using the variational baeriswyl wave function," *Phys. Rev. B*, vol. 93, p. 115124, Mar 2016. [Online]. Available: https://link.aps.org/doi/10.1103/PhysRevB.93.115124

[73] I. V. Blinov, P. Ribeiro, and A. N. Rubtsov, "Post-quench dynamics and suppression of thermalization in an open half-filled hubbard layer," *Phys. Rev. B*, vol. 95, p. 024309, Jan 2017. [Online]. Available: https://link.aps.org/doi/10.1103/PhysRevB.95.024309

[74] Y.-Z. Chou, Y. Liao, and M. S. Foster, "Twisting anderson pseudospins with light: Quench dynamics in terahertz-pumped bcs superconductors," *Phys. Rev. B*, vol. 95, p. 104507, Mar 2017. [Online]. Available: https://link.aps.org/doi/10.1103/PhysRevB.95.104507

[75] S. Yoon and G. Watanabe, "Pairing dynamics of polar states in a quenched p-wave superfluid fermi gas," *Phys. Rev. Lett.*, vol. 119, p. 100401, Sep 2017. [Online]. Available: https://link.aps.org/doi/10.1103/PhysRevLett.119.100401

[76] S. Hannibal, P. Kettmann, M. D. Croitoru, V. M. Axt, and T. Kuhn, "Dynamical vanishing of the order parameter in a confined bardeen-cooper-schrieffer fermi gas after an interaction quench," *Phys. Rev. A*, vol. 97, p. 013619, Jan 2018. [Online]. Available: https://link.aps.org/doi/10.1103/PhysRevA.97.013619

[77] S. Hannibal, P. Kettmann, M. D. Croitoru, V. M. Axt, and T. Kuhn, "Persistent oscillations of the order parameter and interaction quench phase diagram for a confined bardeen-cooper-schrieffer fermi gas," *Phys. Rev. A*, vol. 98, p. 053605, Nov 2018. [Online]. Available: https://link.aps.org/doi/10.1103/PhysRevA.98.053605

[78] T. Cui, M. Schütt, P. P. Orth, and R. M. Fernandes, "Postquench gap dynamics of two-band superconductors," *Phys. Rev. B*, vol. 100, p. 144513, Oct 2019. [Online]. Available: https://link.aps.org/doi/10.1103/PhysRevB.100.144513

[79] J. A. Scaramazza, P. Smacchia, and E. A. Yuzbashyan, "Consequences of integrability breaking in quench dynamics of pairing hamiltonians," *Phys. Rev. B*, vol. 99, p. 054520, Feb 2019. [Online]. Available: https://link.aps.org/doi/10.1103/PhysRevB.99.054520

[80] Y. Chen and Z. Cai, "Persistent oscillations versus thermalization in the quench dynamics of quantum gases with long-range interactions," *Phys. Rev. A*, vol. 101, p. 023611, Feb 2020. [Online]. Available: https://link.aps.org/doi/10.1103/PhysRevA.101.023611

[81] P. W. Anderson, "Random-phase approximation in the theory of superconductivity," *Phys. Rev.*, vol. 112, pp. 1900–1916, Dec 1958. [Online]. Available: https://link.aps.org/doi/10.1103/PhysRev.112.1900

[82] T. W. B. Kibble, "Topology of cosmic domains and strings," *Journal of Physics A: Mathematical and General*, vol. 9, no. 8, p. 1387, aug 1976. [Online]. Available: https://dx.doi.org/10.1088/0305-4470/9/8/029

[83] W. H. Zurek, "Cosmological experiments in superfluid helium?" *Nature*, vol. 317, no. 6037, pp. 505–508, Oct 1985. [Online]. Available: https://doi.org/10.1038/317505a0

[84] A. Chandran, A. Erez, S. S. Gubser, and S. L. Sondhi, "Kibble-zurek problem: Universality and the scaling limit," *Phys. Rev. B*, vol. 86, p. 064304, Aug 2012. [Online]. Available: https://link.aps.org/doi/10.1103/PhysRevB.86.064304

[85] B. Damski, "The simplest quantum model supporting the kibble-zurek mechanism of topological defect production: Landau-zener transitions from a new perspective," *Phys. Rev. Lett.*, vol. 95, p. 035701, Jul 2005. [Online]. Available: https://link.aps.org/doi/10.1103/PhysRevLett.95.035701

[86] K. Sengupta, D. Sen, and S. Mondal, "Exact results for quench dynamics and defect production in a two-dimensional model," *Phys. Rev. Lett.*, vol. 100, p. 077204, Feb 2008. [Online]. Available: https://link.aps.org/doi/10.1103/PhysRevLett.100.077204

[87] W. H. Zurek, U. Dorner, and P. Zoller, "Dynamics of a quantum phase transition," *Phys. Rev. Lett.*, vol. 95, p. 105701, Sep 2005. [Online]. Available: https://link.aps.org/doi/10.1103/PhysRevLett.95.105701

[88] L. Mathey and A. Polkovnikov, "Light cone dynamics and reverse kibble-zurek mechanism in two-dimensional superfluids following a quantum quench," *Phys. Rev. A*, vol. 81, p. 033605, Mar 2010. [Online]. Available: https://link.aps.org/doi/10.1103/PhysRevA.81.033605

[89] A. del Campo, "Universal statistics of topological defects formed in a quantum phase transition," *Phys. Rev. Lett.*, vol. 121, p. 200601, Nov 2018. [Online]. Available: https://link.aps.org/doi/10.1103/PhysRevLett.121.200601

[90] M. Dzero, E. A. Yuzbashyan, and B. L. Altshuler, "Cooper pair turbulence in atomic fermi gases," *Europhysics Letters*, vol. 85, no. 2, p. 20004, jan 2009. [Online]. Available: https://dx.doi.org/10.1209/0295-5075/85/20004

[91] G.-W. Chern and K. Barros, "Nonequilibrium dynamics of superconductivity in the attractive hubbard model," *Phys. Rev. B*, vol. 99, p. 035162, Jan 2019. [Online]. Available: https://link.aps.org/doi/10.1103/PhysRevB.99.035162

[92] B. Huang, X. Yang, N. Xu, J. Zhou, and M. Gong, "Dynamical instability with respect to finite-momentum pairing in quenched bcs superconducting phases," *Phys. Rev. B*, vol. 99, p. 014517, Jan 2019. [Online]. Available: https://link.aps.org/doi/10.1103/PhysRevB.99.014517

[93] M. Eckstein, M. Kollar, and P. Werner, "Thermalization after an interaction quench in the hubbard model," *Phys. Rev. Lett.*, vol. 103, p. 056403, Jul 2009. [Online]. Available: https://link.aps.org/doi/10.1103/PhysRevLett.103.056403

[94] M. Schiró and M. Fabrizio, "Time-dependent mean field theory for quench dynamics in correlated electron systems," *Phys. Rev. Lett.*, vol. 105, p. 076401, Aug 2010. [Online]. Available: https://link.aps.org/doi/10.1103/PhysRevLett.105.076401

[95] G.-W. Chern, "Dynamic inhomogeneities and phase separation after quantum quenches in strongly correlated systems," *arXiv preprint arXiv:1711.07972*, 2017. [Online]. Available: https://arxiv.org/abs/1711.07972

[96] G. Nicolis and I. Prigogine, *Self Organization in Non Equilibrium Systems*. Wiley, 1977.

[97] M. C. Cross and P. C. Hohenberg, "Pattern formation outside of equilibrium," *Rev. Mod. Phys.*, vol. 65, pp. 851–1112, Jul 1993. [Online]. Available: https://link.aps.org/doi/10.1103/RevModPhys.65.851

[98] A. J. Koch and H. Meinhardt, "Biological pattern formation: from basic mechanisms to complex structures," *Rev. Mod. Phys.*, vol. 66, pp. 1481–1507, Oct 1994. [Online]. Available: https://link.aps.org/doi/10.1103/RevModPhys.66.1481

[99] L. Pismen, *Patterns and Interfaces in Dissipative Dynamics*. Springer, 2006.

[100] M. Cross and H. Greenside, *Pattern Formation and Dynamics in Non-Equilibrium Systems*. Cambridge University Press, 2009.

[101] G. Grüner, "The dynamics of charge-density waves," *Rev. Mod. Phys.*, vol. 60, pp. 1129–1181, Oct 1988. [Online]. Available: https://link.aps.org/doi/10.1103/RevModPhys.60.1129

[102] R. E. Thorne, "Charge-density-wave conductors," *Physics Today*, vol. 49, no. 5, pp. 42–47, 1996. [Online]. Available: https://doi.org/10.1063/1.881498

[103] S. V. Zaitsev-Zotov, "Finite-size effects in quasi-one-dimensional conductors with a charge-density wave," *Physics-Uspekhi*, vol. 47, no. 6, p. 533, 2004. [Online]. Available: https://doi.org/10.1070/pu2004v047n06abeh001675

[104] P. Monceau, "Electronic crystals: an experimental overview," *Advances in Physics*, vol. 61, no. 4, pp. 325–581, 2012. [Online]. Available: https://doi.org/10.1080/00018732.2012.719674

[105] Y. Yu, F. Yang, X. F. Lu, Y. J. Yan, Y.-H. Cho, L. Ma, X. Niu, S. Kim, Y.-W. Son, D. Feng *et al.*, "Gate-tunable phase transitions in thin flakes of 1T-TaS_2," *Nature Nanotechnology*, vol. 10, no. 3, pp. 270–276, 2015. [Online]. Available: https://doi.org/10.1038/nnano.2014.323

[106] R. Samnakay, D. Wickramaratne, T. Pope, R. Lake, T. Salguero, and A. Balandin, "Zone-folded phonons and the commensurate–incommensurate charge-density-wave transition in 1T-TaS_2 thin films," *Nano Letters*, vol. 15, no. 5, pp. 2965–2973, 2015. [Online]. Available: https://pubs.acs.org/doi/10.1021/nl504811s

[107] X. Xi, L. Zhao, Z. Wang, H. Berger, L. Forró, J. Shan, and K. F. Mak, "Strongly enhanced charge-density-wave order in monolayer $NbSe_2$," *Nature Nanotechnology*, vol. 10, no. 9, pp. 765–769, 2015. [Online]. Available: https://doi.org/10.1038/nnano.2015.143

[108] D. Cho, S. Cheon, K.-S. Kim, S.-H. Lee, Y.-H. Cho, S.-W. Cheong, and H. W. Yeom, "Nanoscale manipulation of the mott insulating state coupled to charge order in 1T-TaS_2," *Nature Communications*, vol. 7, no. 1, p. 10453, 2016. [Online]. Available: https://doi.org/10.1038/ncomms10453

[109] G. Liu, B. Debnath, T. R. Pope, T. T. Salguero, R. K. Lake, and A. A. Balandin, "A charge-density-wave oscillator based on an integrated tantalum disulfide–boron nitride–graphene device operating at room temperature,"

Nature Nanotechnology, vol. 11, no. 10, pp. 845–850, 2016. [Online]. Available: https://doi.org/10.1038/nnano.2016.108

[110] S. Vogelgesang, G. Storeck, J. Horstmann, T. Diekmann, M. Sivis, S. Schramm, K. Rossnagel, S. Schäfer, and C. Ropers, "Phase ordering of charge density waves traced by ultrafast low-energy electron diffraction," *Nature Physics*, vol. 14, no. 2, pp. 184–190, 2018. [Online]. Available: https://doi.org/10.1038/nphys4309

[111] A. K. Geremew, S. Rumyantsev, F. Kargar, B. Debnath, A. Nosek, M. A. Bloodgood, M. Bockrath, T. T. Salguero, R. K. Lake, and A. A. Balandin, "Bias-voltage driven switching of the charge-density-wave and normal metallic phases in $1T$-TaS_2 thin-film devices," *ACS Nano*, vol. 13, no. 6, pp. 7231–7240, 2019. [Online]. Available: https://pubs.acs.org/doi/10.1021/acsnano.9b02870

[112] A. A. Balandin, S. V. Zaitsev-Zotov, and G. Grüner, "Charge-density-wave quantum materials and devices—New developments and future prospects," *Applied Physics Letters*, vol. 119, no. 17, 2021. [Online]. Available: https://pubs.aip.org/aip/apl/article/119/17/170401/1022999/

[113] S. Iwai, K. Yamamoto, A. Kashiwazaki, F. Hiramatsu, H. Nakaya, Y. Kawakami, K. Yakushi, H. Okamoto, H. Mori, and Y. Nishio, "Photoinduced melting of a stripe-type charge-order and metallic domain formation in a layered

BEDT-TTF-based organic salt," *Phys. Rev. Lett.*, vol. 98, p. 097402, Mar 2007. [Online]. Available: https://link.aps.org/doi/10.1103/PhysRevLett.98.097402

[114] C. Kübler, H. Ehrke, R. Huber, R. Lopez, A. Halabica, R. F. Haglund, and A. Leitenstorfer, "Coherent structural dynamics and electronic correlations during an ultrafast insulator-to-metal phase transition in VO_2," *Phys. Rev. Lett.*, vol. 99, p. 116401, Sep 2007. [Online]. Available: https://link.aps.org/doi/10.1103/PhysRevLett.99.116401

[115] F. Schmitt, P. S. Kirchmann, U. Bovensiepen, R. G. Moore, L. Rettig, M. Krenz, J.-H. Chu, N. Ru, L. Perfetti, D. Lu *et al.*, "Transient electronic structure and melting of a charge density wave in $TbTe_3$," *Science*, vol. 321, no. 5896, pp. 1649–1652, 2008. [Online]. Available: https://www.science.org/doi/abs/10.1126/science.1160778

[116] A. Tomeljak, H. Schäfer, D. Städter, M. Beyer, K. Biljakovic, and J. Demsar, "Dynamics of photoinduced charge-density-wave to metal phase transition in $\mathbf{K}_{0.3}MoO_3$," *Phys. Rev. Lett.*, vol. 102, p. 066404, Feb 2009. [Online]. Available: https://link.aps.org/doi/10.1103/PhysRevLett.102.066404

[117] S. Hellmann, M. Beye, C. Sohrt, T. Rohwer, F. Sorgenfrei, H. Redlin, M. Kalläne, M. Marczynski-Bühlow, F. Hennies, M. Bauer, A. Föhlisch, L. Kipp, W. Wurth, and K. Rossnagel, "Ultrafast melting of a charge-density wave in the mott insulator $1T$-TaS_2," *Phys. Rev. Lett.*, vol. 105, p. 187401,

Oct 2010. [Online]. Available: https://link.aps.org/doi/10.1103/PhysRevLett.105.187401

[118] Y. Kawakami, T. Fukatsu, Y. Sakurai, H. Unno, H. Itoh, S. Iwai, T. Sasaki, K. Yamamoto, K. Yakushi, and K. Yonemitsu, "Early-stage dynamics of light-matter interaction leading to the insulator-to-metal transition in a charge ordered organic crystal," *Phys. Rev. Lett.*, vol. 105, p. 246402, Dec 2010. [Online]. Available: https://link.aps.org/doi/10.1103/PhysRevLett.105.246402

[119] A. Cavalleri, T. Dekorsy, H. H. W. Chong, J. C. Kieffer, and R. W. Schoenlein, "Evidence for a structurally-driven insulator-to-metal transition in VO_2: A view from the ultrafast timescale," *Phys. Rev. B*, vol. 70, p. 161102, Oct 2004. [Online]. Available: https://link.aps.org/doi/10.1103/PhysRevB.70.161102

[120] J. C. Petersen, S. Kaiser, N. Dean, A. Simoncig, H. Y. Liu, A. L. Cavalieri, C. Cacho, I. C. E. Turcu, E. Springate, F. Frassetto, L. Poletto, S. S. Dhesi, H. Berger, and A. Cavalleri, "Clocking the melting transition of charge and lattice order in $1T$-TaS_2 with ultrafast extreme-ultraviolet angle-resolved photoemission spectroscopy," *Phys. Rev. Lett.*, vol. 107, p. 177402, Oct 2011. [Online]. Available: https://link.aps.org/doi/10.1103/PhysRevLett.107.177402

[121] S. Wall, B. Krenzer, S. Wippermann, S. Sanna, F. Klasing, A. Hanisch-Blicharski, M. Kammler, W. G. Schmidt, and M. Horn-von Hoegen, "Atomistic picture of charge density wave formation at surfaces," *Phys.*

Rev. Lett., vol. 109, p. 186101, Nov 2012. [Online]. Available: https://link.aps.org/doi/10.1103/PhysRevLett.109.186101

[122] H. Y. Liu, I. Gierz, J. C. Petersen, S. Kaiser, A. Simoncig, A. L. Cavalieri, C. Cacho, I. C. E. Turcu, E. Springate, F. Frassetto, L. Poletto, S. S. Dhesi, Z.-A. Xu, T. Cuk, R. Merlin, and A. Cavalleri, "Possible observation of parametrically amplified coherent phasons in $K_{0.3}MoO_3$ using time-resolved extreme-ultraviolet angle-resolved photoemission spectroscopy," *Phys. Rev. B*, vol. 88, p. 045104, Jul 2013. [Online]. Available: https://link.aps.org/doi/10.1103/PhysRevB.88.045104

[123] S. Mathias, S. Eich, J. Urbancic, S. Michael, A. Carr, S. Emmerich, A. Stange, T. Popmintchev, T. Rohwer, M. Wiesenmayer *et al.*, "Self-amplified photo-induced gap quenching in a correlated electron material," *Nature Communications*, vol. 7, no. 1, p. 12902, 2016. [Online]. Available: https://doi.org/10.1038/ncomms12902

[124] L. Rettig, R. Cortés, J.-H. Chu, I. Fisher, F. Schmitt, R. Moore, Z.-X. Shen, P. Kirchmann, M. Wolf, and U. Bovensiepen, "Persistent order due to transiently enhanced nesting in an electronically excited charge density wave," *Nature Communications*, vol. 7, no. 1, p. 10459, 2016. [Online]. Available: https://doi.org/10.1038/ncomms10459

[125] M. Chavez-Cervantes, G. E. Topp, S. Aeschlimann, R. Krause, S. A. Sato, M. A. Sentef, and I. Gierz, "Charge density wave melting in one-dimensional wires with femtosecond subgap excitation," *Phys. Rev. Lett.*, vol. 123, p. 036405, Jul 2019. [Online]. Available: https://link.aps.org/doi/10.1103/PhysRevLett.123.036405

[126] J. Diego, A. Said, S. K. Mahatha, R. Bianco, L. Monacelli, M. Calandra, F. Mauri, K. Rossnagel, I. Errea, and S. Blanco-Canosa, "van der waals driven anharmonic melting of the 3d charge density wave in VSe_2," *Nature Communications*, vol. 12, no. 1, p. 598, 2021. [Online]. Available: https://doi.org/10.1038/s41467-020-20829-2

[127] R. Yusupov, T. Mertelj, V. V. Kabanov, S. Brazovskii, P. Kusar, J.-H. Chu, I. R. Fisher, and D. Mihailovic, "Coherent dynamics of macroscopic electronic order through a symmetry breaking transition," *Nature Physics*, vol. 6, no. 9, pp. 681–684, 2010. [Online]. Available: https://doi.org/10.1038/nphys1738

[128] M. Porer, U. Leierseder, J.-M. Ménard, H. Dachraoui, L. Mouchliadis, I. Perakis, U. Heinzmann, J. Demsar, K. Rossnagel, and R. Huber, "Non-thermal separation of electronic and structural orders in a persisting charge density wave," *Nature Materials*, vol. 13, no. 9, pp. 857–861, 2014. [Online]. Available: https://doi.org/10.1038/nmat4042

[129] T. Rohwer, S. Hellmann, M. Wiesenmayer, C. Sohrt, A. Stange, B. Slomski, A. Carr, Y. Liu, L. M. Avila, M. Kalläne *et al.*, "Collapse of long-range

charge order tracked by time-resolved photoemission at high momenta," *Nature*, vol. 471, no. 7339, pp. 490–493, 2011. [Online]. Available: https://doi.org/10.1038/nature09829

[130] S. Hellmann, T. Rohwer, M. Kalläne, K. Hanff, C. Sohrt, A. Stange, A. Carr, M. Murnane, H. Kapteyn, L. Kipp *et al.*, "Time-domain classification of charge-density-wave insulators," *Nature Communications*, vol. 3, no. 1, p. 1069, 2012. [Online]. Available: https://doi.org/10.1038/ncomms2078

[131] H. Hedayat, C. J. Sayers, D. Bugini, C. Dallera, D. Wolverson, T. Batten, S. Karbassi, S. Friedemann, G. Cerullo, J. van Wezel, S. R. Clark, E. Carpene, and E. Da Como, "Excitonic and lattice contributions to the charge density wave in $1T$-TaS_2 revealed by a phonon bottleneck," *Phys. Rev. Res.*, vol. 1, p. 023029, Sep 2019. [Online]. Available: https://link.aps.org/doi/10.1103/PhysRevResearch.1.023029

[132] C. J. Sayers, H. Hedayat, A. Ceraso, F. Museur, M. Cattelan, L. S. Hart, L. S. Farrar, S. Dal Conte, G. Cerullo, C. Dallera, E. Da Como, and E. Carpene, "Coherent phonons and the interplay between charge density wave and mott phases in $1T$-TaS_2," *Phys. Rev. B*, vol. 102, p. 161105, Oct 2020. [Online]. Available: https://link.aps.org/doi/10.1103/PhysRevB.102.161105

[133] S. R. White, "Density matrix formulation for quantum renormalization groups," *Phys. Rev. Lett.*, vol. 69, pp. 2863–2866, Nov 1992. [Online]. Available:

https://link.aps.org/doi/10.1103/PhysRevLett.69.2863

[134] U. Schollwöck, "The density-matrix renormalization group," *Rev. Mod. Phys.*, vol. 77, pp. 259–315, Apr 2005. [Online]. Available: https://link.aps.org/doi/10.1103/RevModPhys.77.259

[135] G. Vidal, "Efficient classical simulation of slightly entangled quantum computations," *Phys. Rev. Lett.*, vol. 91, p. 147902, Oct 2003. [Online]. Available: https://link.aps.org/doi/10.1103/PhysRevLett.91.147902

[136] S. R. White and A. E. Feiguin, "Real-time evolution using the density matrix renormalization group," *Phys. Rev. Lett.*, vol. 93, p. 076401, Aug 2004. [Online]. Available: https://link.aps.org/doi/10.1103/PhysRevLett.93.076401

[137] P. Ring and P. Schuck, *The Nuclear Many-Body Problem.* Springer-Verlag, Berlin, 1980.

[138] A. D. McLACHLAN and M. A. BALL, "Time-dependent hartree—fock theory for molecules," *Rev. Mod. Phys.*, vol. 36, pp. 844–855, Jul 1964. [Online]. Available: https://link.aps.org/doi/10.1103/RevModPhys.36.844

[139] E. Deumens, A. Diz, R. Longo, and Y. Öhrn, "Time-dependent theoretical treatments of the dynamics of electrons and nuclei in molecular systems," *Rev. Mod. Phys.*, vol. 66, pp. 917–983, Jul 1994. [Online]. Available: https://link.aps.org/doi/10.1103/RevModPhys.66.917

[140] P. A. M. Dirac, "Note on exchange phenomena in the thomas atom," *Mathematical Proceedings of the Cambridge Philosophical Society*, vol. 26, no. 3, p. 376–385, 1930.

[141] J. Frenkel, *Wave Mechanics: Advanced General Theory*. Clarendon, Oxford University Press, 1934.

[142] J. Haegeman, J. I. Cirac, T. J. Osborne, I. Pižorn, H. Verschelde, and F. Verstraete, "Time-dependent variational principle for quantum lattices," *Phys. Rev. Lett.*, vol. 107, p. 070601, Aug 2011. [Online]. Available: https://link.aps.org/doi/10.1103/PhysRevLett.107.070601

[143] J. Haegeman, C. Lubich, I. Oseledets, B. Vandereycken, and F. Verstraete, "Unifying time evolution and optimization with matrix product states," *Phys. Rev. B*, vol. 94, p. 165116, Oct 2016. [Online]. Available: https://link.aps.org/doi/10.1103/PhysRevB.94.165116

[144] F. Bloch, "Nuclear induction," *Phys. Rev.*, vol. 70, pp. 460–474, Oct 1946. [Online]. Available: https://link.aps.org/doi/10.1103/PhysRev.70.460

[145] A. F. Volkov and S. M. Kogan, "Collisionless relaxation of the energy gap in superconductors," *J. Exp. Theor. Phys.*, vol. 38, p. 1018, 1974. [Online]. Available: http://www.jetp.ras.ru/cgi-bin/e/index/r/65/5/p2038?a=list

[146] A. J. Bray, "Theory of phase-ordering kinetics," *Advances in Physics*, vol. 43, no. 3, pp. 357–459, 1994. [Online]. Available: https://doi.org/10.1080/00018739400101505

[147] S. Puri and V. Wadhawan, *Kinetics of phase transitions*. CRC press, 2009.

[148] A. C. Newell and Y. Pomeau, "Turbulent crystals in macroscopic systems," *Journal of Physics A: Mathematical and General*, vol. 26, no. 8, p. L429, apr 1993. [Online]. Available: https://dx.doi.org/10.1088/0305-4470/26/8/006

[149] M. Le Berre, E. Ressayre, A. Tallet, Y. Pomeau, and L. Di Menza, "Example of a chaotic crystal: The labyrinth," *Phys. Rev. E*, vol. 66, p. 026203, Aug 2002. [Online]. Available: https://link.aps.org/doi/10.1103/PhysRevE.66.026203

[150] T. Holstein, "Studies of polaron motion: Part I. the molecular-crystal model," *Annals of Physics*, vol. 8, no. 3, pp. 325–342, 1959. [Online]. Available: https://www.sciencedirect.com/science/article/pii/0003491659900028

[151] T. Holstein, "Studies of polaron motion: Part II. the "small" polaron," *Annals of Physics*, vol. 8, no. 3, pp. 343–389, 1959. [Online]. Available: https://www.sciencedirect.com/science/article/pii/000349165990003X?via%3Dihub

[152] R. T. Scalettar, N. E. Bickers, and D. J. Scalapino, "Competition of pairing and peierls–charge-density-wave correlations in a two-dimensional electron-phonon model," *Phys. Rev. B*, vol. 40, pp. 197–200, Jul 1989. [Online]. Available: https://link.aps.org/doi/10.1103/PhysRevB.40.197

[153] J. Bonča, S. A. Trugman, and I. Batistić, "Holstein polaron," *Phys. Rev. B*, vol. 60, pp. 1633–1642, Jul 1999. [Online]. Available: https://link.aps.org/doi/10.1103/PhysRevB.60.1633

[154] D. Golež, J. Bonča, L. Vidmar, and S. A. Trugman, "Relaxation dynamics of the Holstein polaron," *Phys. Rev. Lett.*, vol. 109, p. 236402, Dec 2012. [Online]. Available: https://link.aps.org/doi/10.1103/PhysRevLett.109.236402

[155] A. S. Mishchenko, N. Nagaosa, and N. Prokof'ev, "Diagrammatic monte carlo method for many-polaron problems," *Phys. Rev. Lett.*, vol. 113, p. 166402, Oct 2014. [Online]. Available: https://link.aps.org/doi/10.1103/PhysRevLett.113.166402

[156] N. C. Costa, T. Blommel, W.-T. Chiu, G. Batrouni, and R. T. Scalettar, "Phonon dispersion and the competition between pairing and charge order," *Phys. Rev. Lett.*, vol. 120, p. 187003, May 2018. [Online]. Available: https://link.aps.org/doi/10.1103/PhysRevLett.120.187003

[157] O. Bradley, G. G. Batrouni, and R. T. Scalettar, "Superconductivity and charge density wave order in the two-dimensional Holstein model," *Phys. Rev. B*, vol. 103, p. 235104, Jun 2021. [Online]. Available: https://link.aps.org/doi/10.1103/PhysRevB.103.235104

[158] I. Esterlis, S. A. Kivelson, and D. J. Scalapino, "Pseudogap crossover in the electron-phonon system," *Phys. Rev. B*, vol. 99, p. 174516, May 2019. [Online].

Available: https://link.aps.org/doi/10.1103/PhysRevB.99.174516

[159] T. Holstein, "Studies of polaron motion: Part i. the molecular-crystal model," *Annals of Physics*, vol. 8, no. 3, pp. 325–342, 1959. [Online]. Available: https://www.sciencedirect.com/science/article/pii/0003491659900028

[160] J. Luo and G.-W. Chern, "Dynamics of electronically phase-separated states in the double exchange model," *Phys. Rev. B*, vol. 103, p. 115137, Mar 2021. [Online]. Available: https://link.aps.org/doi/10.1103/PhysRevB.103.115137

[161] W. Koshibae, N. Furukawa, and N. Nagaosa, "Photo-induced insulator-metal transition of a spin-electron coupled system," *Europhysics Letters*, vol. 94, no. 2, p. 27003, 2011. [Online]. Available: https://iopscience.iop.org/article/10.1209/0295-5075/94/27003

[162] A. Ono and S. Ishihara, "Double-exchange interaction in optically induced nonequilibrium state: A conversion from ferromagnetic to antiferromagnetic structure," *Phys. Rev. Lett.*, vol. 119, p. 207202, Nov 2017. [Online]. Available: https://link.aps.org/doi/10.1103/PhysRevLett.119.207202

[163] S. Huh, K. Mukherjee, K. Kwon, J. Seo, J. Hur, S. I. Mistakidis, H. Sadeghpour, and J.-y. Choi, "Universality class of a spinor bose–einstein condensate far from equilibrium," *Nature Physics*, pp. 1–7, 2024. [Online]. Available: https://www.nature.com/articles/s41567-023-02339-2

[164] C. Cheng, S. Zhang, and G.-W. Chern, "Machine learning for phase ordering dynamics of charge density waves," *Phys. Rev. B*, vol. 108, p. 014301, Jul 2023. [Online]. Available: https://link.aps.org/doi/10.1103/PhysRevB.108.014301

[165] S. Puri, "Kinetics of phase transitions," in *Kinetics of phase transitions*. CRC press, 2009, pp. 13–74.

[166] A. J. Bray, "Theory of phase-ordering kinetics," *Advances in Physics*, vol. 51, no. 2, pp. 481–587, 2002. [Online]. Available: https://www.tandfonline.com/doi/abs/10.1080/00018730110117433

[167] S. M. Bhattacharjee and F. Seno, "A measure of data collapse for scaling," *Journal of Physics A: Mathematical and General*, vol. 34, no. 33, p. 6375, 2001. [Online]. Available: https://iopscience.iop.org/article/10.1088/0305-4470/34/33/302/meta

[168] N. C. Costa, T. Blommel, W.-T. Chiu, G. Batrouni, and R. T. Scalettar, "Phonon dispersion and the competition between pairing and charge order," *Phys. Rev. Lett.*, vol. 120, p. 187003, May 2018. [Online]. Available: https://link.aps.org/doi/10.1103/PhysRevLett.120.187003

[169] O. Bradley, G. G. Batrouni, and R. T. Scalettar, "Superconductivity and charge density wave order in the two-dimensional holstein model," *Phys. Rev. B*, vol. 103, p. 235104, Jun 2021. [Online]. Available: https://link.aps.org/doi/10.1103/PhysRevB.103.235104

[170] J. Bonča, S. A. Trugman, and I. Batistić, "Holstein polaron," *Phys. Rev. B*, vol. 60, pp. 1633–1642, Jul 1999. [Online]. Available: https://link.aps.org/doi/10.1103/PhysRevB.60.1633

[171] A. S. Mishchenko, N. Nagaosa, and N. Prokof'ev, "Diagrammatic monte carlo method for many-polaron problems," *Phys. Rev. Lett.*, vol. 113, p. 166402, Oct 2014. [Online]. Available: https://link.aps.org/doi/10.1103/PhysRevLett.113.166402

[172] R. M. Noack, D. J. Scalapino, and R. T. Scalettar, "Charge-density-wave and pairing susceptibilities in a two-dimensional electron-phonon model," *Phys. Rev. Lett.*, vol. 66, pp. 778–781, Feb 1991. [Online]. Available: https://link.aps.org/doi/10.1103/PhysRevLett.66.778

[173] Y.-X. Zhang, W.-T. Chiu, N. C. Costa, G. G. Batrouni, and R. T. Scalettar, "Charge order in the holstein model on a honeycomb lattice," *Phys. Rev. Lett.*, vol. 122, p. 077602, Feb 2019. [Online]. Available: https://link.aps.org/doi/10.1103/PhysRevLett.122.077602

[174] C. Chen, X. Y. Xu, Z. Y. Meng, and M. Hohenadler, "Charge-density-wave transitions of dirac fermions coupled to phonons," *Phys. Rev. Lett.*, vol. 122, p. 077601, Feb 2019. [Online]. Available: https://link.aps.org/doi/10.1103/PhysRevLett.122.077601

[175] I. Esterlis, S. A. Kivelson, and D. J. Scalapino, "Pseudogap crossover in the electron-phonon system," *Phys. Rev. B*, vol. 99, p. 174516, May 2019. [Online]. Available: https://link.aps.org/doi/10.1103/PhysRevB.99.174516

[176] L. Yang, Y. Yang, and G.-W. Chern, "Pattern formation in charge density wave states after a quantum quench," *Phys. Rev. B*, vol. 109, p. 195133, May 2024. [Online]. Available: https://link.aps.org/doi/10.1103/PhysRevB.109.195133

[177] M. van Veenendaal, "Photoinduced ultrafast charge-order melting: Charge-order inversion and nonthermal effects," *Phys. Rev. B*, vol. 94, p. 115101, Sep 2016. [Online]. Available: https://link.aps.org/doi/10.1103/PhysRevB.94.115101

[178] M. D. Petrovic, M. Weber, and J. K. Freericks, "Theoretical description of time-resolved photoemission in charge-density-wave materials out to long times," *arXiv preprint arXiv:2203.11880*, 2022. [Online]. Available: https://arxiv.org/abs/2203.11880

[179] H. Ning, O. Mehio, M. Buchhold, T. Kurumaji, G. Refael, J. G. Checkelsky, and D. Hsieh, "Signatures of ultrafast reversal of excitonic order in ta_2nise_5," *Phys. Rev. Lett.*, vol. 125, p. 267602, Dec 2020. [Online]. Available: https://link.aps.org/doi/10.1103/PhysRevLett.125.267602

[180] M. Guan, D. Chen, Q. Chen, Y. Yao, and S. Meng, "Coherent phonon assisted ultrafast order-parameter reversal and hidden metallic state in

ta_2nise_5," *Phys. Rev. Lett.*, vol. 131, p. 256503, Dec 2023. [Online]. Available: https://link.aps.org/doi/10.1103/PhysRevLett.131.256503

[181] H. Seo, Y. Tanaka, and S. Ishihara, "Photoinduced collective mode, inhomogeneity, and melting in a charge-order system," *Phys. Rev. B*, vol. 98, p. 235150, Dec 2018. [Online]. Available: https://link.aps.org/doi/10.1103/PhysRevB.98.235150

[182] H. Krull, N. Bittner, G. Uhrig, D. Manske, and A. Schnyder, "Coupling of higgs and leggett modes in non-equilibrium superconductors," *Nature communications*, vol. 7, no. 1, p. 11921, 2016. [Online]. Available: https://www.nature.com/articles/ncomms11921

[183] H. Hashimoto and S. Ishihara, "Photoinduced charge-order melting dynamics in a one-dimensional interacting holstein model," *Phys. Rev. B*, vol. 96, p. 035154, Jul 2017. [Online]. Available: https://link.aps.org/doi/10.1103/PhysRevB.96.035154

[184] J. Stolpp, J. Herbrych, F. Dorfner, E. Dagotto, and F. Heidrich-Meisner, "Charge-density-wave melting in the one-dimensional holstein model," *Phys. Rev. B*, vol. 101, p. 035134, Jan 2020. [Online]. Available: https://link.aps.org/doi/10.1103/PhysRevB.101.035134